High Energy Density Physics and Inertial Confinement Fusion

V. T. Tikhonchuk

Centre Lasers Intenses et Applications, University of Bordeaux – CNRS – CEA, Talence, France

ELI-Beamlines, Institute of Physics, CSR, Dolní Břežany, Czech Republic

eli beamlines

université de BORDEAUX

CELIA

Outline

- **Place of high energy density physics in the modern science**
- **Physics of inertial confinement fusion**
- **High energy density laboratory astrophysics**

Place of high energy density physics in the modern science

Place of high energy density physics in science

Extreme physics is ubiquitous in the Universe, can be assessed remotely only

Experiments are limited by the conditions that can be achieved in laboratory

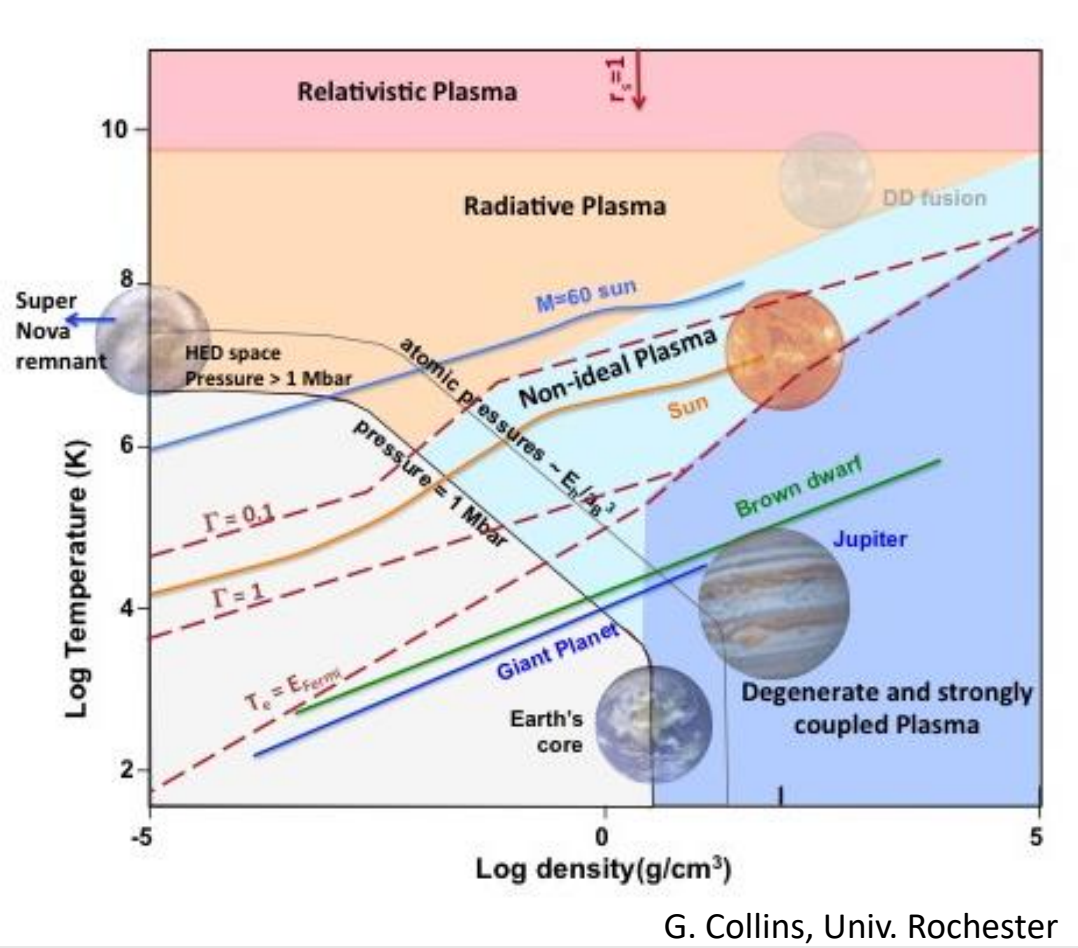

G. Collins, Univ. Rochester

High energy density physics is defined by pressures exceeding the value of 1 Mbar

Lasers are unique tools providing access to such extreme conditions

R. P. Drake, High-Energy-Density Physics, Springer, 2006
Frontiers in High Energy Density Physics: The X-Games of Contemporary Science, www.nap.edu, 2003

Extreme physics: high pressures and densities

Lasers are offering a unique possibility to create (for a short period of time) pressures that are much larger than any other methods in laboratory thus opening new ways for studying materials at extreme conditions P, T

- **Diamond anvil cells – maximum pressure 8 Mbar**
- **Imploded laser fusion targets – achieved pressure 2-250 Gbar**

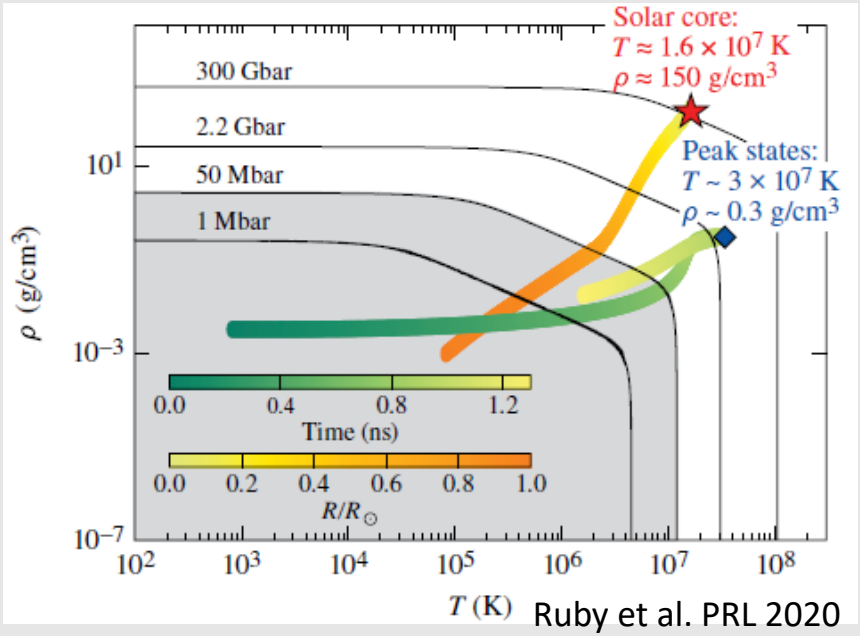

Ruby et al. PRL 2020

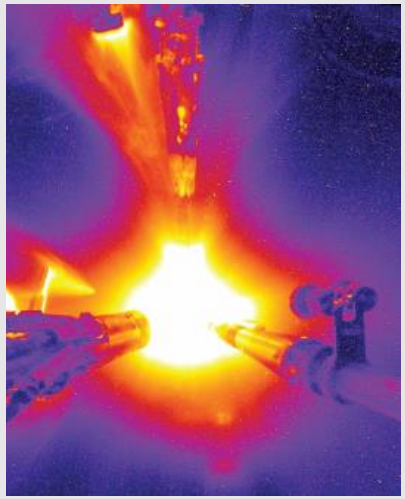
NIF expt. 2016


S. Merkel, Univ. Lille

Two methods of creation pressure:

- **Laser ablation (shock or implosion)**
- **Laser radiation pressure (reflection)**

Laser high energy facilities worldwide

There are only few lasers capable to deliver energies at a MJ scale with multiple beams of a ns pulse length

National Ignition facility operates since 2009 with maximum energy 1.9 MJ and power 450 TW

Laser MegaJoule will have energy 1.5 MJ with 176 beams (actually 300 kJ)


LMJ, CEA, 2016

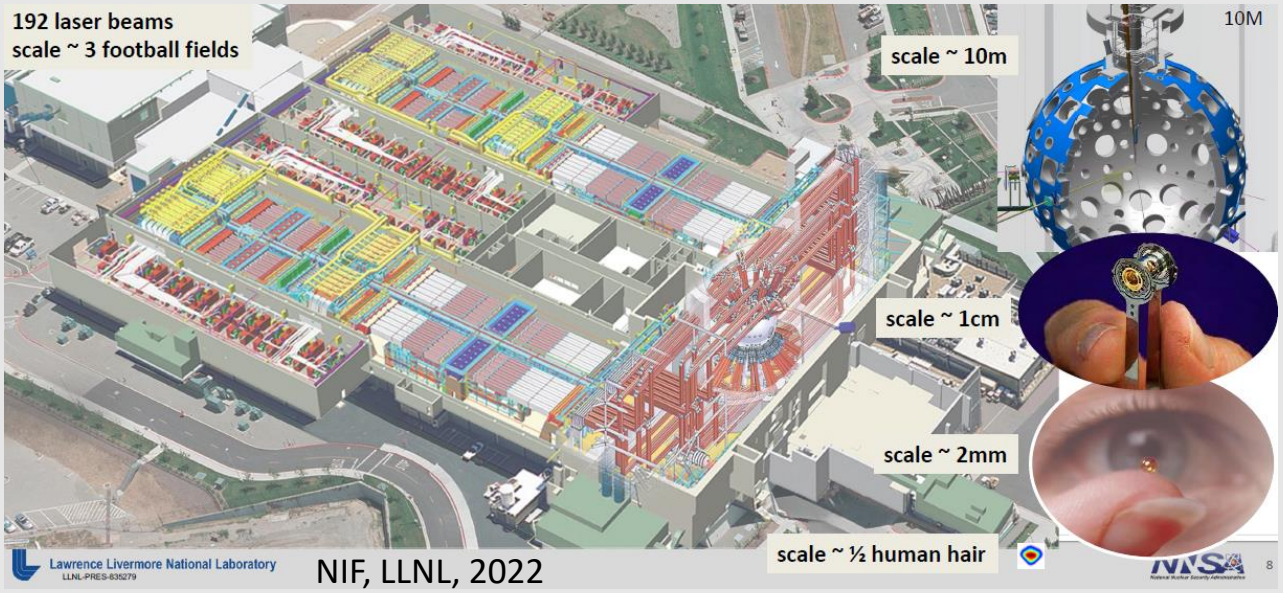

NIF, LLNL, 2022

Energy concentration in time and in space

ELI laser facilities can make significant contribution to HED science: coupling kJ and ps laser beams

Part 1:
Inertial confinement fusion

- Basic principles of energy production from fusion reactions
- Physics of inertial confinement fusion
- Recent results and inertial fusion research

Basic principles of energy production from fusion reactions

Energy production in fusion reactions

The major obstacle are elastic collisions: cross section of elastic collisions

$$\sigma_{\text{elast}} \cong (\hbar/m_r v)^2$$

is more than 4 orders of magnitude larger than the fusion reaction cross section:

$$\sigma_{\text{fus}} \cong (\hbar/m_r v)^2 \exp - \sqrt{\varepsilon_G/\varepsilon}$$

ε_G ~2 MeV - Gamov energy; for $\varepsilon = 100$ keV, $\sigma_{\text{elast}} \cong 10^{-19}$ cm², compared to $\sigma_{\text{fus DT}} \cong 3 \times 10^{-24}$ cm²

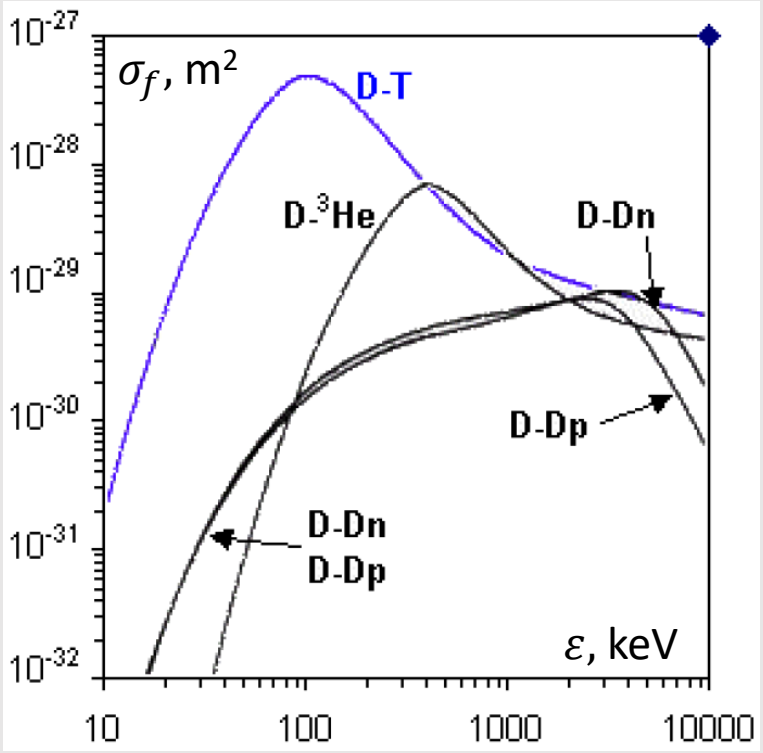

The only solution to overcome elastic collisions is to heat the fuel and to maintain it for a time sufficient for the ions to fuse: two main conditions: heating and confinement. Fusion proceeds in a near thermal equilibrium in the plasma state

The most natural process in Universe, which is extremely difficult to realize on the Earth

Lawson criterion for energy production

The life time of a hot plasma is limited: useful energy has to be produced within the energy confinement time: released fusion energy > plasma internal energy

$$E_{\mathrm{fus}} = \varepsilon_\alpha \frac{1}{4} N_i^2 \langle \sigma_{\mathrm{DT}} v \rangle t_{\mathrm{conf}} > E_{\mathrm{th}} = 3 N_i T$$

$\varepsilon_{\mathrm{DT}} \cong 17.6$ MeV
$\varepsilon_\alpha = 0.2 \varepsilon_{\mathrm{DT}} \cong 3.5$ MeV

Magnetic fusion:

$$N_i\, t_{\mathrm{conf}} > \frac{12T}{\varepsilon_\alpha \langle \sigma_{\mathrm{DT}} v \rangle}$$

minimum @ $T_{\mathrm{igDT}} \cong 12$ keV

pressure × time > 8.3 atm·s

Need for a long confinement

Inertial fusion: $t_{\mathrm{conf}} = R_{\mathrm{fuel}}/4c_s$

$$N_i\, R_{\mathrm{fuel}} > \frac{48 T c_s}{\varepsilon_\alpha \langle \sigma_{\mathrm{DT}} v \rangle}$$

areal density > 2.5 g/cm²

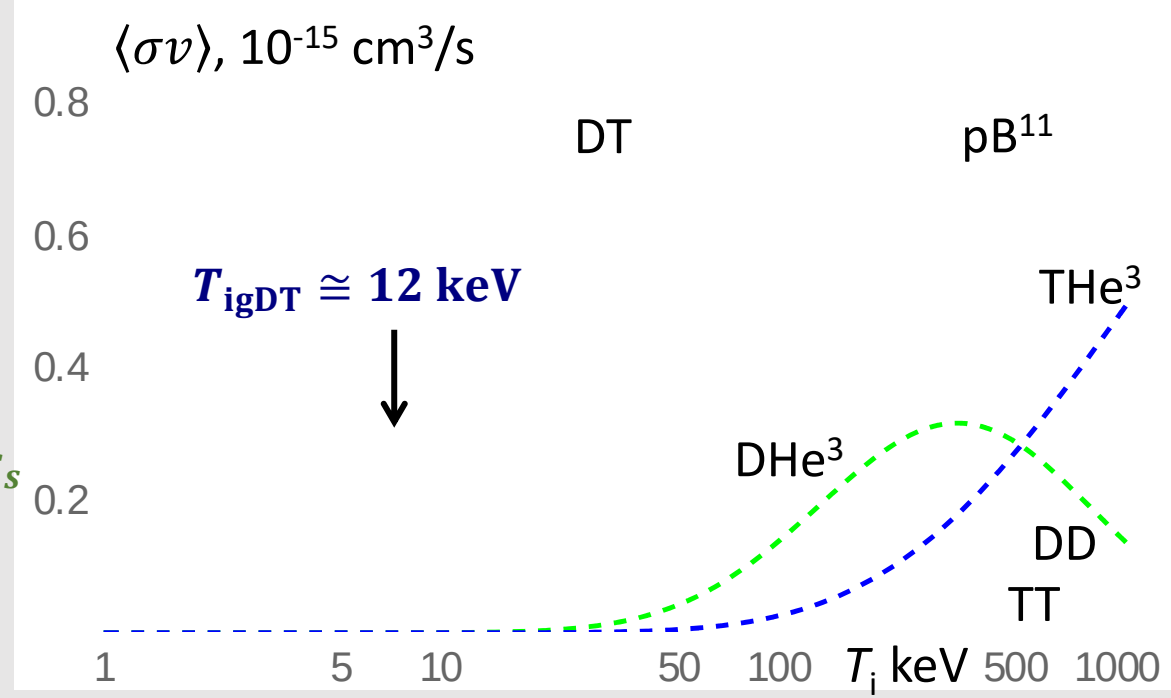

Need for a strong compression: $\rho_0 = 0.25$ g/cm³

Energy balance in fusion reactions

Fusion reactions proceed in a local thermal equilibrium at high temperatures

The intrinsic yield is defined as a ratio of the fusion energy to the fuel thermal energy

$$E_{\mathrm{fus}} = \frac{1}{2} N_i \varepsilon_{\mathrm{fus}} \qquad E_{\mathrm{th}} = \frac{3}{2}(N_i + N_e) T_{\mathrm{ig}} \qquad Y = E_{\mathrm{fus}}/E_{\mathrm{th}} \qquad T_{\mathrm{igDT}} \cong 12\ \mathrm{keV}$$

$$\varepsilon_{\mathrm{DT}} \cong 17.6\ \mathrm{MeV} \quad (\mathrm{n} + \alpha)$$

Intrinsic gain $Y_{\mathrm{DT}} \cong 300$

Disadvantages of DT:

- **Tritium**
- **neutrons**

Two other potential fuels (aneutronic):

$$Y_{\mathrm{DHe^3}} \cong 60 \quad (\mathrm{p} + \alpha)$$

$$Y_{\mathrm{pB^{11}}} \cong 5 \quad (3\alpha)$$

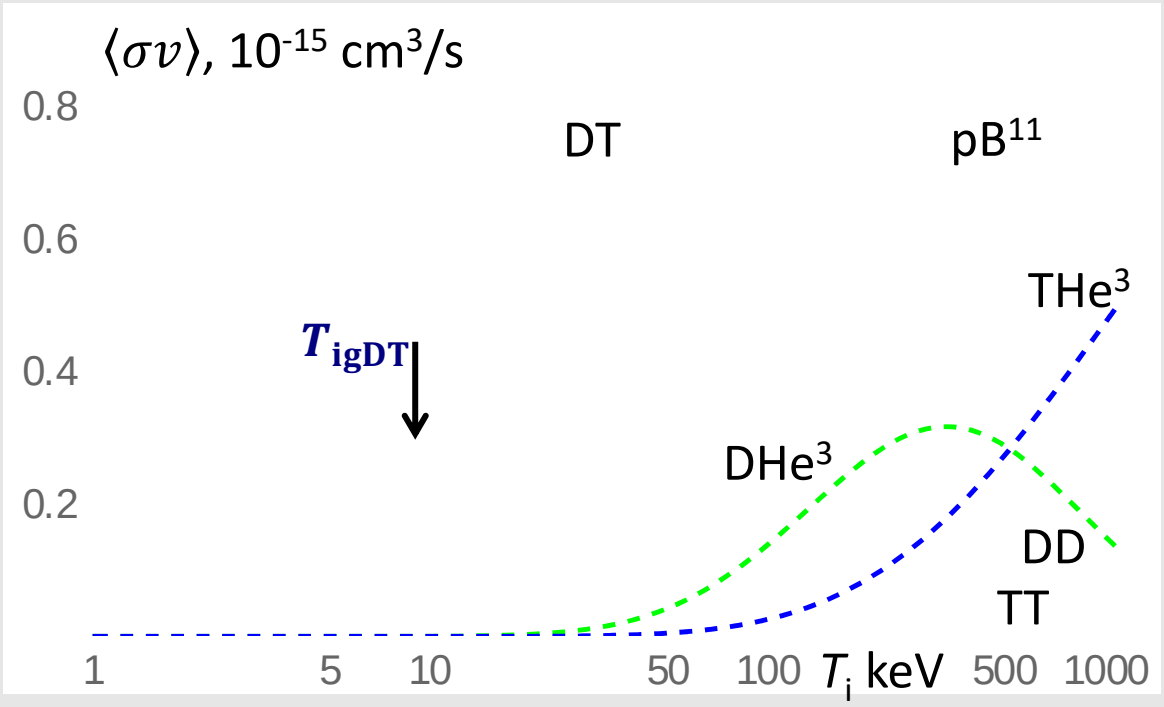

Hot spot ignition concept

If all fuel will be compressed and heated, the energy gain is limited by the intrinsic yield

It is too small to provide economically efficient fusion energy production

There are two ways to increase the fusion energy yield:

- **Continuous operation of power plant – constraint on the confinement system → low plasma density (magnetic confinement fusion)**
- **Pulsed operation – constraint on the confinement time → high plasma density (inertial confinement fusion)**

Fusion gain in the ICF scheme can be increased by the hot spot concept: this is a two-step process

- **all fuel is compressed to the density needed for an efficient fusion burn**
- **a small fraction of fuel is compressed and heated to the temperature needed for the positive yield**

Compression requires less energy then heating, so the fuel can be ignited with a smaller amount of laser energy

Alpha-particles produced in the hot spot provide additional energy for heating remaining part of the fuel to the fusion temperature

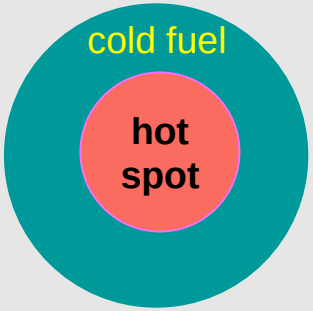

Conditions on the fusion energy production

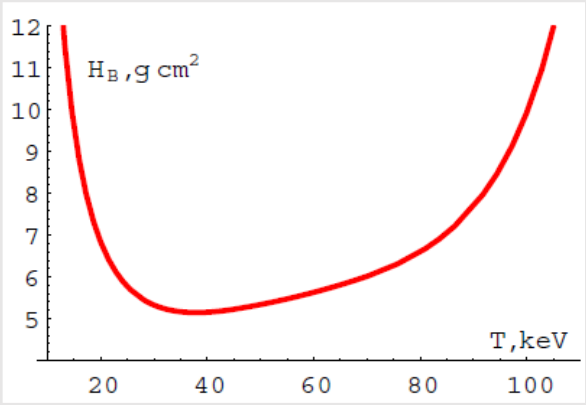

All fuel cannot be burnt in the inertial fusion scheme

- **confinement time:** $t_{\mathrm{conf}} = R_f/4c_s$
- **burn fraction**

$$\Phi_B = \frac{1}{2} n_i \langle \sigma_{\mathrm{DT}} v \rangle t_{\mathrm{conf}} \rightarrow \frac{\rho_f R_f}{H_B(T) + \rho_f R_f}$$

$H_B = 8 m_i c_s / \langle \sigma_{\mathrm{DT}} v \rangle$ **minimum value is 5.5 g/cm^2 → Fusion burn fraction of 30%:**

$$\rho_f R_f \geq 2.5 \text{ g/cm}^2$$

For a fuel mass of 1 mg (total fusion energy is 340 MJ = 80 kg TNT) and fuel density $\rho_0 = 0.25$ g/cm^3, the radius of a liquid fuel droplet R_0 =1 mm and areal density $\rho_0 R_0 = 0.025$ g/cm^2

Increase of $\rho_f R_f$ by a factor of 100 requires a compression in volume of 10^3, that is, radial compression $C_R > 10$

For $\rho_f = 500$ g/cm^3, the radius of a compressed fuel droplet $R_f = 40$ μm and confinement time ~40 ps (to compare with magnetic confinement of ~ 4 s)

Principles of ICF: implosion and ignition

Inertial confinement fusion is realized in two steps:

- **Compression of the fuel to the needed areal density**
- **Ignition of fusion reactions: confinement of alpha-particles**

Compression of fuel is achieved by laser ablation and implosion of a spherical shell

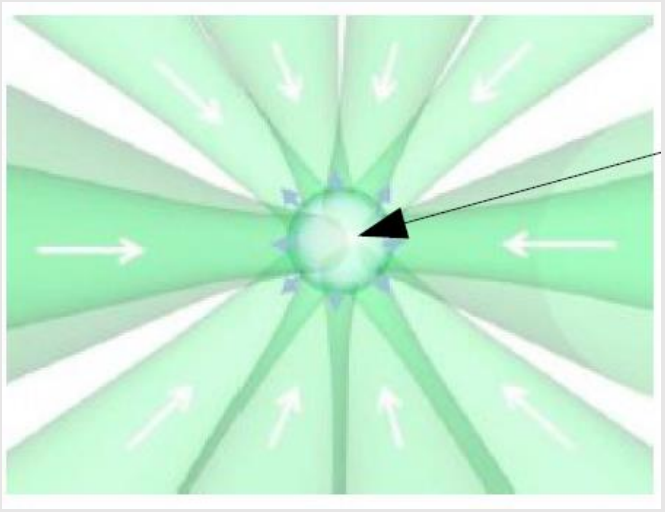

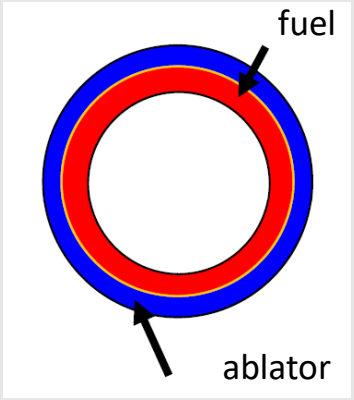

Principle of power amplification: (i) laser energy is converted into the kinetic energy of the inward moving fuel (efficiency < 10-15%, long time ~10 ns); (ii) at stagnation, kinetic energy is converted into the internal energy of collapsed fuel (efficiency < 40%)

Mainstream scheme: indirect drive

Standard ICF approach uses a single, temporally shaped laser pulse for compression and ignition. Laser energy is converted in thermal X-rays that symmetrically irradiate the pellet. Low efficiency but good symmetry.

Best result on NIF: 1.3 MJ fusion energy with 1.9 MJ laser energy delivered

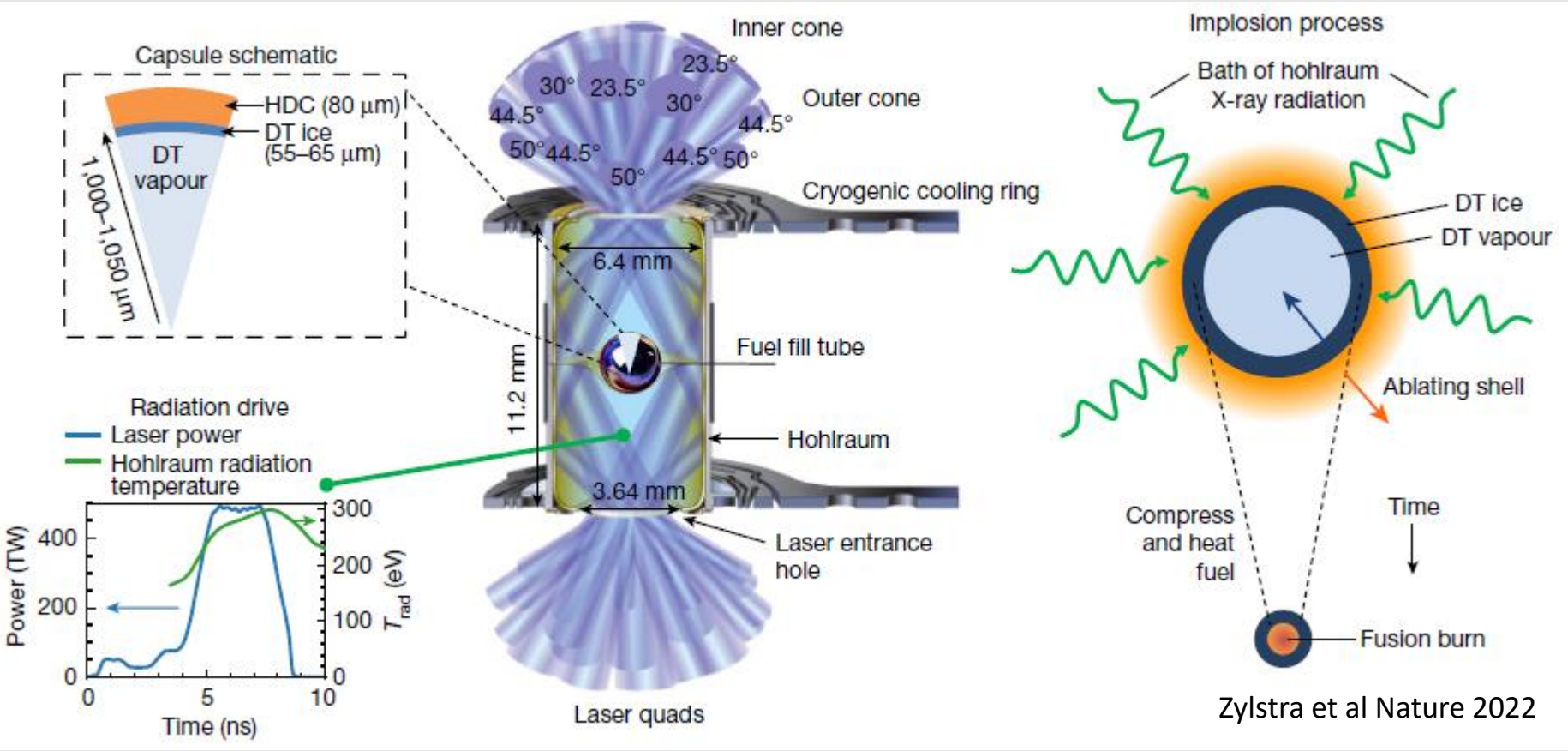

Zylstra et al Nature 2022

Mainstream scheme: direct drive

Standard ICF approach uses a single laser pulse for compression and ignition. Laser energy is delivered directly on the pellet. Much better energy coupling to hot spot but there are issues related to the laser energy deposition and implosion symmetry

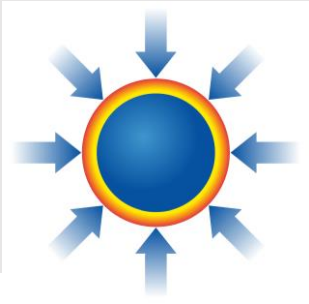

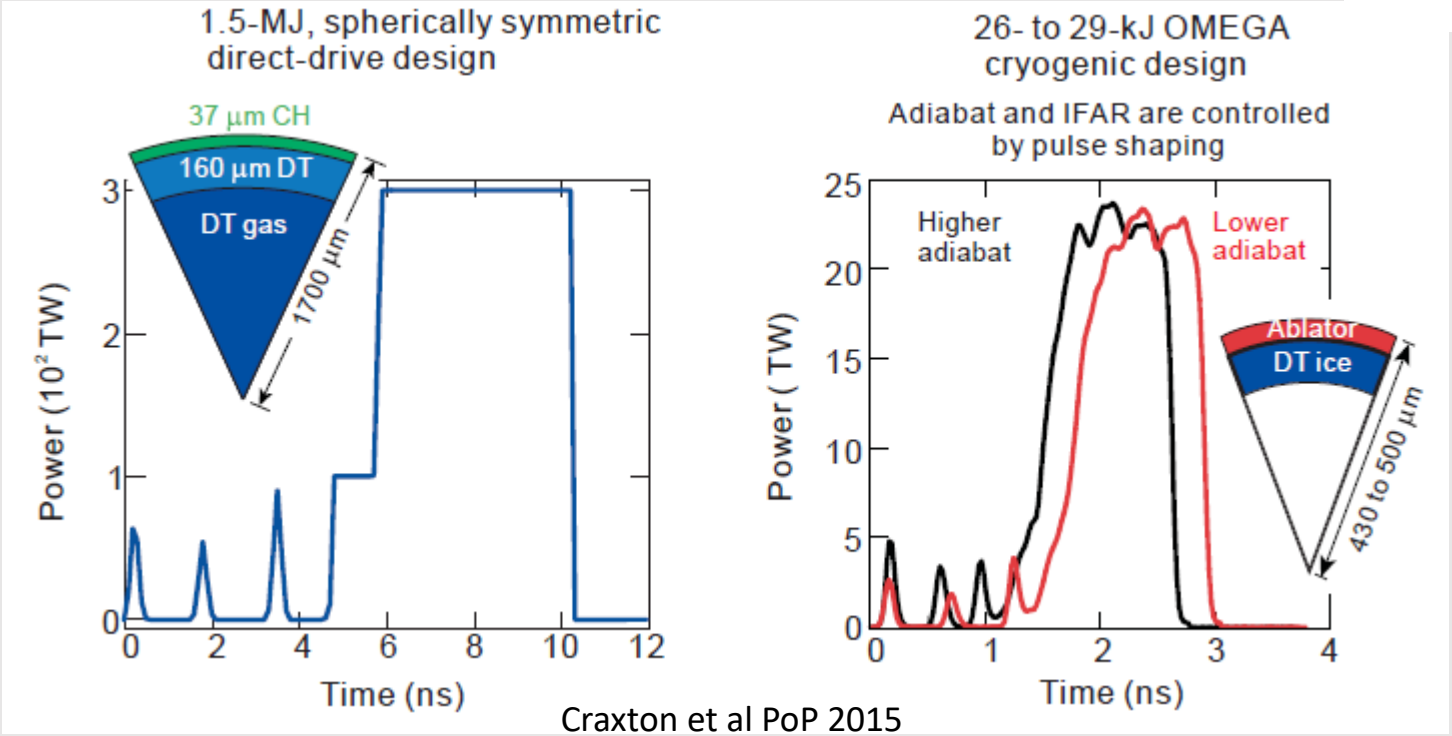

Craxton et al PoP 2015

Best result on OMEGA: hot spot energy 1.2 kJ and neutron yield 2.5e14

Alternative ignition schemes: fast ignition

Alternative schemes – fast and shock ignition – use two separate laser pulses for compression and for ignition. This allows for a better stability of implosion and lower total laser energy in exchange for higher laser power and higher laser intensity

Fast ignition uses a lower intensity main pulse for a more stable fuel compression. Ignition is achieved with a laser-driven intense beam of electrons or ions creating a hot spot off center

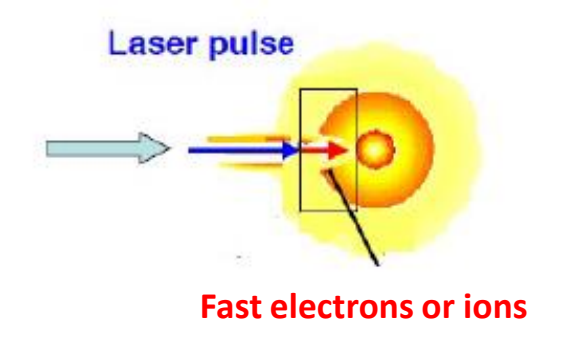

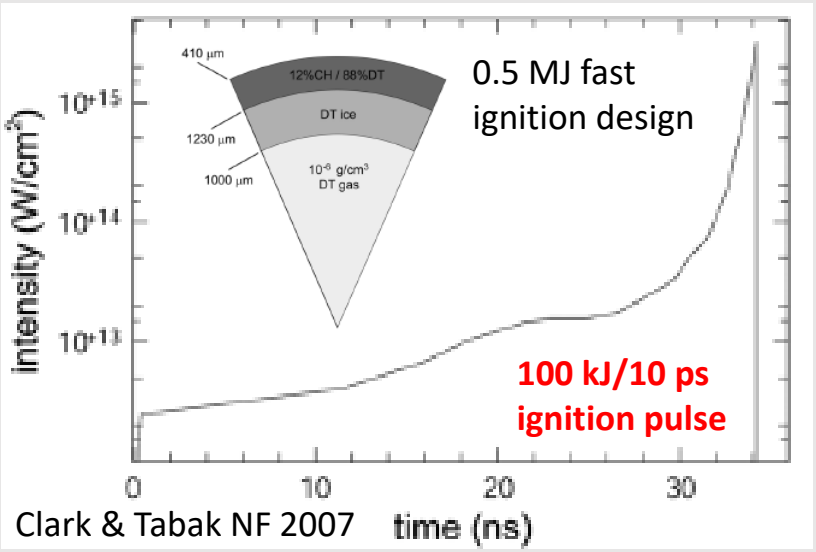

Issues:

- **The need of extremely high intensity lasers ~10 PW to drive electron or ion beams**
- **Focusing of intense beams into a small hot spot**
- **Ion FI is not yet explored experimentally**

Alternative ignition schemes: shock ignition

In shock ignition the shell is imploded at a lower velocity and the central hot spot is created by a strong convergent shock driven by a 1 ns laser spike of a high power and high intensity

0.7 MJ shock ignition design

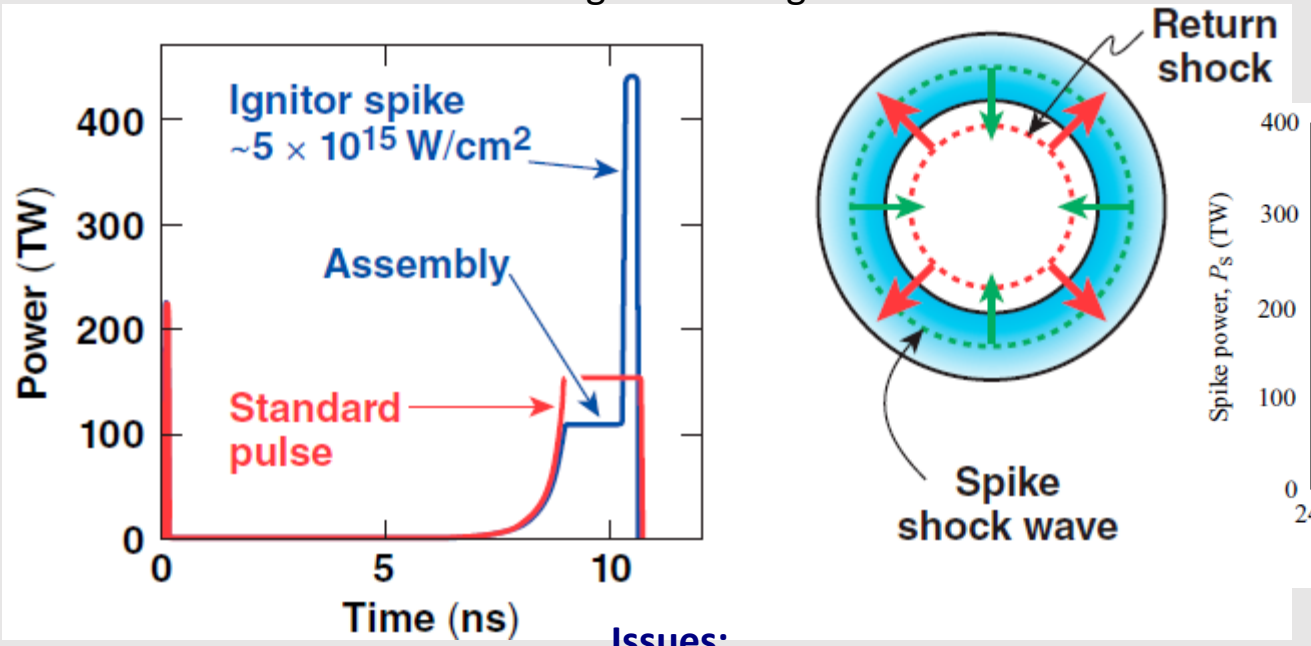

Anderson et al PoP 2013

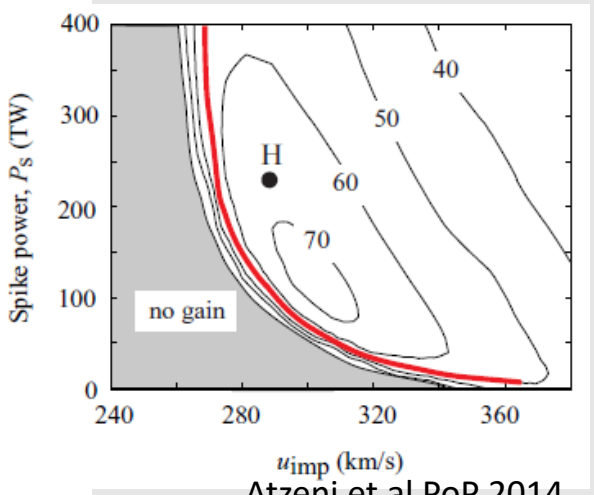

Atzeni et al PoP 2014

Issues:

- **Timing of the spike: tuning the collision time of the spike-driven and return shock**
- **Fuel preheat by the spike-driven hot electrons**
- **Ablation pressure of 300 Mbar is demonstrated**

Physics of inertial confinement fusion

Laser target implosion

Shell-like spherical target is best suited for hot spot creation: ablator-solid DT-gas DT

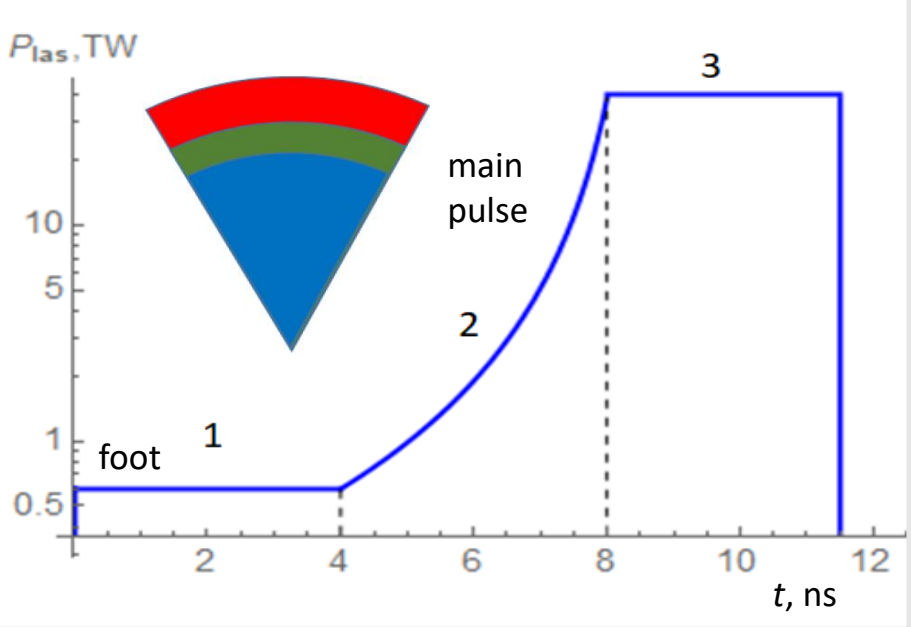

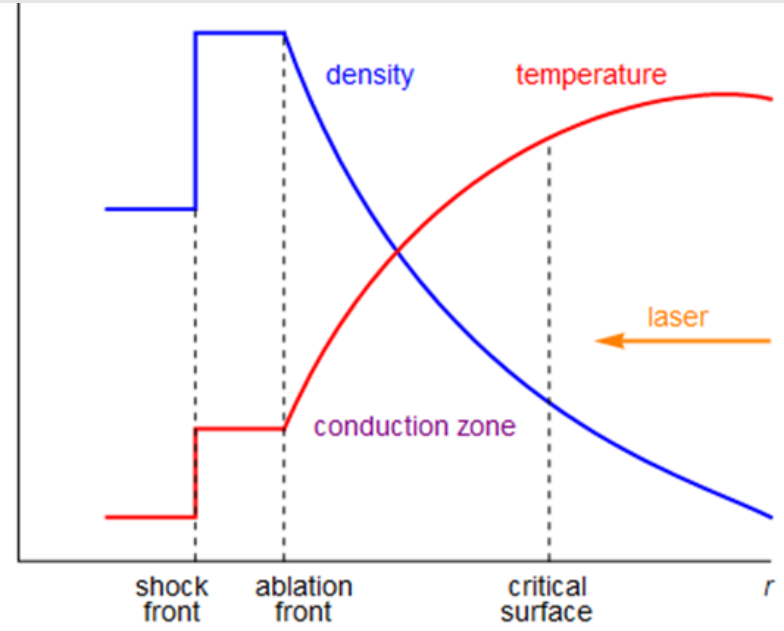

Target implosion is driven by laser assisted ablation:

- **Laser absorption at near-critical density $\rho_{cr} \cong 0.01 - 0.1$ g/cm³** $\quad I_{\text{las abs}} = 4\rho_{cr}c_s^3$
- **Electron energy transport to the ablation surface: balance with ion outflow**
- **Ablation pressure is defined by the recoil momentum**

$$p_{\text{abl}} = \rho_{cr}c_s^2 = 57\left(\frac{I_{\text{las}}}{10^{15}\ \text{W/cm2}}\right)^{2/3}\left(\frac{\lambda_{\text{las}}}{1\ \mu\text{m}}\right)^{-2/3}\ \text{Mbar}$$

Laser target implosion

Implosion proceeds in three steps:

- **shell pre-compression by a first shock,**
- **isentropic shell acceleration,**
- **free flight of the fuel: compression, stagnation and ignition**
- **at stagnation:** $P_{sh} = P_h$

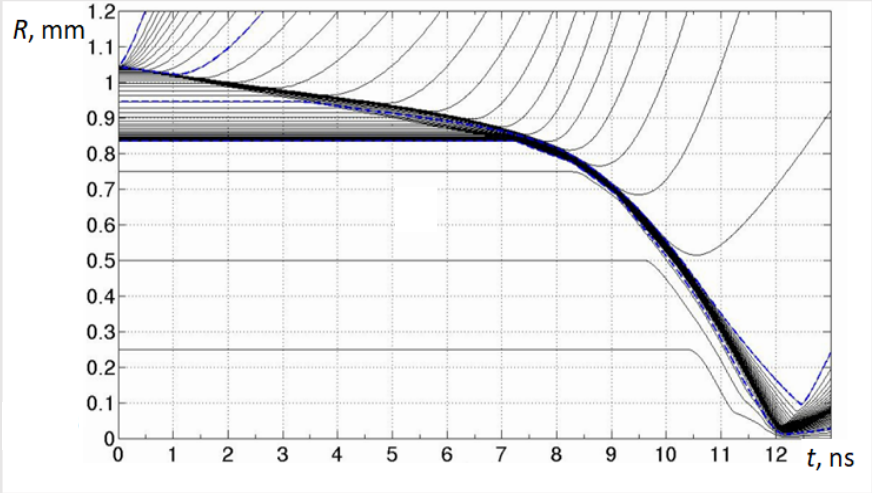

- **Shell implosion velocity is proportional to the ablation velocity:** $U_{imp} = D_{abl} A_{if}$
- **Fuel compression is proportional to the implosion velocity: shell kinetic energy is equal to the work done for shell compression:** $\frac{1}{2} M_{sh} U_{imp}^2 = 4\pi \int_{R_f}^{R_0} R^2 p_{sh}(R)\, dR$
- **Low hydrodynamic efficiency:** $\eta_{hydro} \leq 10\%$

$$C_R = R_0/R_f \cong \left(1 + M_{sh} U_{imp}^2 / 4 A_{if} E_{int}\right)^3$$

Hot spot energy balance

Energy conveyed to hot spot by implosion should overcome the radiation and thermal losses:

$$\frac{dE_h}{dt} = -\frac{4\pi}{3} P_h \frac{dV_h}{dt} + (f_\alpha W_\alpha - W_{\mathrm{br}}) V_h - q_e S_h$$

Pressure work — Alpha heating — Radiation losses — Thermal losses

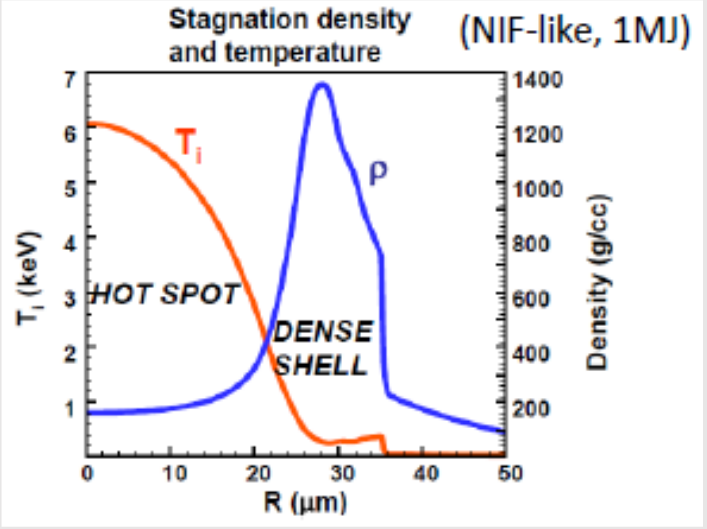

Fusion energy: $W_\alpha = 1.5 \times 10^{19} \left(\frac{n_e}{10^{25}\,\mathrm{cm}^{-3}}\right)^2 \left(\frac{T_e}{1\,\mathrm{keV}}\right)^2$ W/cm³

Radiation losses: $W_{\mathrm{br}} = 5.3 \times 10^{19} \left(\frac{n_e}{10^{25}\,\mathrm{cm}^{-3}}\right)^2 \left(\frac{T_e}{1\,\mathrm{keV}}\right)^{1/2}$ W/cm³ $\quad T_{\mathrm{min}} = 4$ keV

Thermal losses: $q_e = 0.57 \kappa_{\mathrm{SH}} T_e / R_h \propto n_e T_e^{7/2}$ dominate at high temperatures

Ignition: explosive temperature growth if alpha heating dominates: $\frac{dT_h}{dt} \propto T_h^2$

Hot spot energy balance

Standard hot spot ignition is isobaric at stagnation: ***hot spot pressure = cold shell pressure***

Alternative ignition schemes are isochoric: ***hot spot pressure > cold shell pressure***

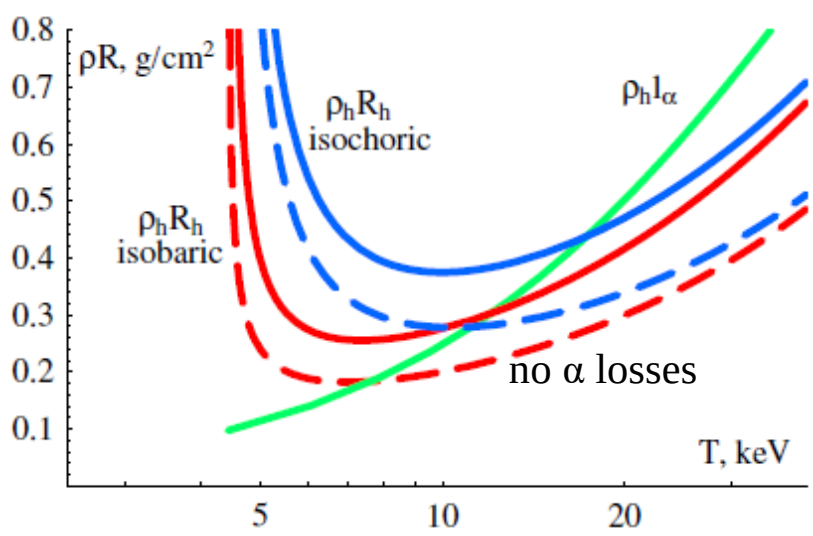

Hot spot pressure and energy at ignition conditions:

$$\rho_h R_h T_h > 0.3 \text{ g/cm}^2 \times 5 \text{ keV}$$

$$P_h > 100 \left(\frac{R_h}{100\ \mu\text{m}}\right)^{-1} \text{Gbar}$$

$$E_h \propto P_h R_h^3 > 5.2 \left(\frac{\rho_h}{100\ \text{g/cm3}}\right)^{-2} \text{kJ}$$

$$P_h > 250 \left(\frac{E_h}{10\ \text{kJ}}\right)^{-1/2} \text{kJ}$$

Direct drive scheme has larger energy coupling efficiency: 3-4 times more energy can be deposited in the hot spot for the same laser energy

Alternative ignition schemes require higher areal density and/or higher temperature in order to compensate mechanical work

Comparison direct vs indirect drive

Direct drive scheme has larger energy coupling efficiency: 3-4 times more energy can be deposited in the hot spot for the same laser energy

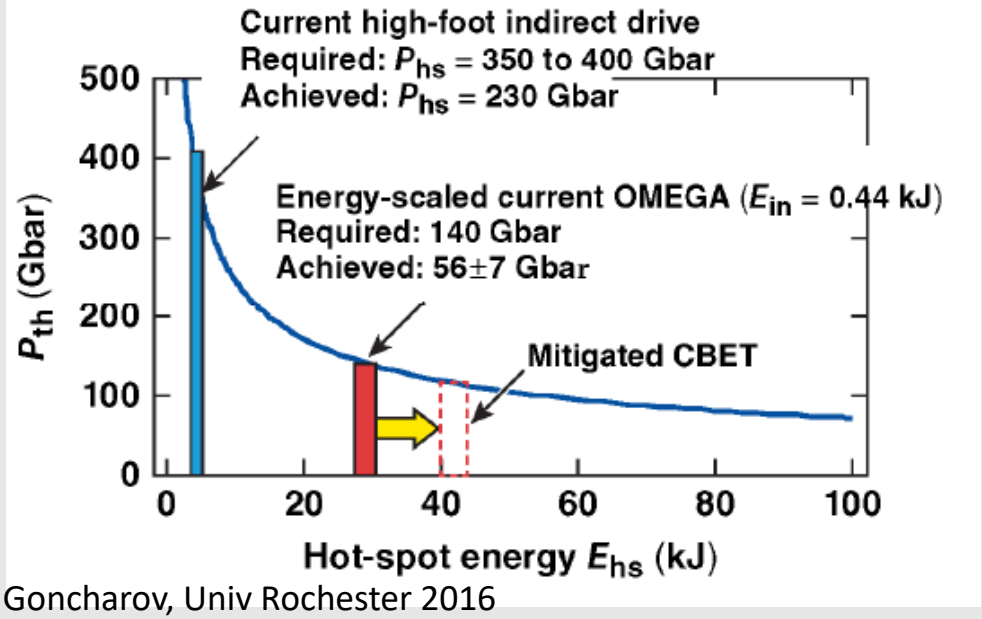

Goncharov, Univ Rochester 2016

$$P_h > 250 \left(\frac{E_h}{10\ \text{kJ}}\right)^{-1/2} \text{Gbar}$$

Fusion yield is proportional to the ignition parameter

$$\bar{P}_h = \frac{P_h}{250\ \text{Gbar}} \sqrt{\frac{E_h}{10\ \text{kJ}}}$$

Direct drive ignition requires shell compression $C > 22$ and hot spot pressure 120 Gbar

Indirect drive ignition requires compression $C > 30$ and pressure > 350 Gbar

Three-dimensional effects: degradation of 1D performance

Implosion of a thin solid shell is intrinsically unstable process. Two undesirable effects: shell breakout and mixing of hot and cold material.

Two sources of initial perturbations:

- **large scale perturbations (target positioning, target defects, tent, filling tube, laser imbalance – low modes)**
- **small scale perturbations (laser beam intensity modulations and small-scale target defects – high modes)**

Large progress is achieved in controlling the low modes: improved target design, more efficient ablators, thinner tent, better laser beam focusing precision and reduction of time jitter

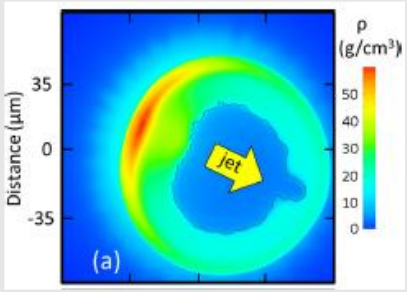

Igumenshchev et al PoP 2017

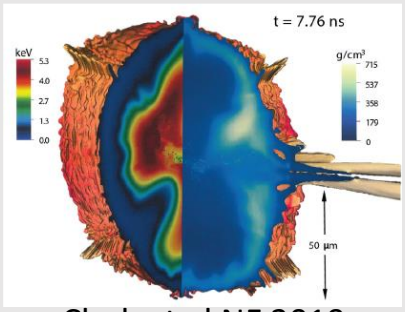

Clark et al NF 2019

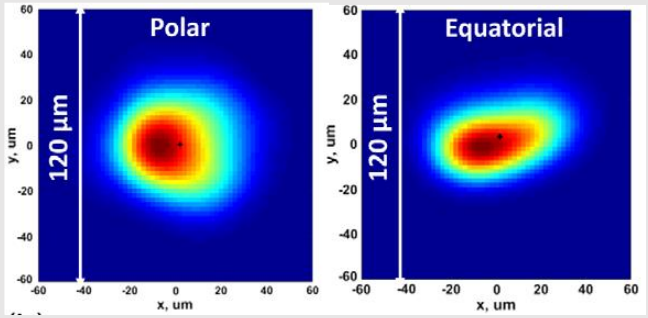

Le Pape et al PRL 2018

Neutron imaging

Hydrodynamic instability: perturbation of shell thickness

Shell perturbations are unstable during the acceleration phase (outer surface) and deceleration phase (inner surface):

Richtmyer-Meshkov instability: oscillations of the ablation surface induced by a corrugated shock front

$$\omega_{RM} \cong k\sqrt{D_{\mathrm{abl}} c_s} \qquad \delta v \cong k\xi_0 D_{\mathrm{shock}}$$

Large-amplitude oscillations seed a RT instability at the acceleration phase

Rayleigh-Taylor instability: exponential temporal growth rate under acceleration:

- **classical RT instability – strong growth**

$$\gamma_{\mathrm{RT}} \cong \alpha\sqrt{kg}$$

- **ablative stabilization: laser heating and mass flow provide a significant reduction of the RT gain**

$$\gamma_{\mathrm{RT}} \cong \alpha\sqrt{\frac{kg}{1+kl_c}} - \beta k D_{\mathrm{abl}}$$

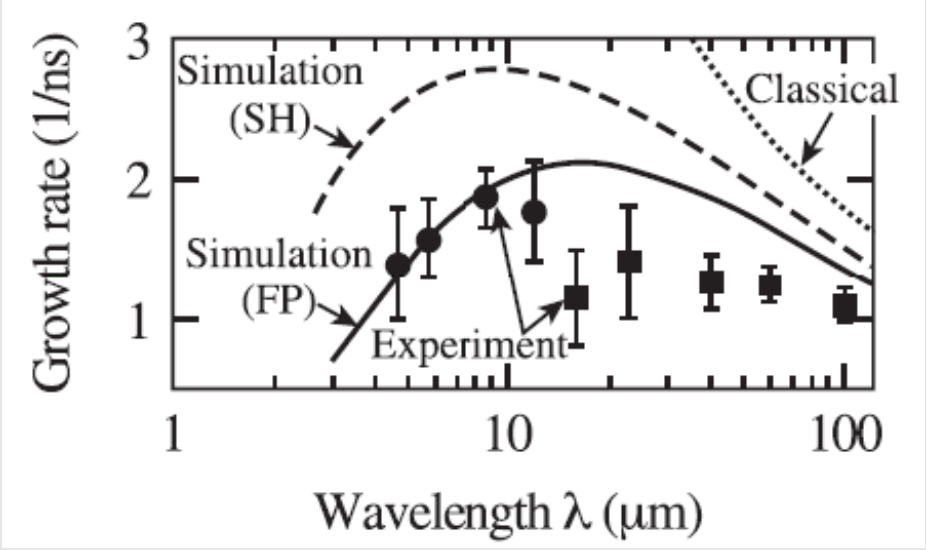

Sakaiya et al PRL 2002

The most dangerous mode $k\,\delta R \sim 1$ corresponds to exponential gain $\sim\sqrt{A_{\mathrm{if}}}$

Hydrodynamic instability at the inner shell surface

Rayleigh-Taylor instability is also excited at the inner shell surface just before stagnation – strong deceleration, fast instability growth

- **outer perturbations penetrate through the shell and seed the instability**
- **Electron heat flux from the hot spot stabilizes growth of high modes**

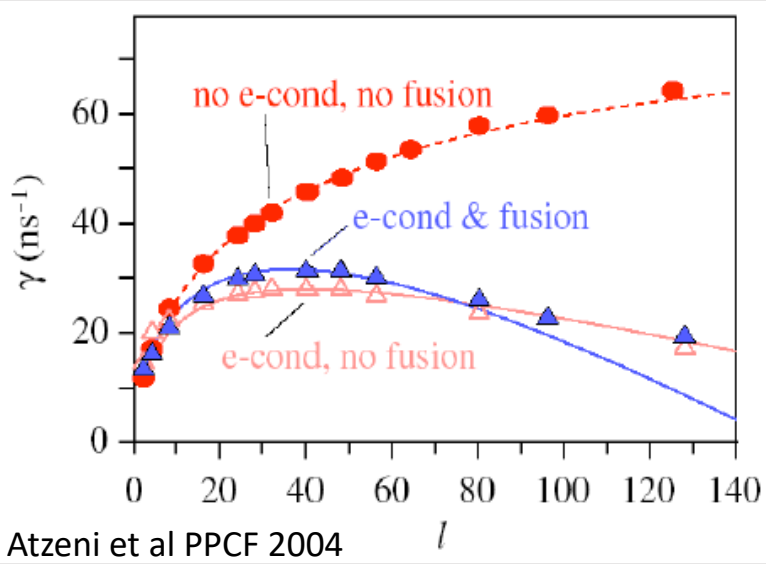

Atzeni et al PPCF 2004

Inner Rayleigh-Taylor instability reduces the effective radius and temperature of hot spot and thus compromises the ignition conditions

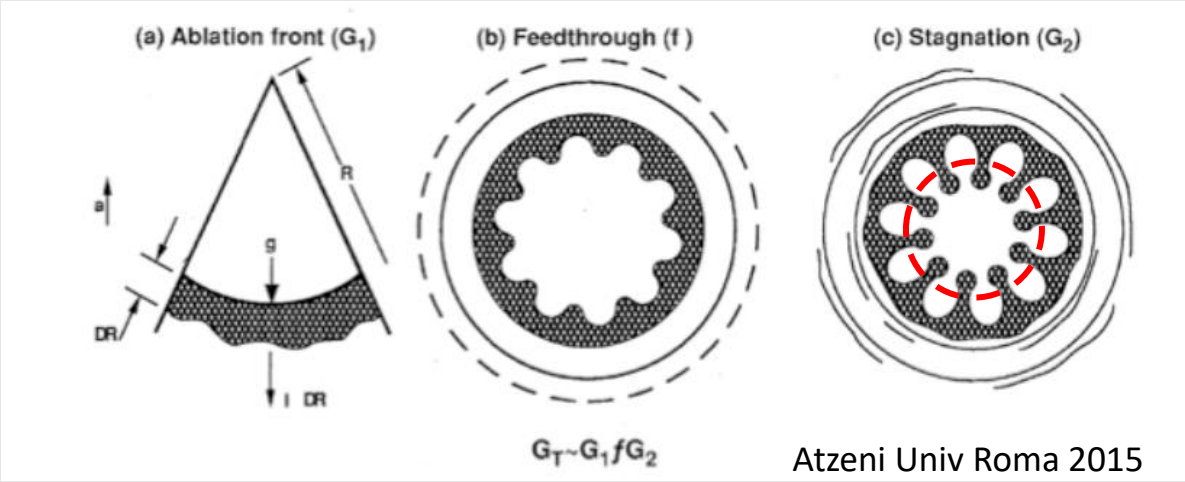

Atzeni Univ Roma 2015

Laser beam smoothing techniques

Laser imprint: intrinsic laser beam intensity modulations present the major source of density perturbations in the direct drive scheme

Amplification of perturbations by shell convergence

$$\delta R_0/R_c = C_R\,\delta R_0/R_0 \ll 1 \quad \rightarrow \quad \delta I_{\rm las}/I_{\rm las} \ll 1/C_{\rm R} \sim \text{a few \%}$$

Methods of suppression of laser-driven perturbations:

- **Laser piquet – a short prepulse vaporizing a thin layer of ablator and creating a plasma that smoothens pressure perturbations by the lateral heat transport**
- **Laser beam smoothing in spatial domain (random phase plates or continuous phase plate)**
- **Laser beam smoothing in temporal domain (spectral broadening and dispersion)**

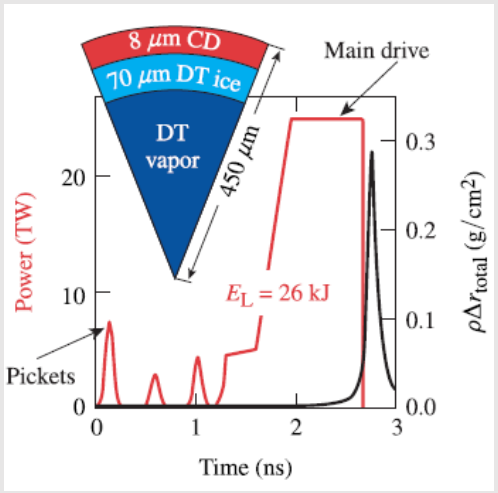

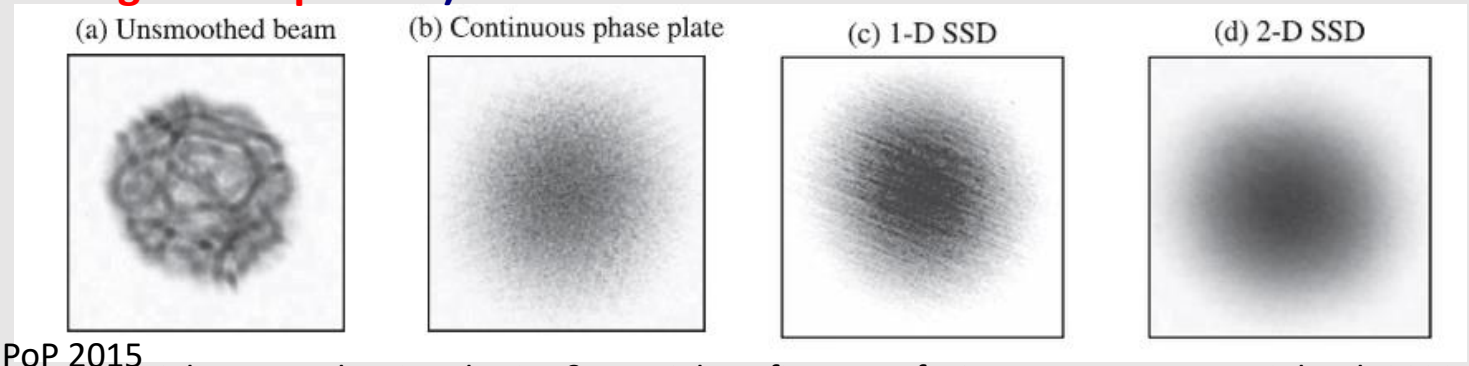

Craxton et al PoP 2015

Electromagnetic instabilities

Laser intensities needed to drive a 100 Mbar pressures are in the range of 10^{15} W/cm^2 Instabilities related to excitation of plasma waves degrade the efficiency and quality of laser absorption (typically 60-70%):

- **Filamentation deteriorate the homogeneity of laser energy deposition and facilitate excitation of secondary instabilities**
- **Stimulated Brillouin and Raman instabilities reflect the laser light and reduce absorption**
- **Stimulated Raman, resonance absorption and two plasmon instability generate supra-thermal electrons which penetrate in the core and may prematurely preheat the fuel**

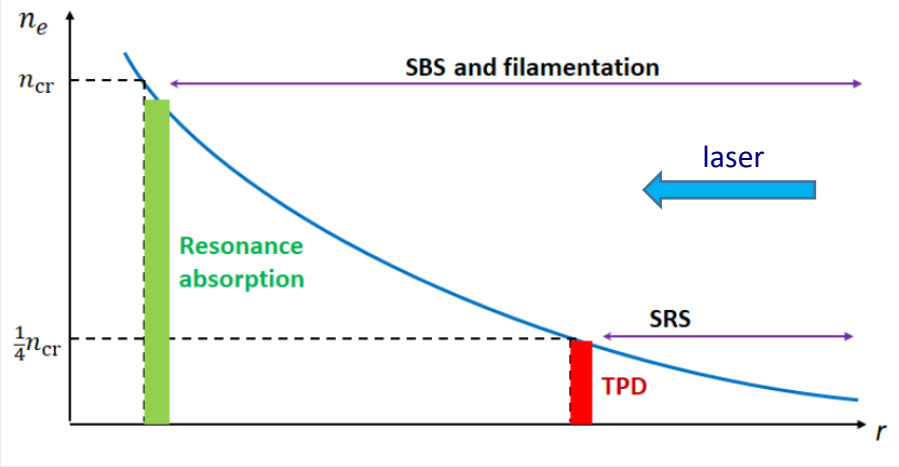

These instabilities can be partially mitigated by laser beam smoothing techniques: spatial smoothing and spectrum broadening

Cross beam energy transfer (CBET)

A homogeneous laser irradiation of the target requires overlapping of many laser beams on the target surface. The beams, however, may interact in a plasma exchange their energy. Cross beam energy transfer deteriorates the homogeneity of laser energy deposition and reduces absorption and ablation pressure up to 40% in the direct drive experiments

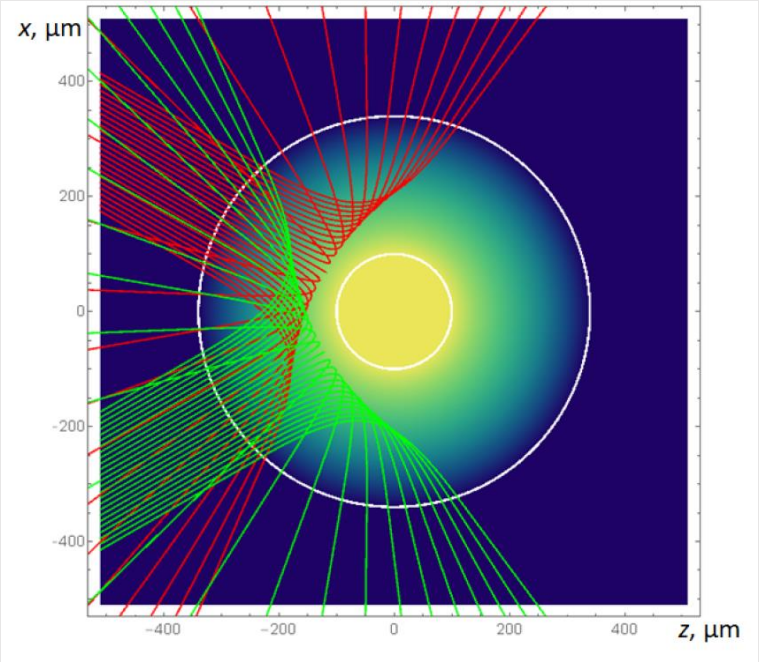

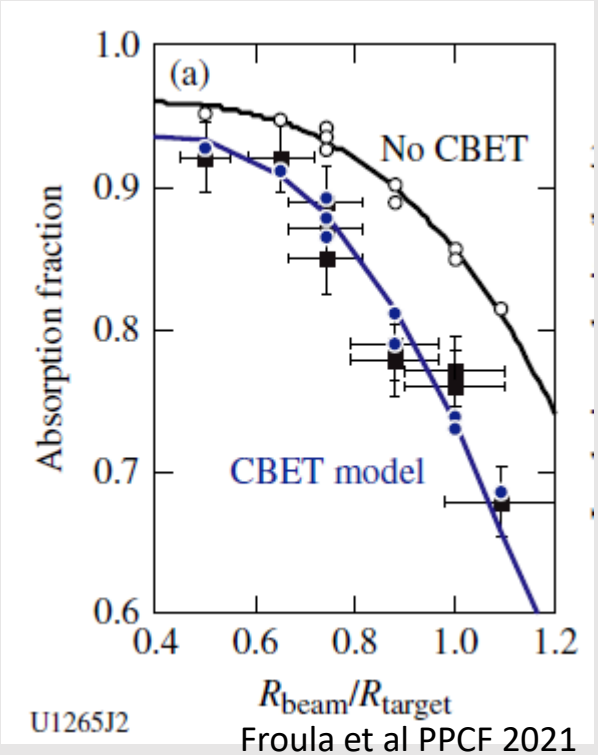

Froula et al PPCF 2021

CBET is a process of resonant interaction of two laser waves with a Doppler shifted ion acoustic wave

$$\Delta\omega - \Delta\boldsymbol{k}\cdot\boldsymbol{u} = |\Delta\boldsymbol{k}|c_s$$

Outgoing – downshifted (in the plasma frame) wave takes energy from incoming (upshifted) laser wave

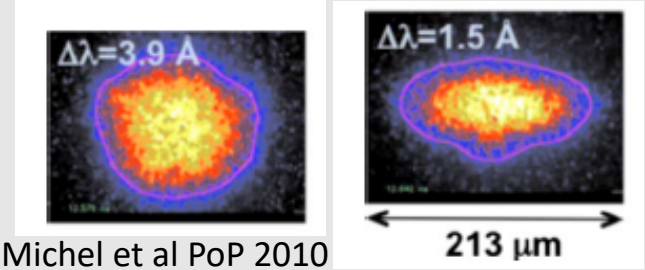

Michel et al PoP 2010

Use of CBET in NIF experiment for compensation of SRS and improving implosion symmetry

Recent results from inertial confinement fusion

Direct drive inertial fusion: USA Omega

Direct drive scheme offers an efficient use of laser energy, but it is sensitive to hydrodynamic and electromagnetic instabilities

Omega laser facility is dedicated to the direct drive experiments: 30 kJ/60 beams at the LLE, University of Rochester; high laser beam quality: RPP, PS and 2D SSD

Neutron yield increase was demonstrated in 2019 in an Optimization Campaign, where implosion design was guided by statistical methods:

1) **First set of 15 experiments was guided by 1D simulations corrected by the training data from the previous experimental campaigns**
2) **Data from these experiments were used for optimization of target design and improved scaling laws for yield and areal density**
3) **Second series experiments guided by the scaling laws produced a record yield and high areal density**

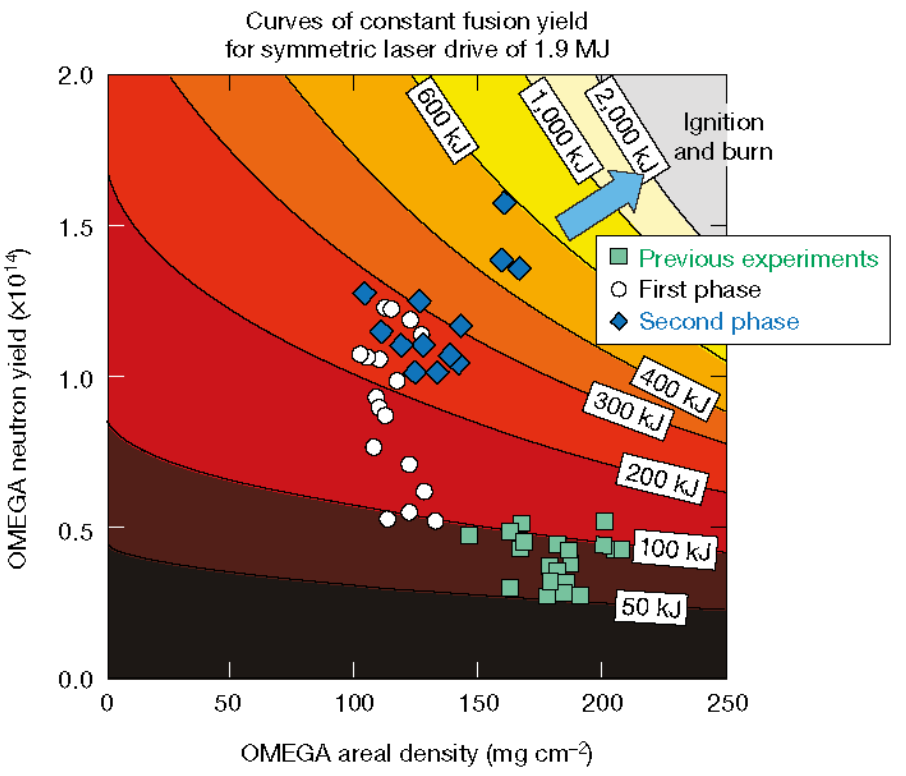

V Gopalaswamy et al. Nature 2019

Direct drive inertial fusion: USA Omega

Direct drive scheme offers an efficient use of laser energy, but it is sensitive to hydrodynamic and electromagnetic instabilities

Omega laser facility is dedicated to the direct drive experiments: 30 kJ/60 beams at the LLE, University of Rochester; high laser beam quality: RPP, PS and 2D SSD

Neutron yield increase was demonstrated in 2019 in an Optimization Campaign, where implosion design was guided by statistical methods

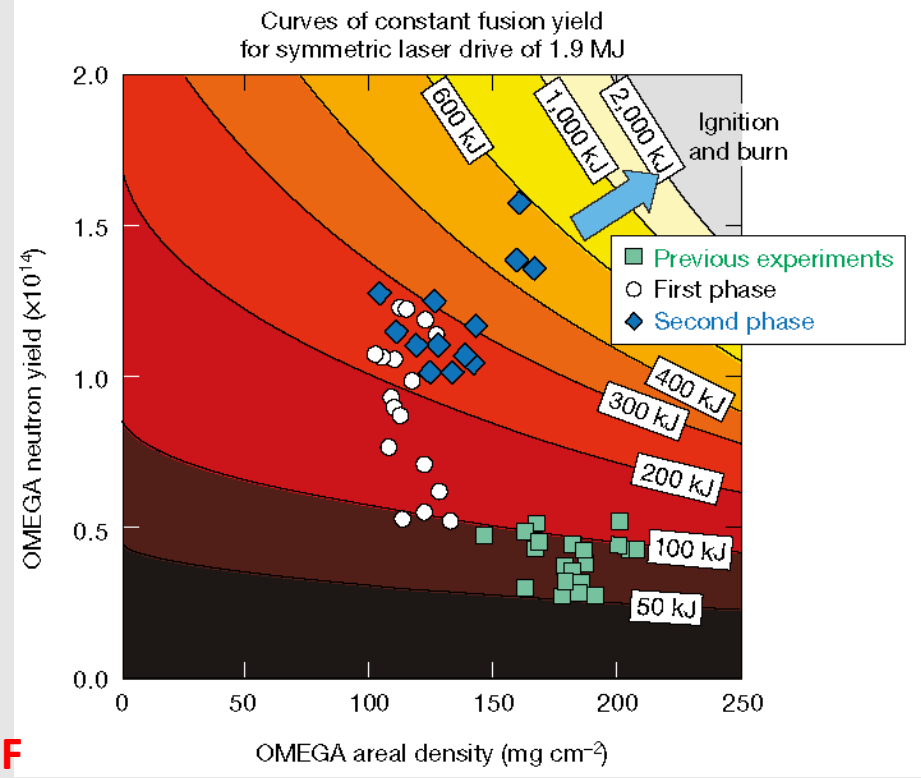

V Gopalaswamy et al. Nature 2019

Hydrodynamic scaling from Omega to NIF:

Factor 60: from 30 kJ to 1.8 MJ

Same performance implies

$$I_{las} = \text{const}, \alpha_{if} = \text{const}, v_{imp} = \text{const}$$

$$M_{fuel} \propto E_{las}, \quad R_{target} \propto E_{las}^{1/3}, \quad t_{imp} \propto E_{las}^{1/3}$$

$E_{las}^{1/3} \cong 4\times$ higher efficiency is expected at NIF in the direct drive implosions

Recent progress in inertial fusion: USA NIF (1)

USA operates NIF laser facility since 2009: 1.9 MJ/192 beams in indirect drive configuration

- **Stockpile stewardship**
- **Indirect drive ICF**
- **Direct drive experiments**
- **High energy density physics**

Indirect drive ICF: a significant progress has been achieved over the period 2011-2021: 3000 implosion experiments in 10 years

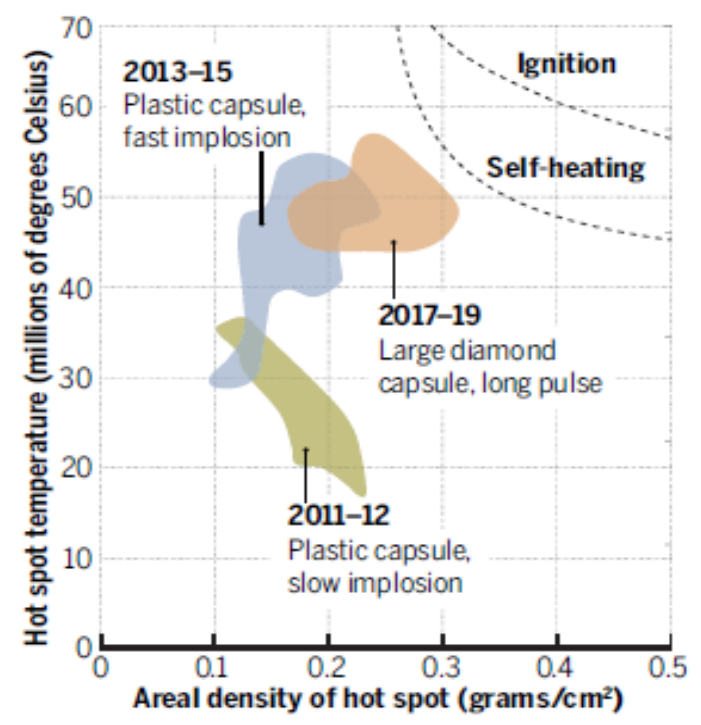

Hermann Science 2020

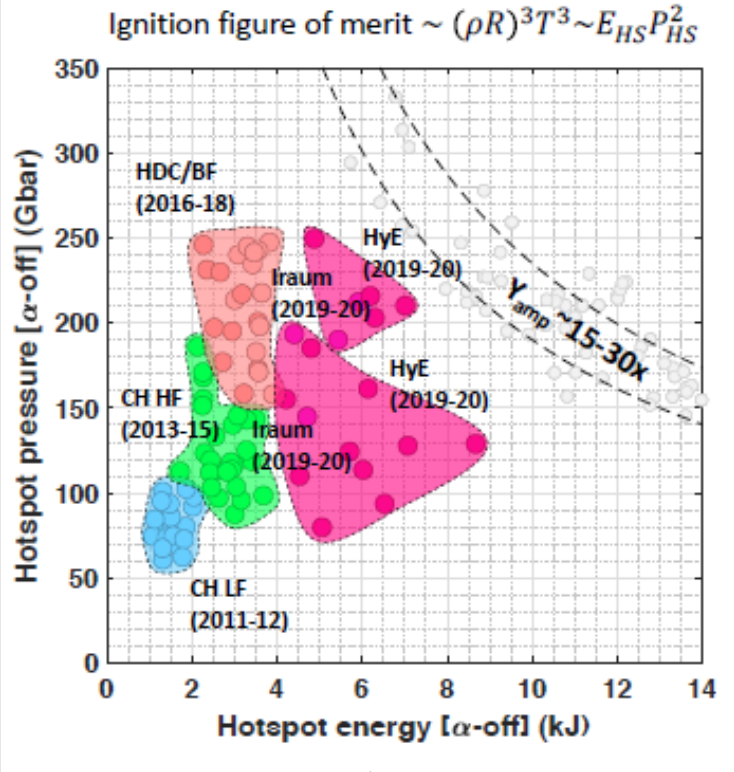

Zylstra, LLNL 2022

Recent progress in inertial fusion: USA NIF (2)

1) LF – original design 2010-12: low adiabat 1.6, long pulse, high density gas fill, slow implosion: failure, max yield 2.5 kJ: low mode asymmetry, tent, RT instability, mixing
2) HF – high foot 2013-15, med adiabat 2.8, high gas fill: max yield 25 kJ: RTI and low mode asymmetry; HDC-VAC – plastic ablator is replaced a diamond shell, no gas fill
3) Since 2016: HDC low gas fill, Be ablator, adiabat shaping, hot spot energy 7 kJ, max yield 56 kJ: improved symmetry and more stable implosion, mixing due to fill tube
4) Since 2019: HYBRID design: larger HDC capsule, 5 µm fill tube, reduced hohlraum size (dep U, gold lined), increase of x-ray coupling, reduced adiabat <2.0, control of asymmetry with CBET, increased ablation velocity > 400 km/s

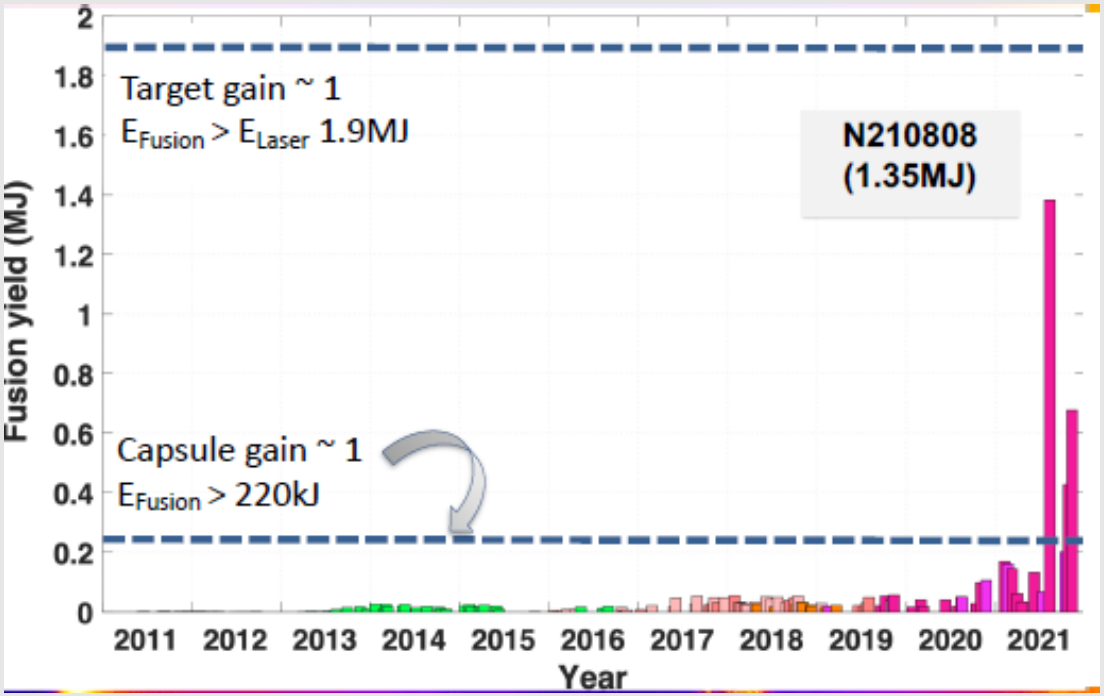

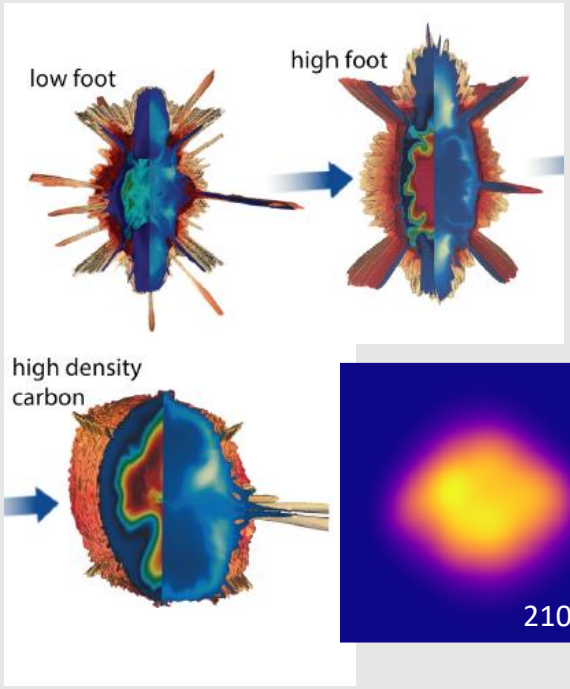

Recent progress in inertial fusion: USA NIF (3)

HYBRID-E campaign the most successful, for the first time, it is provided conditions for the regime of burning plasma: 7 expts in 2020-21 with the yield 100-170 kJ: HS gain >12

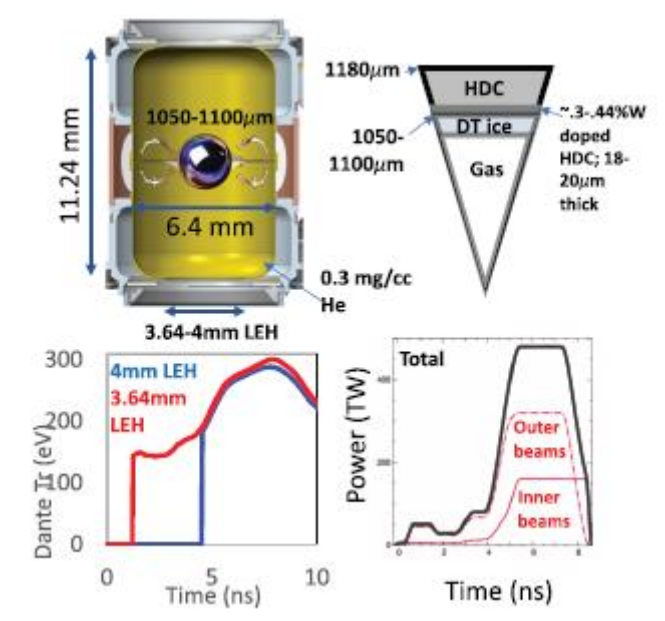

Kritcher et al PoP 2021

- Larger capsule
- Smaller hohlraum
- CBET control
- Smaller LEH
- Larger DT mass
- Low gas fill 0.3 mg/cc
- Suppressed SBS and HE
- Tungsten preheat shield
- 3-shock pulse shape
- 95% shell ablated: 400 km/s
- Max laser capability: 480 TW
- Capsule kin energy > 200 kJ
- Hot spot energy > 10 kJ

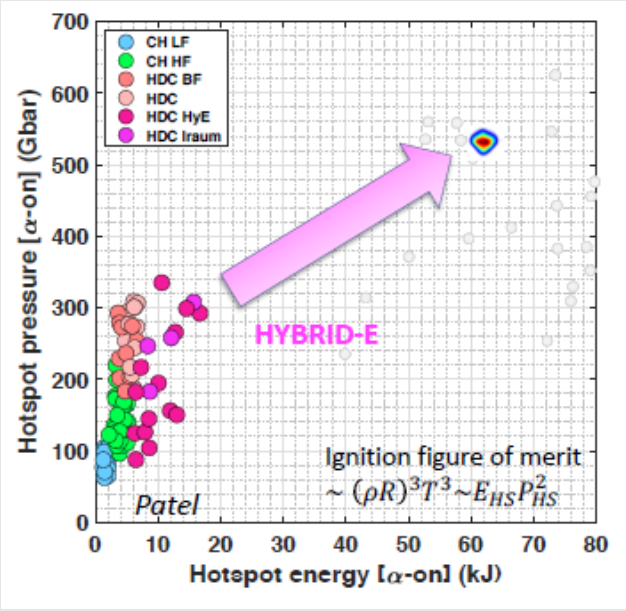

Zylstra, LLNL 2022

Issues and problems:

- Robustness & reproducibility
- Low mode asymmetries
- Hydro instabilities
- Quality of HDC shell (voids)
- Compressibility of the fuel
- Laser beam energy balance

Quest for strong shock generation

Experiments on OMEGA and LMJ at $\sim 3 \times 10^{15}$ W/cm² @ 3ω attempted to achieve shock pressures needed for shock ignition

- **LMJ planar geometry: maximum pressure 110 Mbar, observation of the hot electron preheat**
- **OMEGA spherical geometry: high shock pressure > 300 Mbar**

Omega experiment: 22 kJ/60 beams: shock pressure boosted to 300 Mbar by hot electrons

LMJ experiment: 20 kJ, 3 quads: low energy of hot electrons ~ 10 keV, correlation with SRS

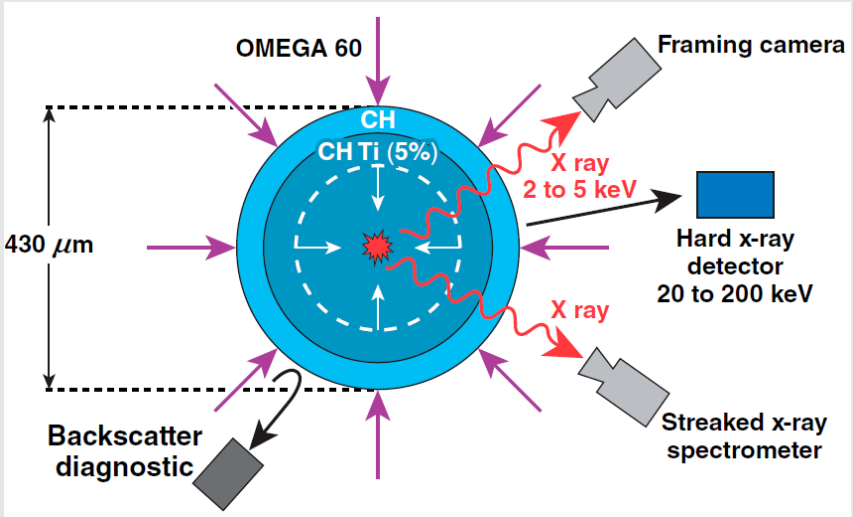

Nora et al, PRL 2015
Llor Aisa et al PoP 2017

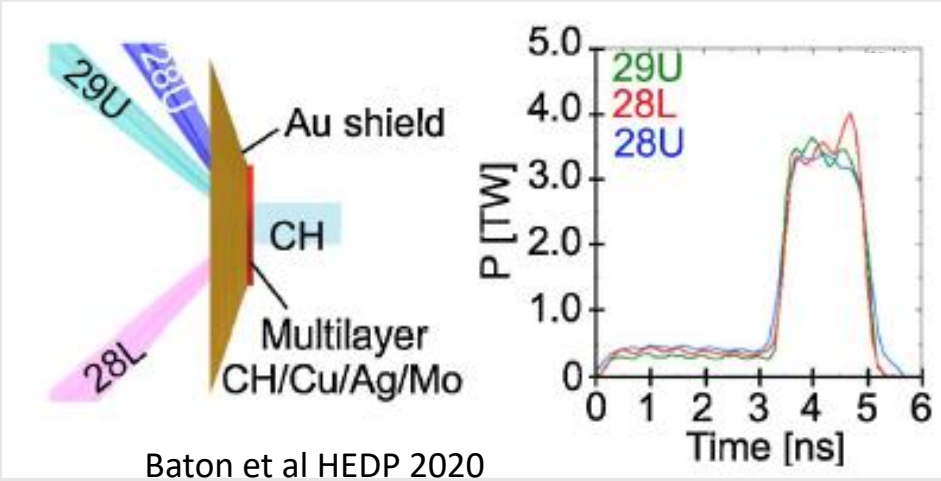

Baton et al HEDP 2020

European approach to inertial fusion:

Academic research in Europe is oriented towards energy production, clear separation from the defense, international collaboration with USA and Japan

Europe does not have its own academic laser installation permitting integrated experiments

First ICF international project HiPER 2007 – 2013: 26 laboratories from 10 countries
EuroFusion support – "keep in touch" projects:

- **Building ICF community**
- **Focusing on realistic ignition scheme: direct drive shock ignition**
- **Experiments on European laser (kJ scale) facilities PALS, LULI, VULCAN, ELI: planar geometry**
- **Implosion experiments on OMEGA: demonstration of a record shock pressure exceeding 300 Mbar**
- **LMJ is under construction – first implosion indirect drive experiments are planned in 2022-2023 campaign**
- **Theory and code developments: 3D simulations, physics of laser plasma interactions, hot electron generation and transport**
- **Demonstration of a high rep rate operation for LPI experiments on ELI L4n**

End of ICF section

Part 2:
High energy density laboratory astrophysics

- **Static experiments: equations of state, opacities, atomic physics, nuclear reactions – realistic conditions**
- **Dynamical experiments: similarity – hydrodynamic scaling**
- **Collisionless shocks and particle acceleration – reproducing similar physics but at different conditions**

Static experiments: equations of state, opacities, atomic physics, nuclear reactions – *realistic conditions*

Equations of state: $P(\rho, T)$

High energy lasers are unique tool for assessment material properties at extreme conditions

- **ICF: DT fuel at ignition conditions - compressibility**
- **Planetary science: formation, evolution and structure of planets**
- **Star formation and evolution**

Experimental approach: matter compression by a strong shock or a sequence of shocks in planar or spherical geometry

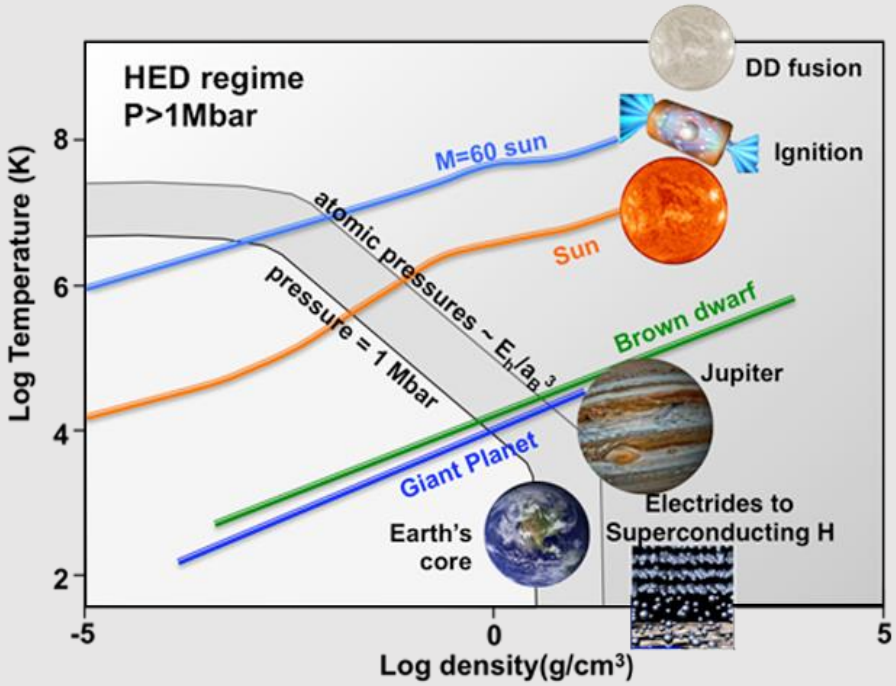

$$P_{\text{abl}} = 57 \left(\frac{I_{\text{las}}}{10^{15}\ \text{W/cm2}} \right)^{2/3} \left(\frac{\lambda_{\text{las}}}{1\ \mu\text{m}} \right)^{-2/3} \text{Mbar}$$

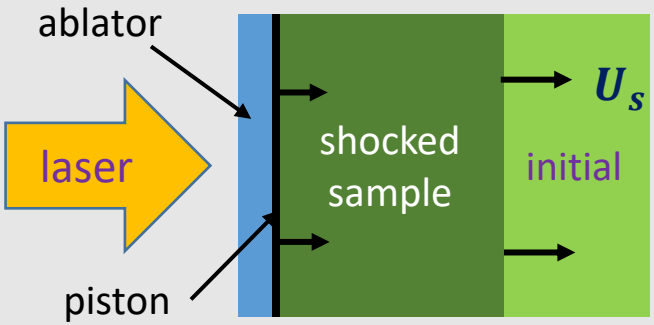

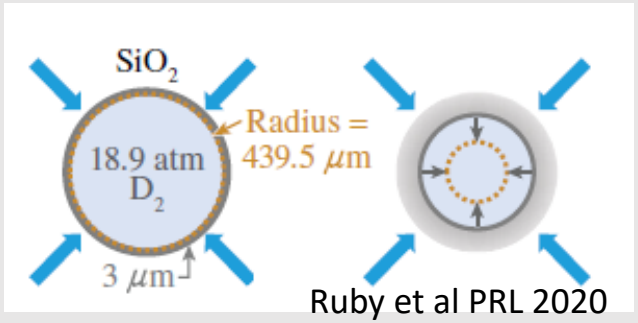

Ruby et al PRL 2020

How to measure EoS in dynamic experiments

Static experiment (Diamond Anvil Cell): T and P known, ρ is measured

Shock experiment: Rankine-Hugoniot conditions at shock front:

- **Mass conservation $\rho_0 U_s = \rho(U_s - U_p)$**
- **Momentum conservation $\rho_0 U_s U_p = P - P_0$**
- **Energy conservation $\rho_0 U_s \left(\varepsilon - \varepsilon_0 + \frac{1}{2}U_p^2\right) = P U_p$**

3 equations

3 init. cond.: $\rho_0, P_0, \varepsilon_0$

5 unknowns: $\rho, P, \varepsilon, U_s, U_p$

Absolute measurement: 2 velocities U_s and U_p

Relative measurement: velocity U_s in 2 materials – one material with known EoS (aluminum or quartz)

Passive diagnostic: thermal emission from the rear side with temporal resolution

Protection of the sample from the laser-induced preheat

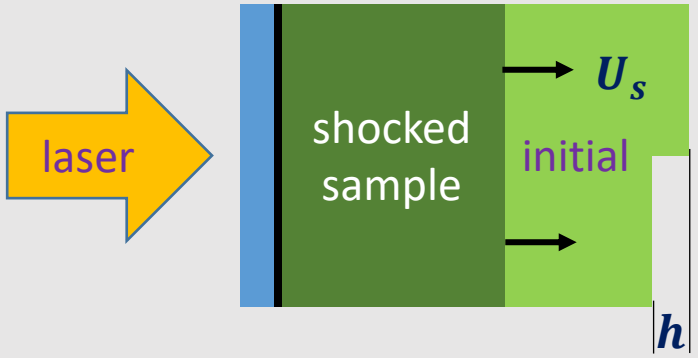

$$U_s = \frac{h}{\Delta t}$$

$$I(\lambda) \rightarrow T$$

Active diagnostics: radiography and VISAR

Material densities and shock velocity can be measured with time-resolved X-ray imaging (absorption or phase contrast)

Shock and material velocities can be measured laser interferometry (Doppler shift)

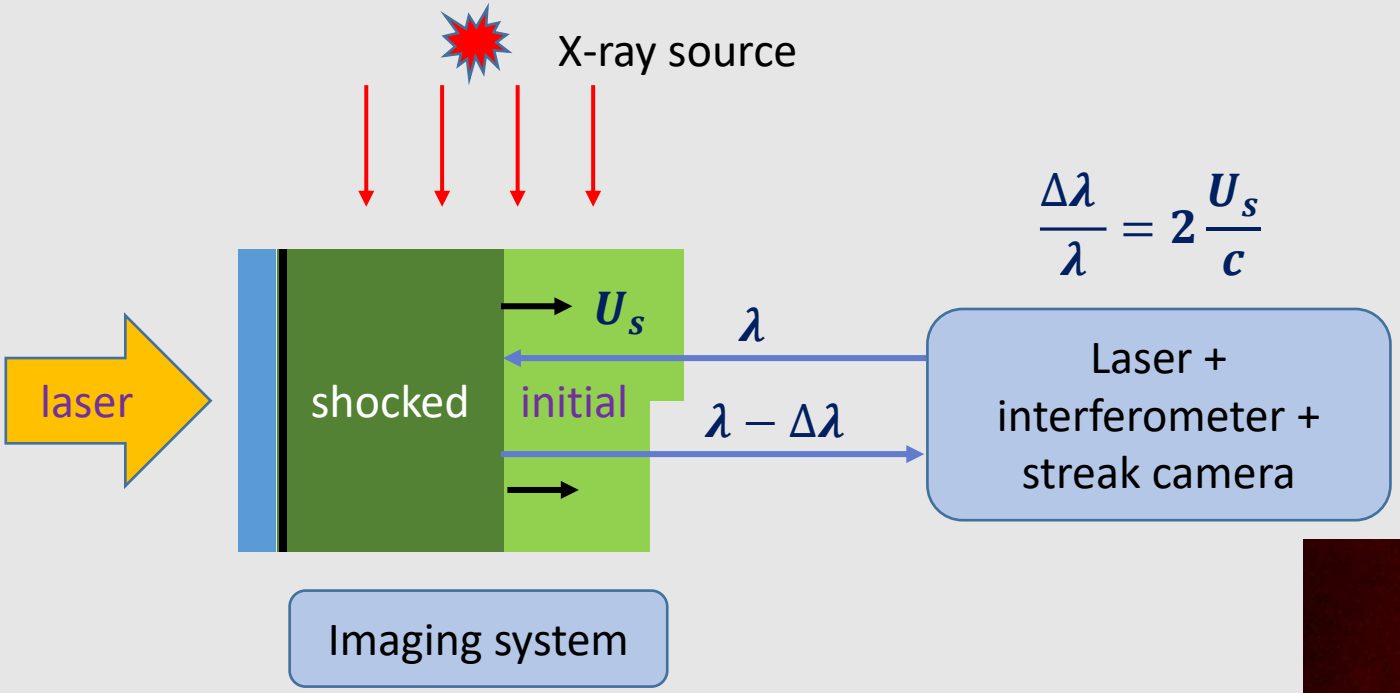

$$\frac{\Delta\lambda}{\lambda} = 2\frac{U_s}{c}$$

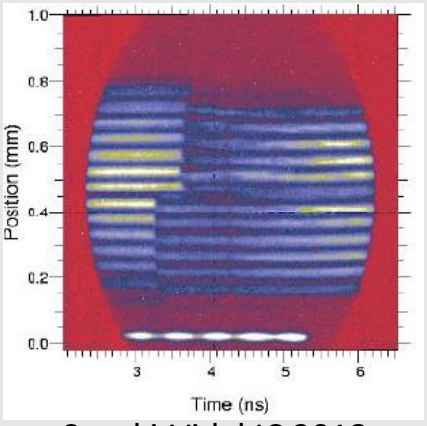

Suzuki-Vidal IC 2018

Precision of measurements depend on the shock planarity:

- **Need for spatial and temporal smoothing (CPP + SSD)**
- **Large focal spot & long pulse: need for a large laser energy**

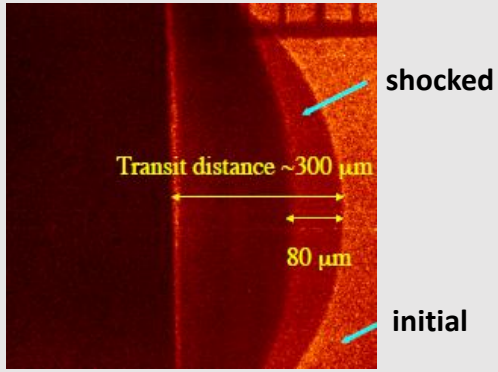

Koenig LULI 2013

Use of the reference material (Al or SiO_2)

Measurement is based on the second Hugoniot relation: $P = \rho_0 U_p U_s = Z U_s$

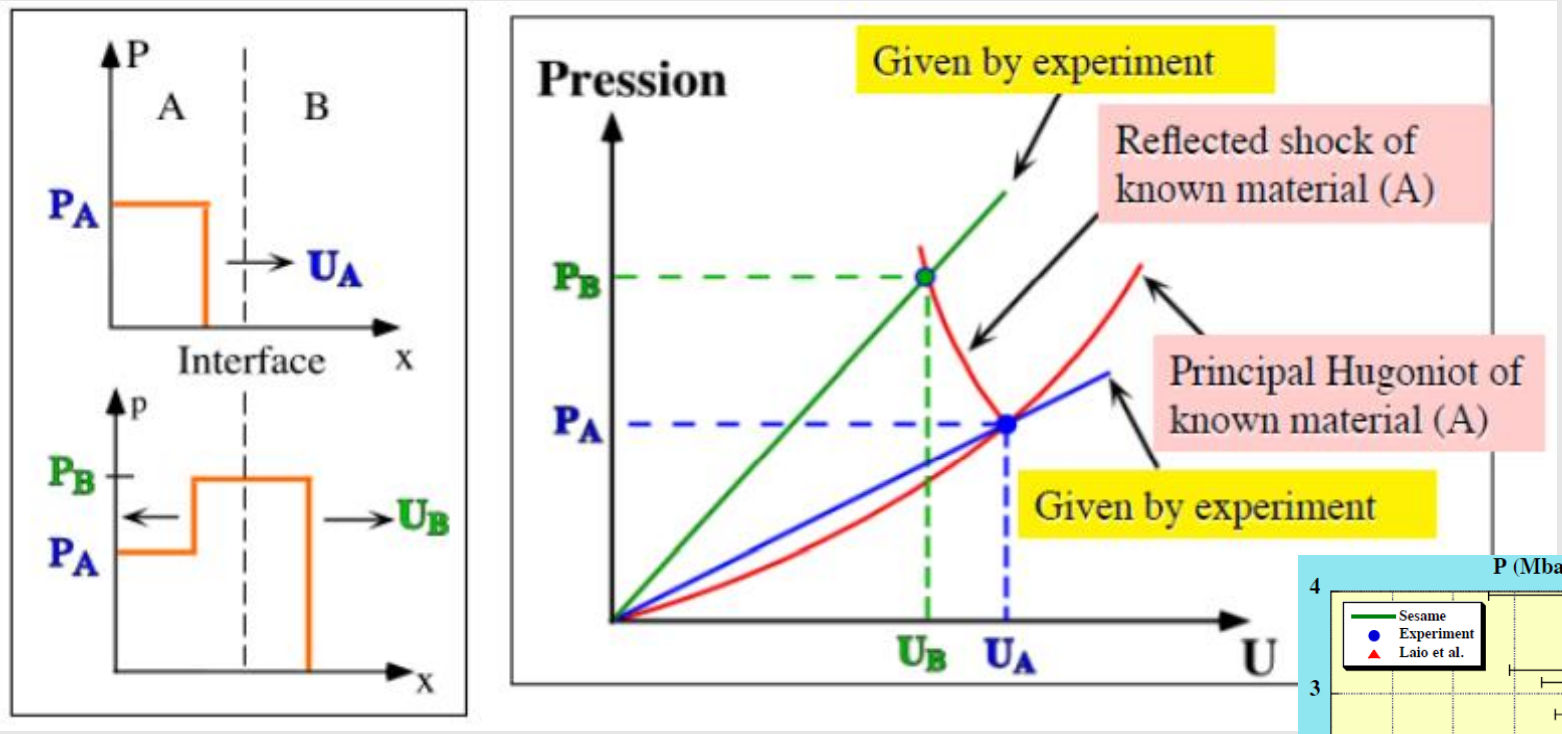

- **Shock velocities U_A and U_B are measured in the experiment**
- **Pressure P_A in the known material is calculated from R-H relation**
- **Pressure P_B is calculated from R-H relation for the reflected shock**

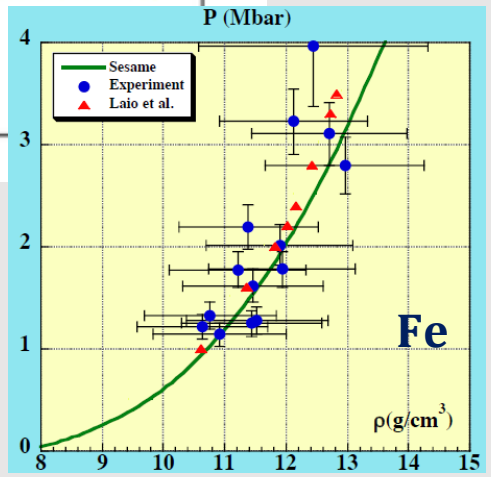

Koenig LULI 2013

How to move out of Hugoniot line

Hugoniot curve: $P(\rho)$ is defined by the initial density and temperature.

There are several methods to explore states out of the principal Hugoniot line:

- **Different initial density: porous material or pre-compression**
- **Compression with two successive shocks**
- **Relaxation – decaying shock**
- **Isentropic (slow) compression**
- **Isochoric heating (ions, X-rays) & isentropic expansion**

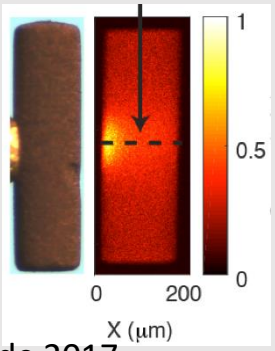

Higginson Univ Strathclyde 2017

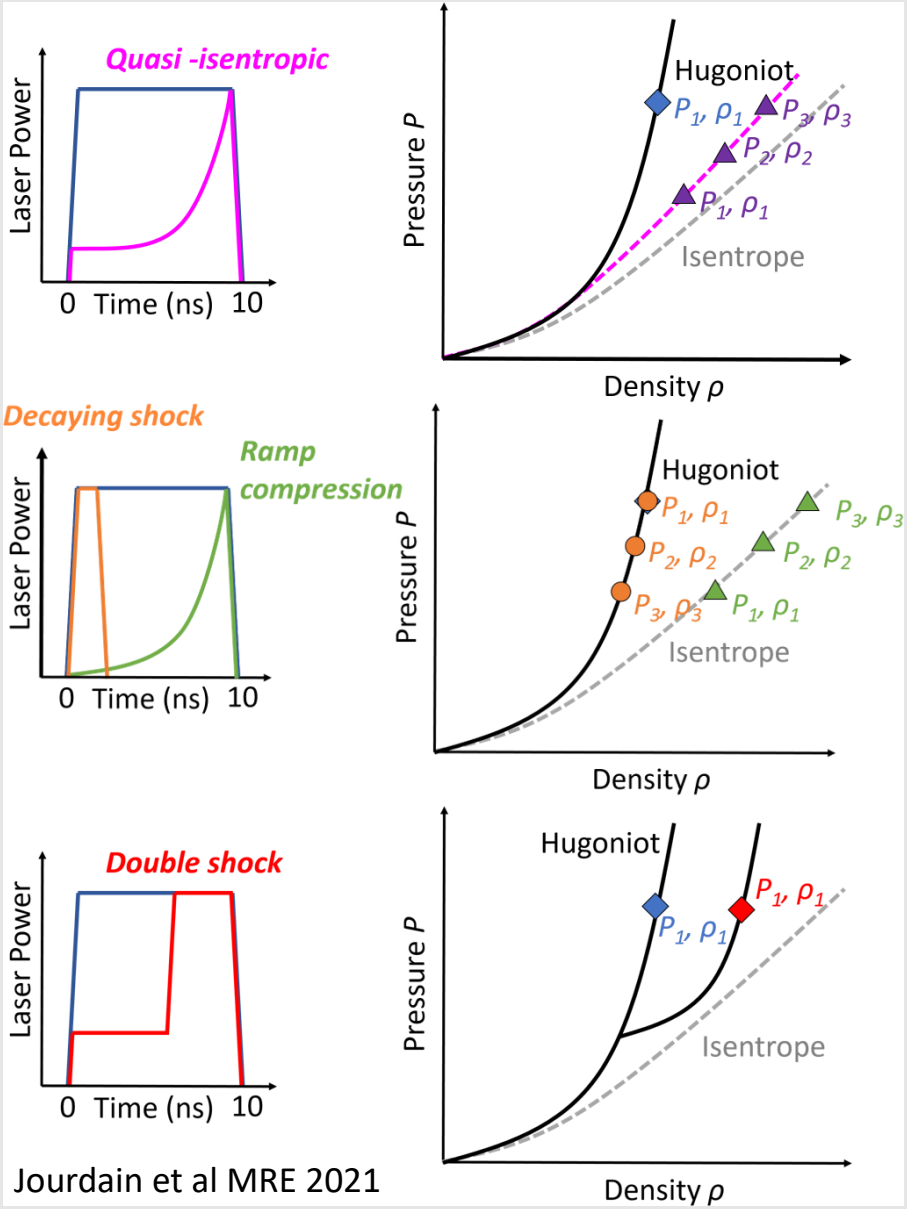

Jourdain et al MRE 2021

Exploring phase transitions

Different techniques of material compression allow to explore large areas in the phase space and obtain high precision data

Magnesium oxide is representative rocky material in Earth mantle and in terrestrial planets

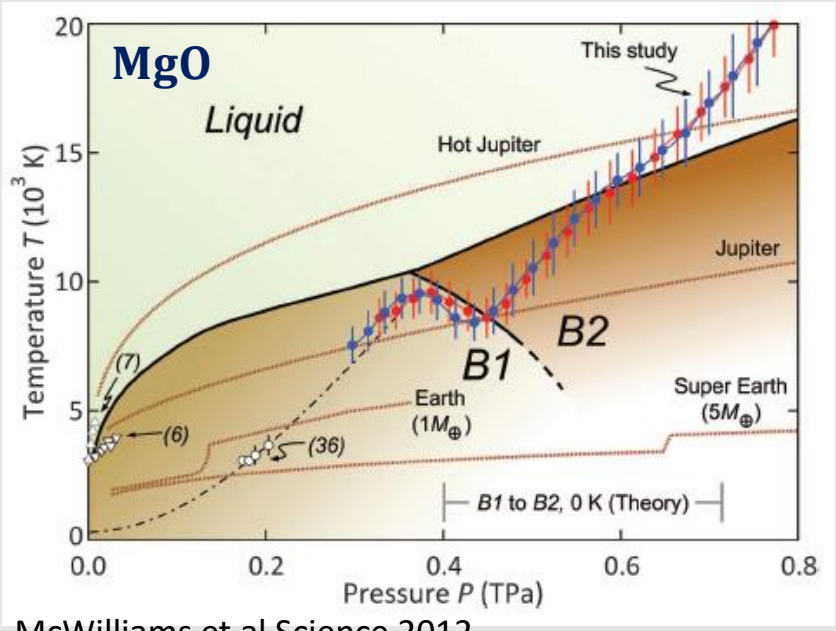

McWilliams et al Science 2012

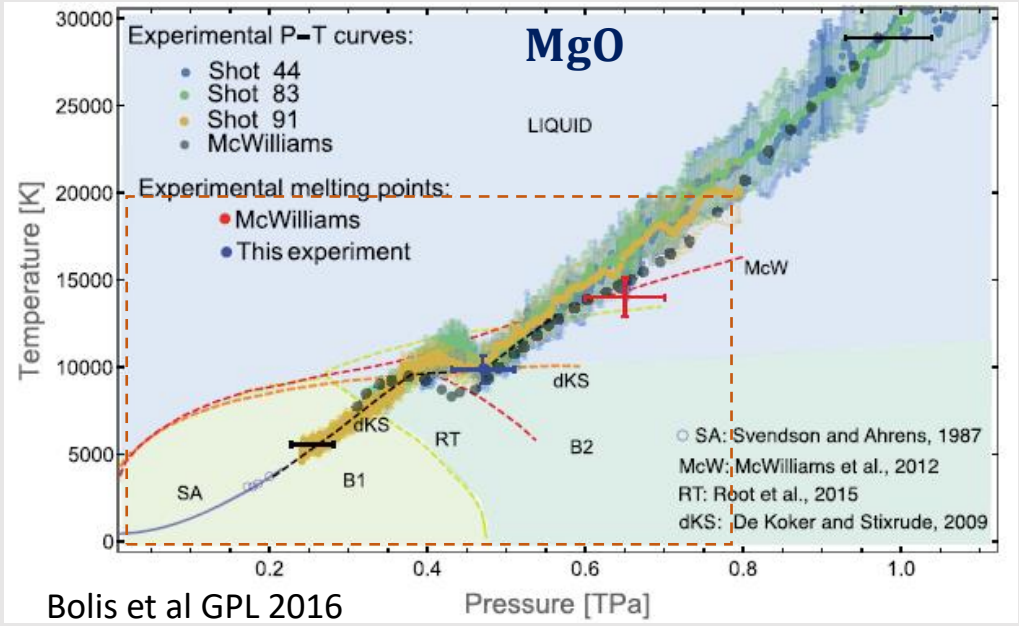

Bolis et al GPL 2016

These data are used for modeling of magnetic field generation in the Earth core and super-Earth evolution

Going to higher pressures: spherical implosion

Spherical implosions provide access to higher pressures and higher compressions

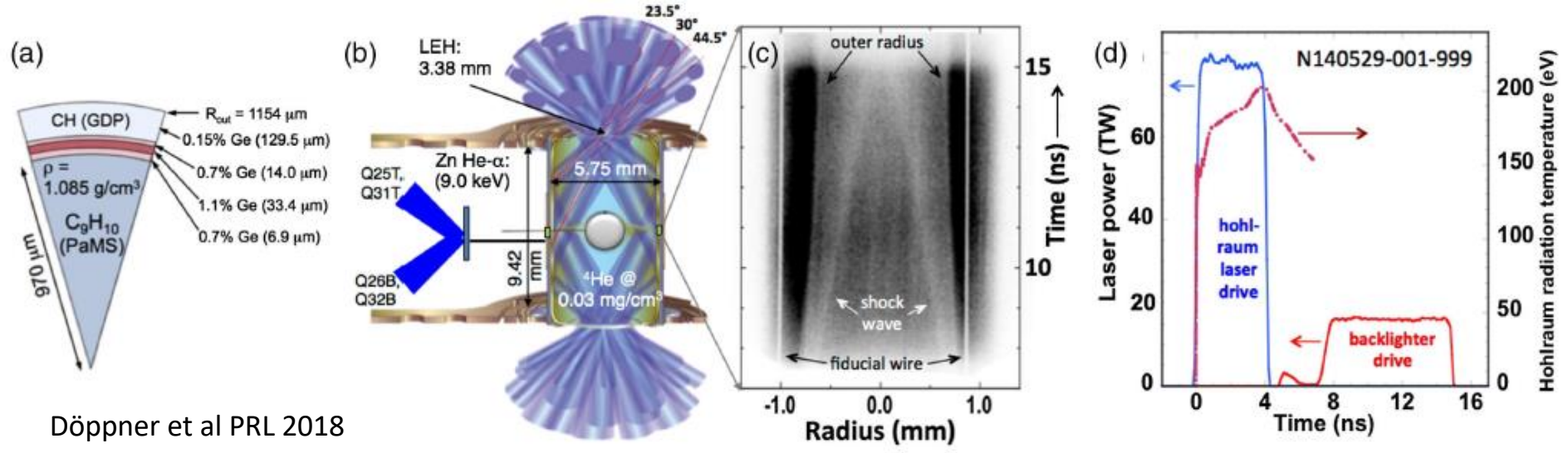

Döppner et al PRL 2018

Measured quantities:

- **Shock position → U_s**
- **Mass density ρ**

Pressure is calculated from R-H relation

$$P = \rho_0 U_s^2 (1 - \rho_0/\rho)$$

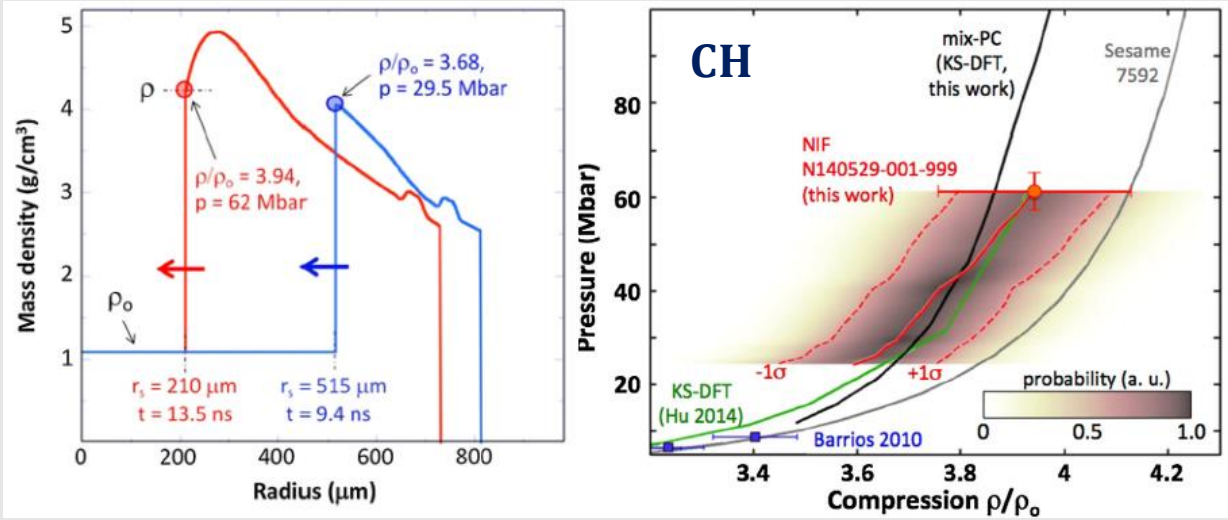

Radiation transport and plasma opacity

Radiation transport dominates energy balance in many astrophysical objects including stars and planets

Equation of radiation transport $\left(\vec{n}\cdot\vec{\nabla}\right) I_\nu = \kappa_\nu (B_\nu - I_\nu)$

Planckian spectrum

spectral opacity

spectral intensity

Opacity describes photon absorption by free an atomic electrons – four processes: free-free, bound-free, free-bound, bound-bound

For many electron atomic systems calculations of κ_ν are very complicated and poorly agree with experiments.

For the systems near equilibrium $B_\nu \approx I_\nu$ it is sufficient to use spectrally-integrated intensity and average (Planck) opacity

$$\kappa_P = \int \kappa_\nu B_\nu \, d\nu \,/\, \int B_\nu \, d\nu$$

Indispensable for understanding the astrophysical observations, both spectral and macroscopic (example Cepheid pulsations: $\frac{d\kappa_P}{dT} > 0$ in H-He mixture)

Emissivity of Al cylinder Ø 2 cm, $l = 3$ cm at $T = 400$ eV and different densities

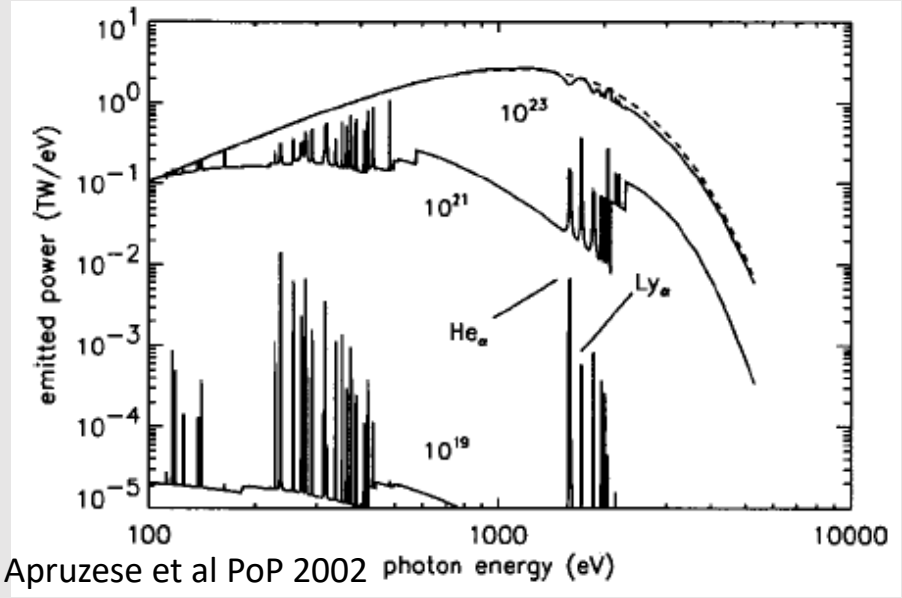

Apruzese et al PoP 2002

Measurements of plasma opacity

Laboratory opacity measurements:

- **aim at reducing uncertainties in stellar interior models**
- **contribute to photo-ionized plasma modeling – creation of the accretion objects**
- **link the radiation transport effects to the plasma source geometry**

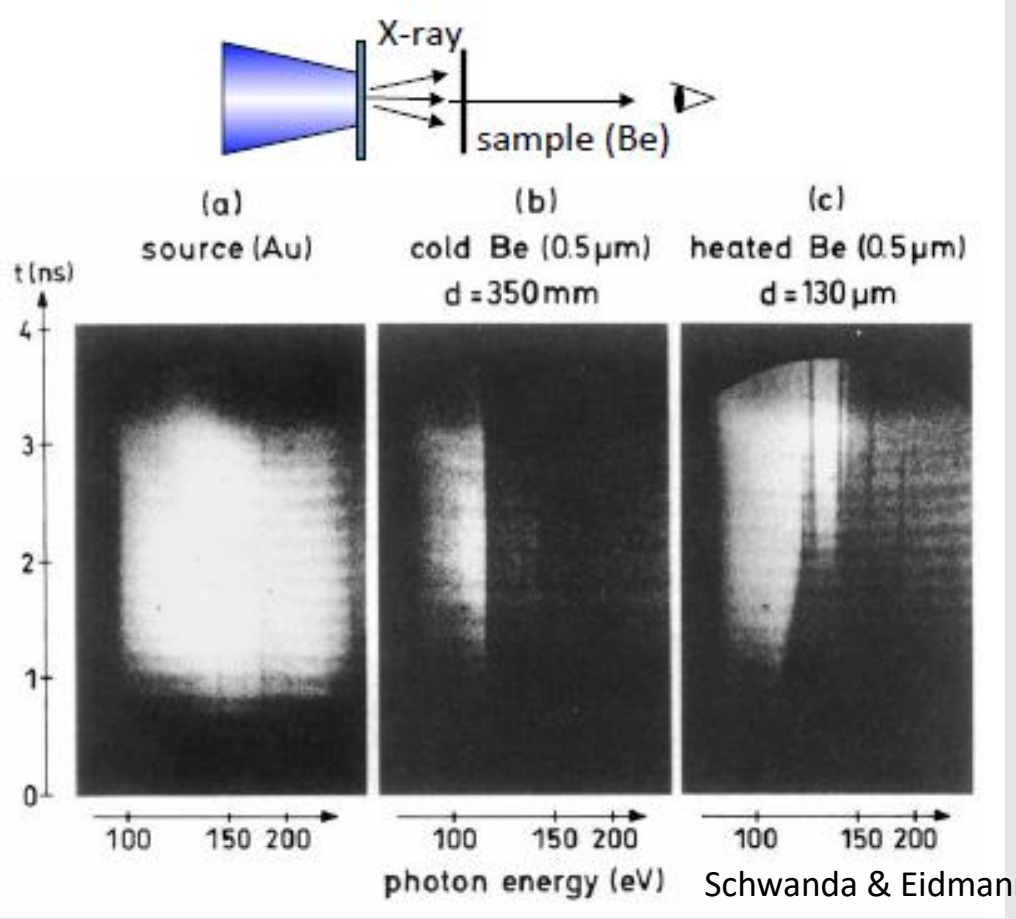

Schwanda & Eidmann PRL 1992

Transmission scheme – strong dependence on the sample density and temperature:

- **shift an smoothing of K edge**
- **electron impact line broadening**

Plasma opacity at extreme conditions

- Sample is enclosed in a temper in order to prevent expansion
- Absorption spectrum of the sample (2) is found by subtraction of the spectrum w/out sample (1)
- Predictivity of the numerical codes is still insufficient

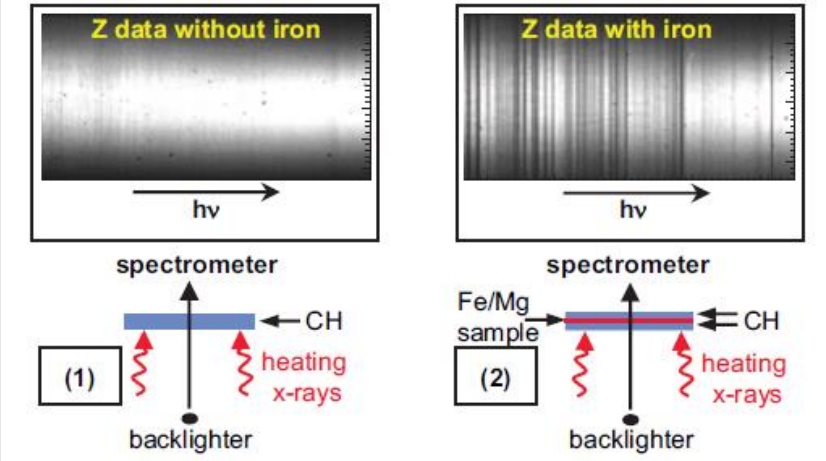

Bailey et al PoP 2009

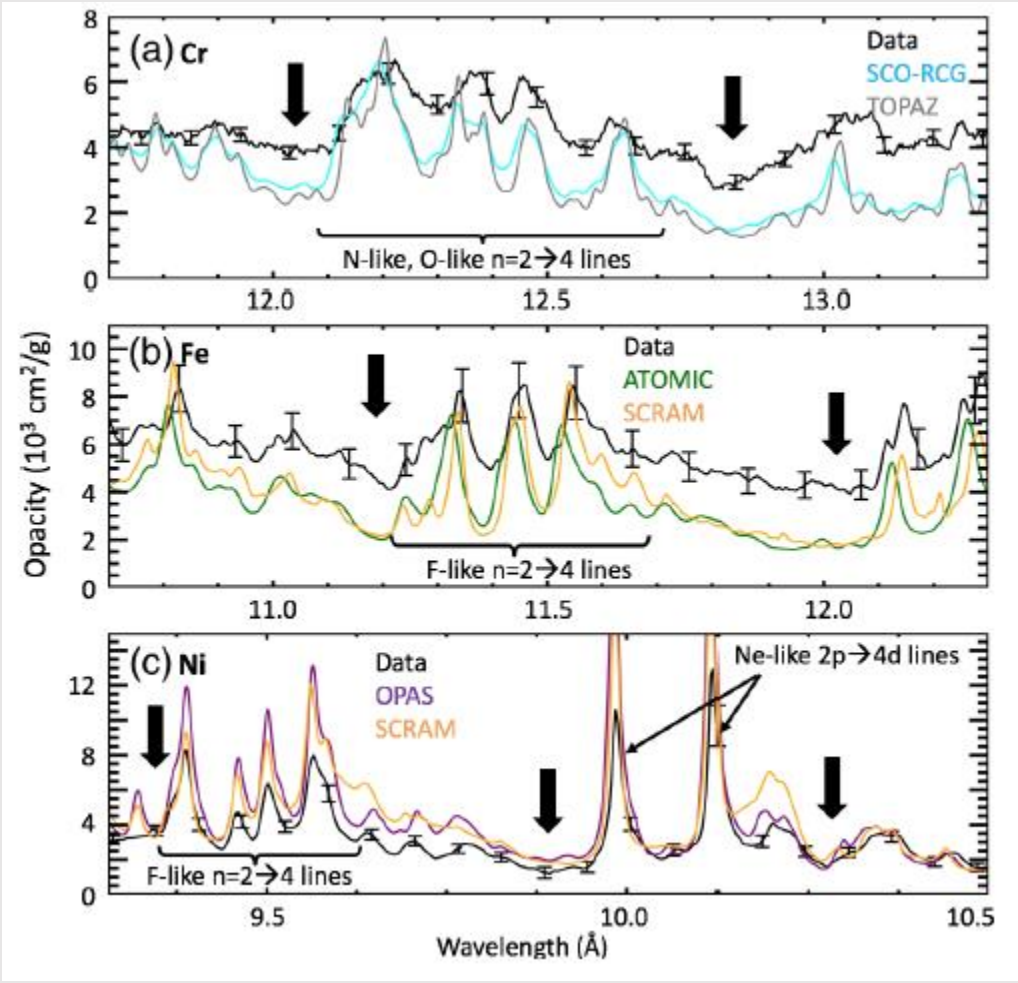

Nagayama et al PRL 2019

Dynamical experiments: similarity – *hydrodynamic scaling*

Dynamic objects in astrophysics: supernova

Supernova: star explosion at the end of life – no more fuel to maintain hot core and hydrostatic equilibrium

- **Very light dying stars form brown dwarfs – cold dense objects**
- **Light stars in binary components, which contain fusible elements (C, O, Si), may accumulate additional mass from a companion and explode: SN Ia – thermonuclear**
- **Heavy stars that burn all fusible elements up to Fe are transformed in a neutron star: ejection of outer shell containing light elements: SN II**

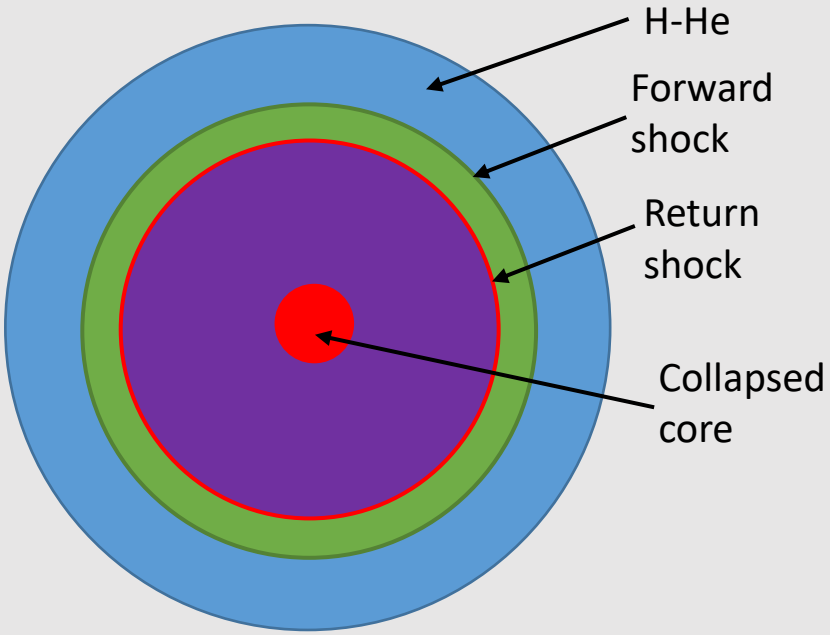

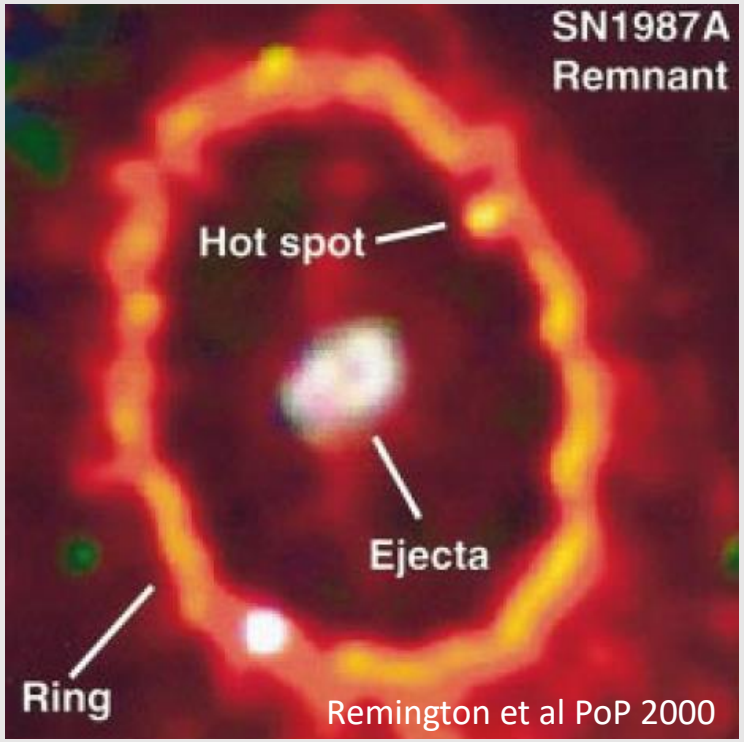

Hydrodynamic scaling

Problem: understand the instability of expanding shell (similarity with ICF), H-He mixing
Principle: hydrodynamic scaling – processes described by same equations proceed similarly at different scales provided the dimensionless parameters are the same and initial conditions are similar
Equations: compressible hydrodynamics

$$d_t\rho + \rho \,\mathrm{div}\, \boldsymbol{u} = 0$$
$$\rho\, d_t\boldsymbol{u} = -\mathrm{grad}\, p$$
$$d_t p + \gamma p \,\mathrm{div}\, \boldsymbol{u}=0$$

$$r \to r'/L^* \qquad \rho \to \rho'/\rho^* \qquad p \to p'/p^*$$

$$u \to u'/u^* \qquad t \to t'/t^* \qquad u^* = L^*/t^*$$

$$\rho(t=0,r) = \rho'(t=0,r')/\rho^*$$
$$p(t=0,r) = p'(t=0,r')/p^*$$
$$u(t=0,r) = u'(t=0,r')/u^*$$

Similarity condition $\mathrm{Eu} = \dfrac{u^*}{\sqrt{p^*/\rho^*}} = \dfrac{u}{\sqrt{p/\rho}}$

Dissipative terms (viscosity, heat conduction) should not make important contributions to the processes considered

Experiment: instability of expanding SN 1987A (1)

Laser-plasma experiments allowed to resolve the physics of instability of expanding shell of SN remnant and validate large scale hydrodynamic simulations

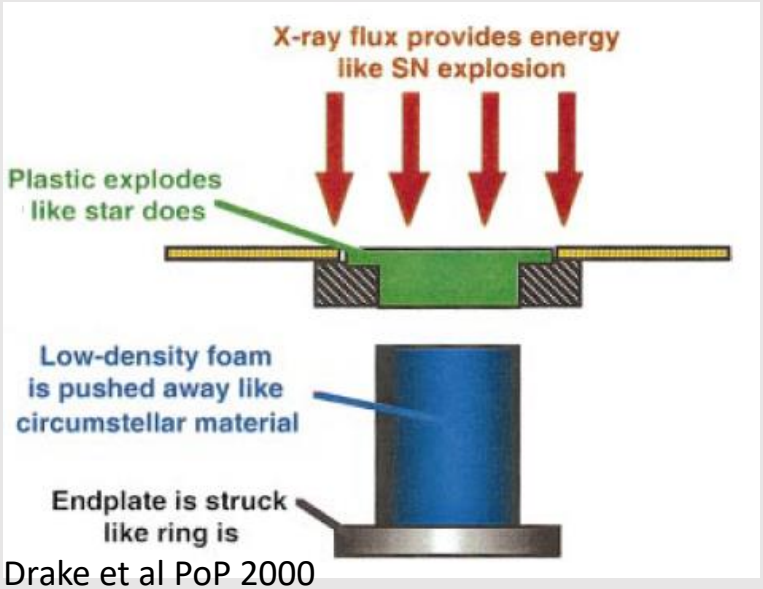

Drake et al PoP 2000

Parameter	Supernova 1987A	Experiment
	(2000 s)	(21 ns)
Length scale (cm)	9×10^{10}	0.0180
Velocity (km/s)	2000	35
Density (g/cm^3)	0.0075	0.4
Pressure (dynes/cm^2)	3.5×10^{13}	5.2×10^{11}
Temperature (eV)	900	7.4
Z_i	2.0	0.6
A	4.0	11.4
Density of nuclei (cm^{-3})	1.1×10^{21}	2.1×10^{22}
$u^*/\sqrt{p^*/\rho^*}$	2.9	3.1
Collisional mfp (cm)	3.5×10^{-3}	7.9×10^{-8}
Kinematic viscosity (cm^2/s)	7.0×10^{7}	0.334
Reynolds number	2.6×10^{11}	1.9×10^{5}

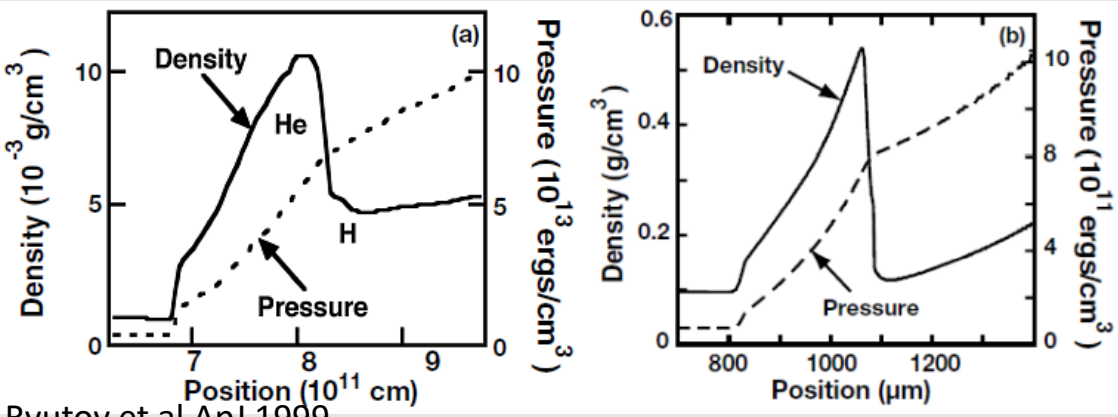

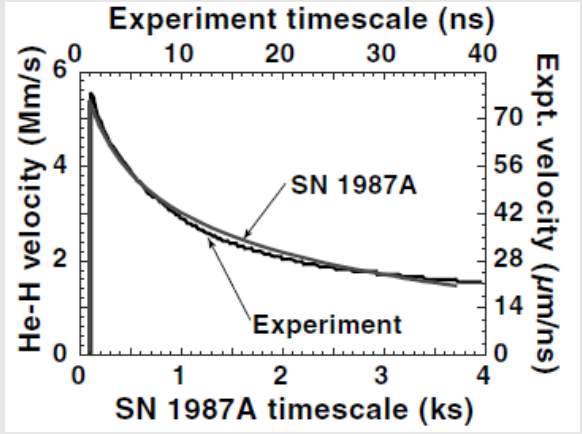

Ryutov et al ApJ 1999

Experiment: instability of expanding SN 1987A (2)

Correct scaling and good agreement with 2D and 3D hydrodynamic simulations

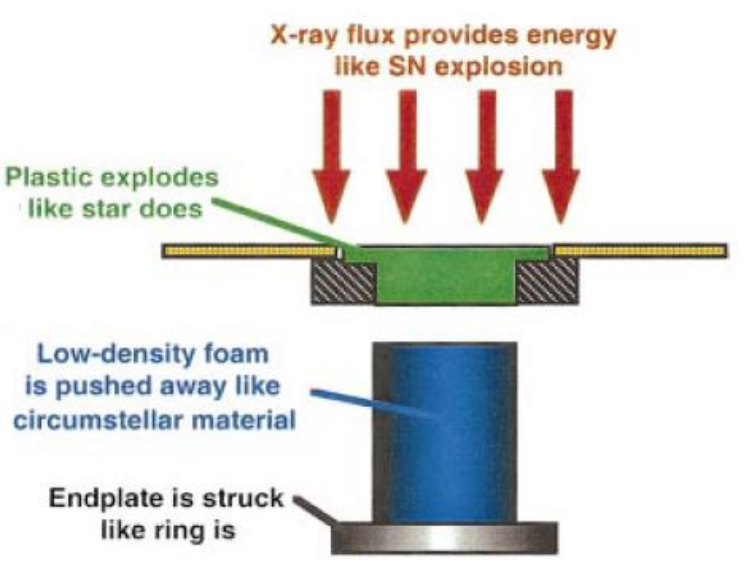

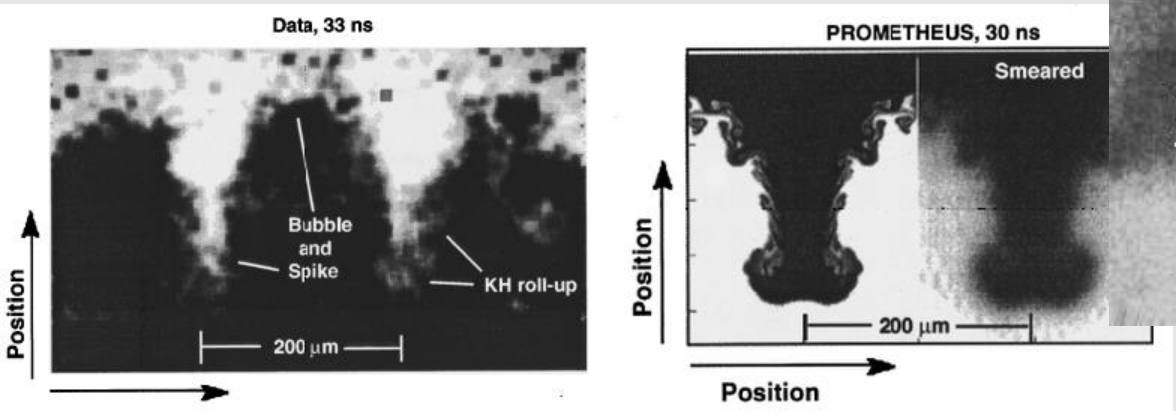

Remington et al PoP 1997

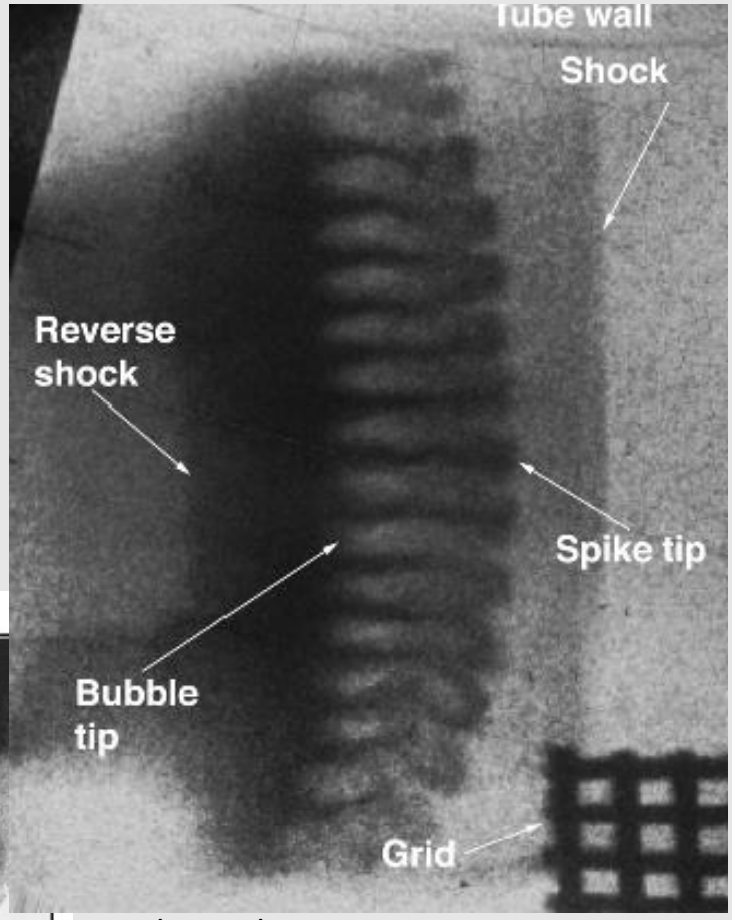

Drake et al PoP 2000

Radiative shocks

Radiative cooling downstream the shock front leads to a stronger compression and may create an upstream precursor
Important in low density plasmas where photon mean free path is large

$$\kappa_P \sigma_{SB} T_e^4 \gg n_e v T_e$$

OMEGA experiment was conducted with Xe, which has a large Planck opacity

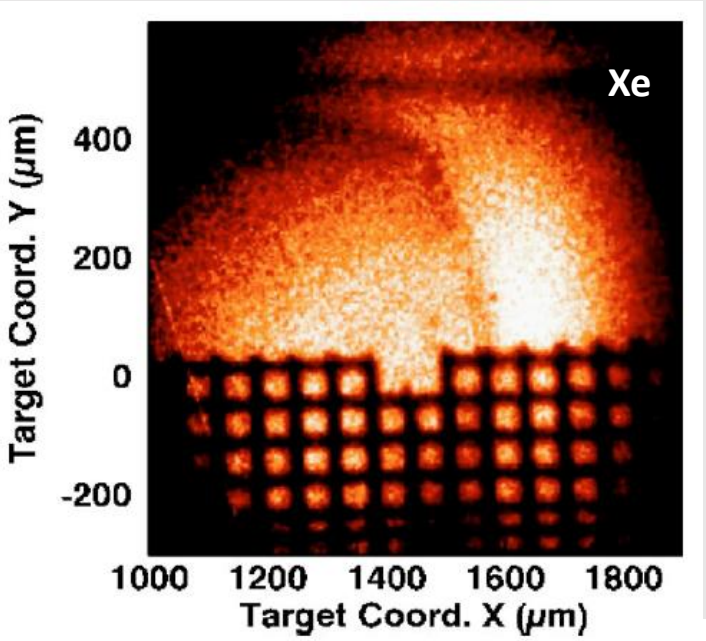

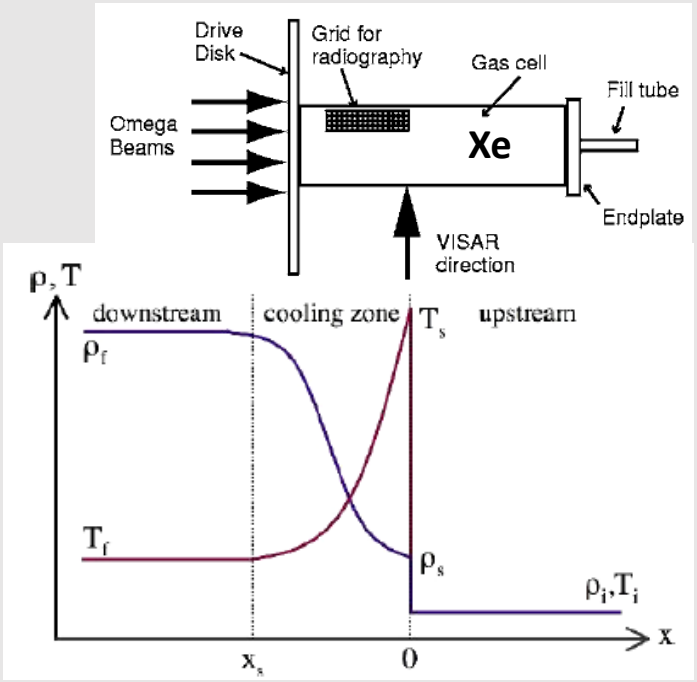

Laser energy 4 kJ
Intensity 10^{15} W/cm^2
Xe pressure 1 bar

Compression more than 40 times is observed

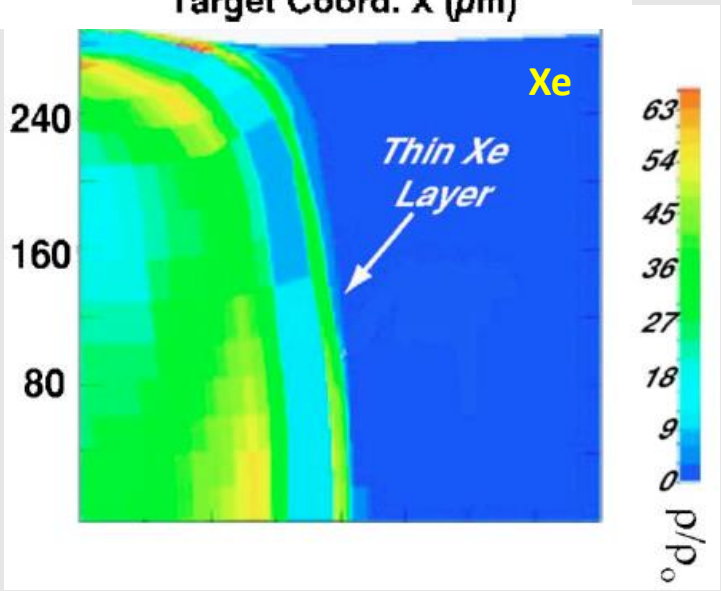

Drake et al PoP 2006

Proto-stellar jets & high Mach number flows

Astrophysical jets (YSO) are ubiquitous features observed in the universe which pose a large number of questions: origin, collimation, bumps, interaction with intergalactic gas and magnetic fields, radiation cooling

- **Hydrodynamic scaling applies to laboratory modeling is these structures**
- **Various experimental setups were tested**

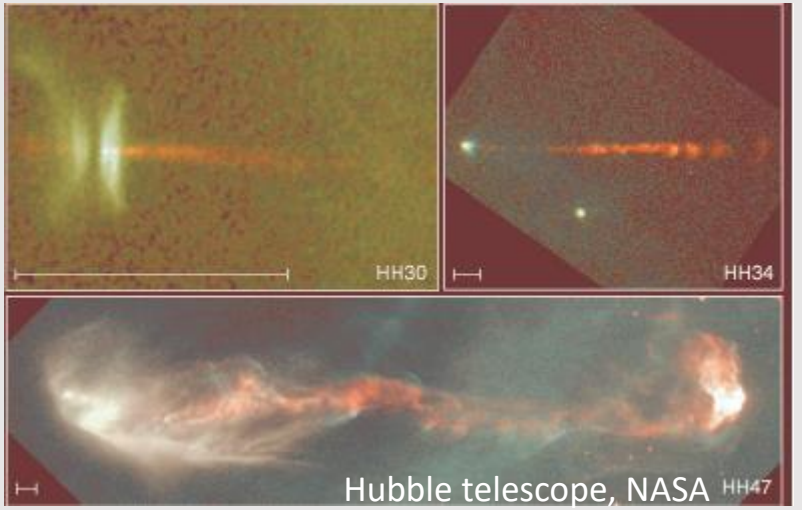

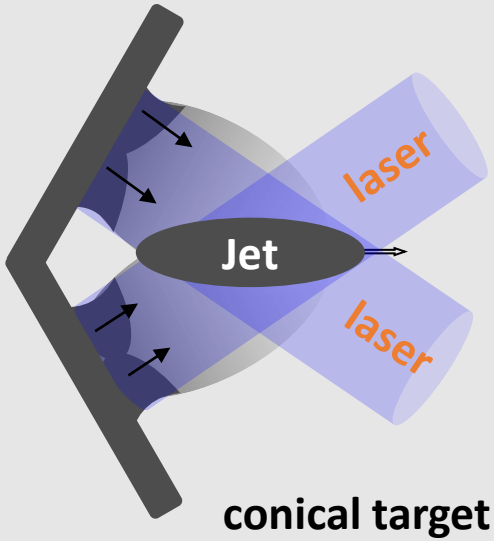

conical target

Farley et al PRL 1999

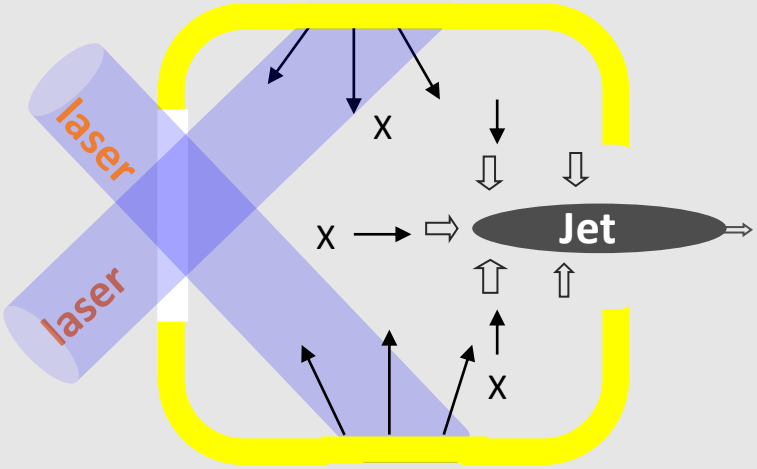

holhraum

Foster et al PoP 2002

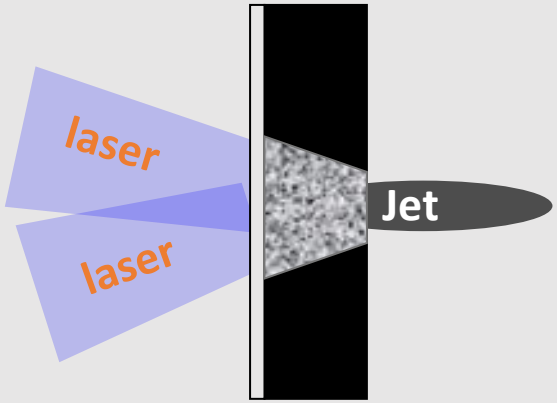

Foam-filled cone target

Loupias et al PRL 2007

Single beam jet formation at PALS

Efficient, reliable and simple jet generation system has been developed on PALS laser

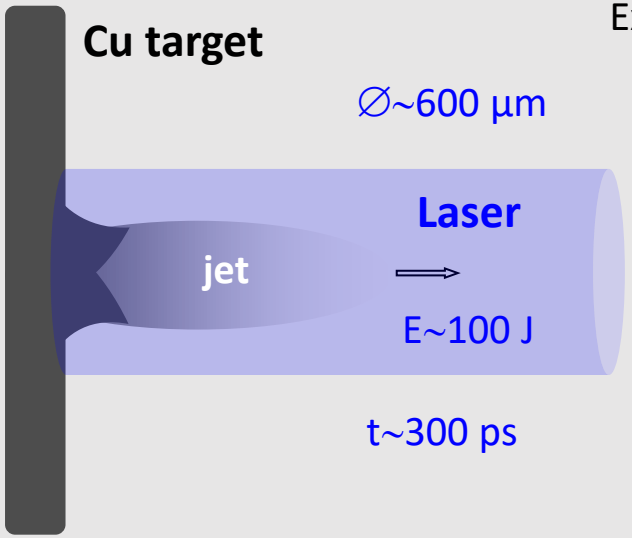

Experimental electron density distribution

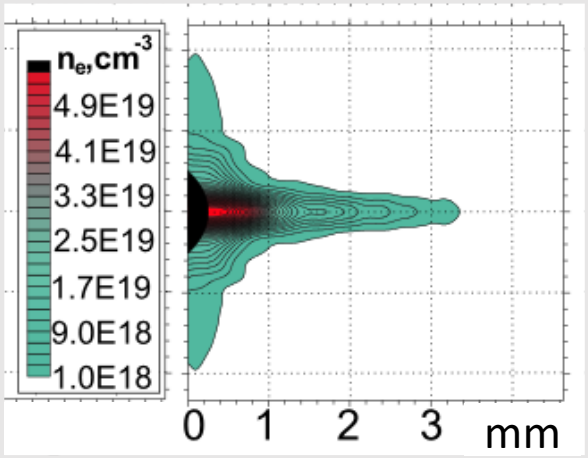

- Velocity 500 km/s
- Duration 10 ns
- Length 3-4 mm
- Mach number 10 -15

These jets have been used for studies of collision with ambient plasma Structure of jet – plasma collision depends on the relative density, velocity and radiation effects

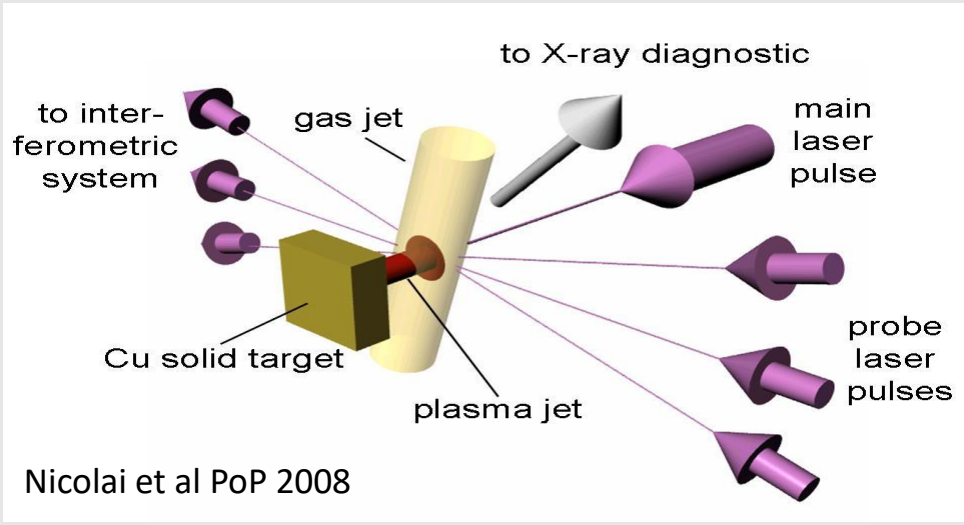

Nicolai et al PoP 2008

Structure of jet-gas interaction zone is investigated

Shadowgraphy and X-ray emission show the jet evolution and formation of the bow shock

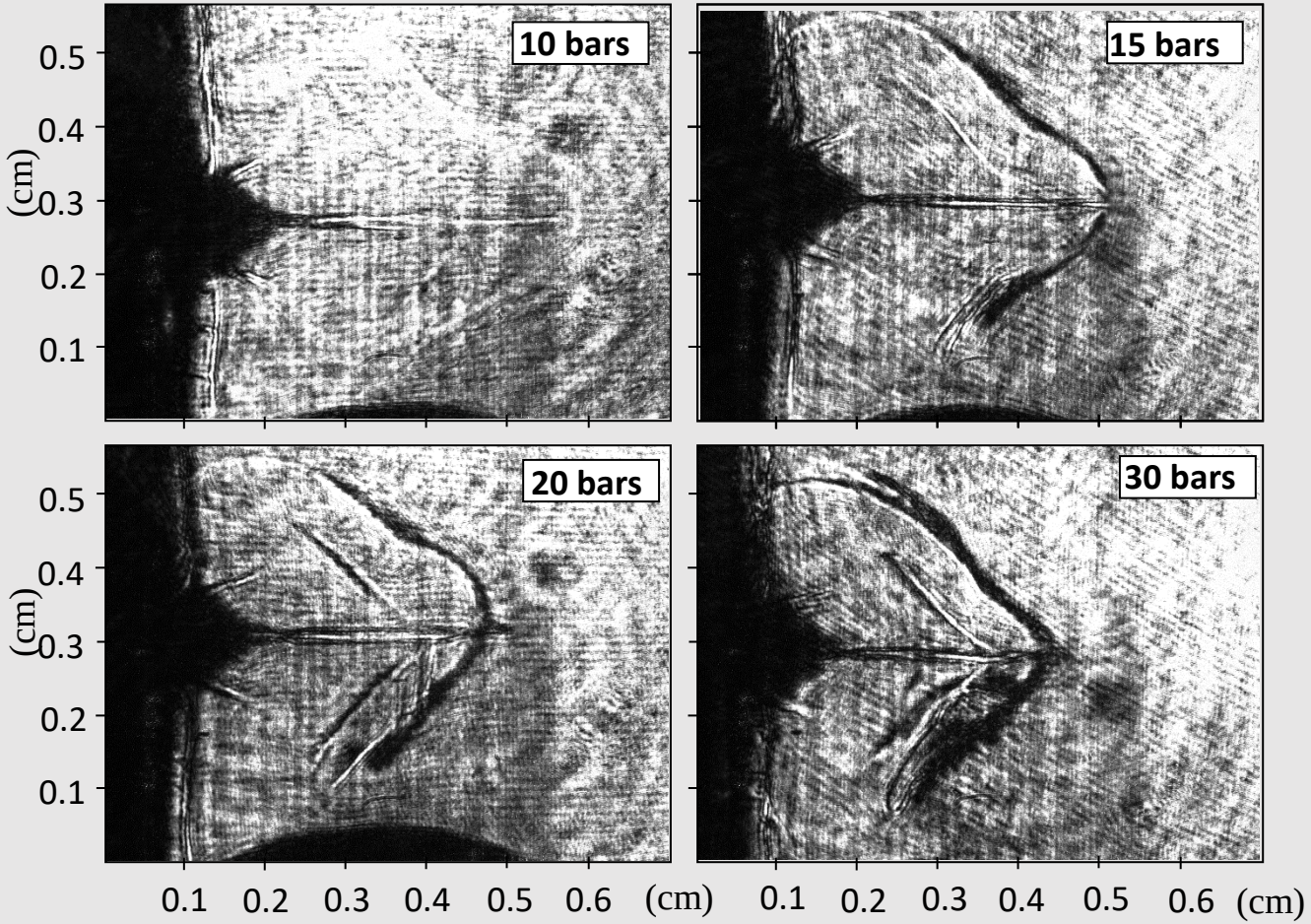

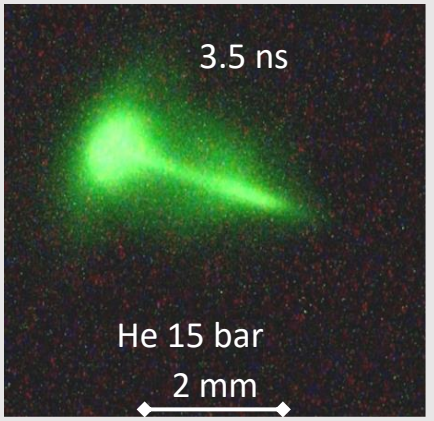

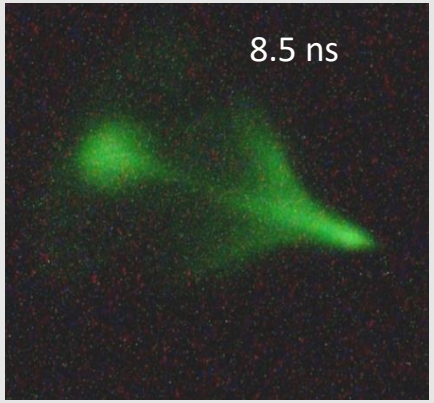

Nicolai et al PoP 2008

Structure of interaction zone depends on the working gas: Helium – adiabatic interaction

Structure of jet- gas zone is investigated

Shape of the jet depends on the ratio of ram/gas pressure and the radiation losses

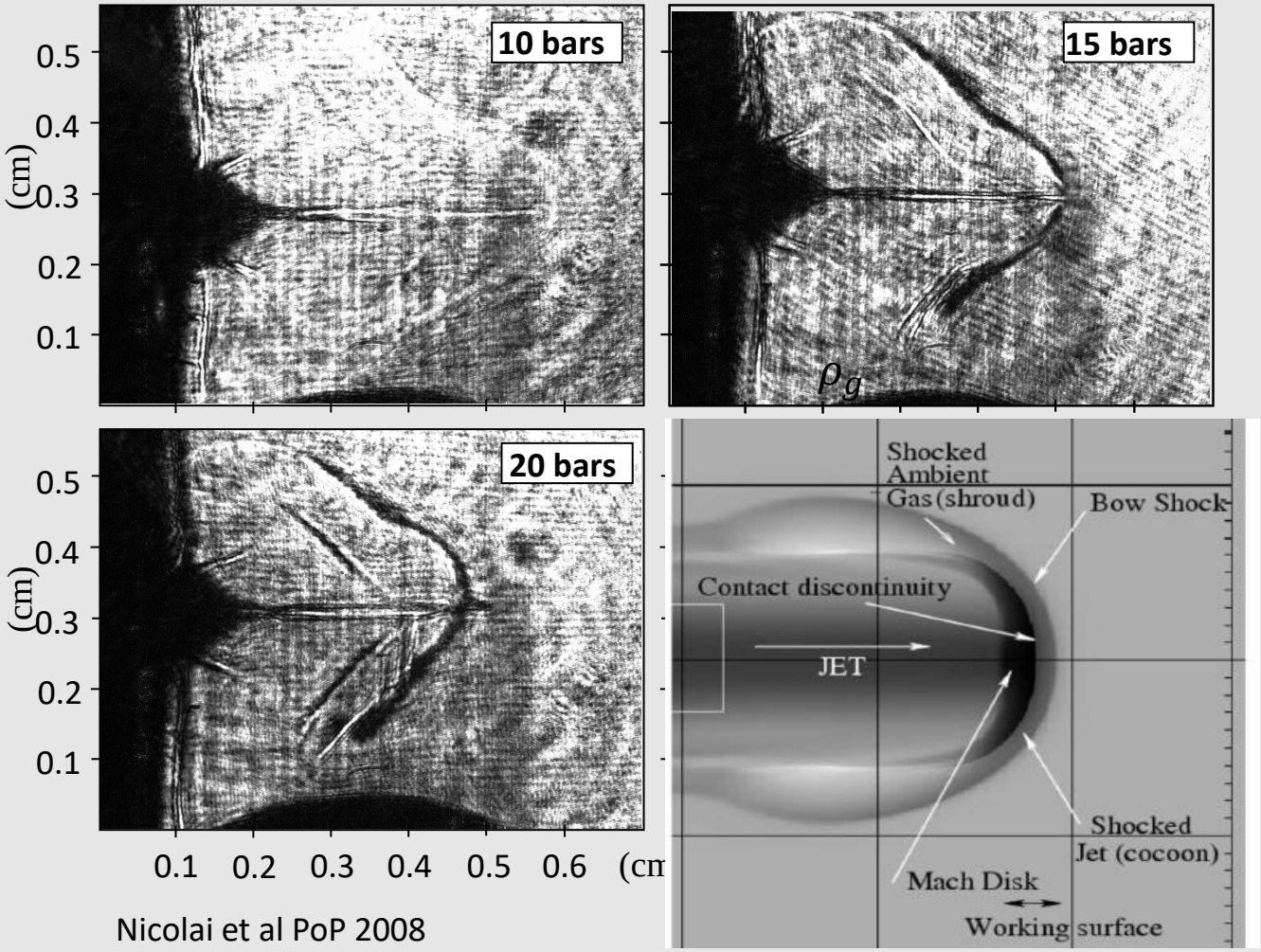

Nicolai et al PoP 2008

Force balance

$\rho_j\left(v_j - v_{bs}\right)^2 = \rho_g v_{bs}^2$ defines the bow shock velocity

$$v_{bs} = v_j\left(1 - \sqrt{\frac{\rho_g}{\rho_j}}\right)^{-1}$$

Radiation cooling time

$$t_{\text{cool}} = \frac{\rho C_v T}{\kappa_{\text{P}} \sigma_{SB} T^4}$$

He $\kappa_{\text{P}} = 0.09$ cm²/g

$t_{\text{cool}} = 2$ μs

Ar $\kappa_{\text{P}} = 80$ cm²/g

$t_{\text{cool}} = 2$ ns

Structure of jet-gas interaction zone is investigated

Structure of interaction zone depends on the working gas: Argon – large radiation losses lead to the formation of a narrow tip

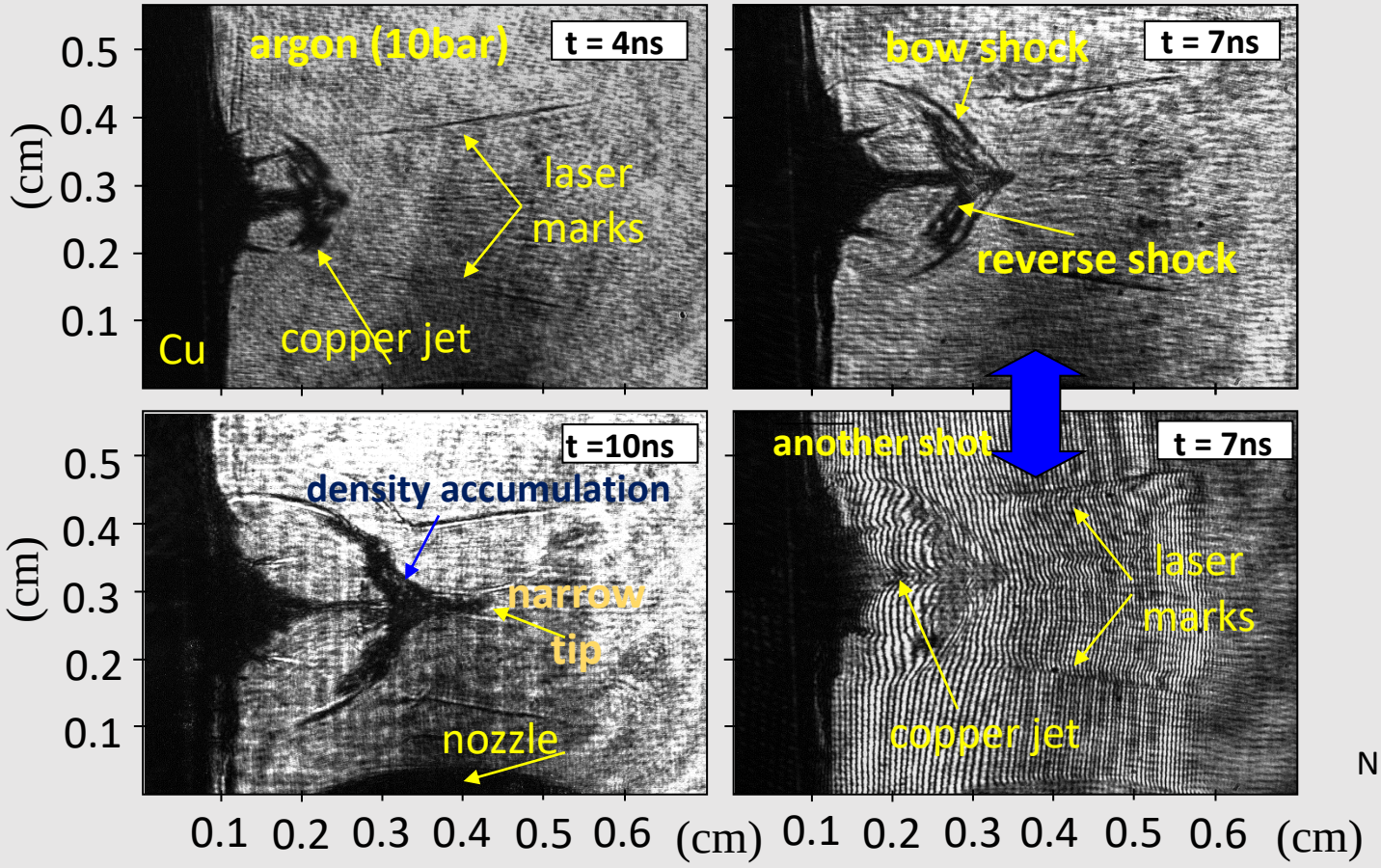

Nicolai et al PoP 2008

Hydrodynamic scaling to astrophysical conditions

Quantity	Herbig–Haro object	Laser experiment	Scaling factor
Jet length (m)	3×10^{15}	5×10^{-3}	$L^* = 6 \times 10^{17}$
Jet radius (m)	7.5×10^{13} m	1.5×10^{-4}	$L^* = 5 \times 10^{17}$
Jet velocity (km s^{-1})	100	500	$v^* = 0.2$
Atomic number	2	15	$Z^* = 0.13$
Mass number	4	40	$A^* = 0.1$
Ion density (cm^{-3})	20	1.5×10^{18}	$n^* = 1.3 \times 10^{-17}$
Mass density (g cm^{-3})	10^{-22}	10^{-4}	$\rho^* = 1 \times 10^{-18}$
Temperature (eV)	1	100	$T^* = 0.01$
Pressure (bar)	10^{-16}	2.5×10^{3}	$P^* = 4 \times 10^{-20}$
Sound speed (km s^{-1})	10	80	$c_s^* = 0.125$
Mach number	9	6	1.5
Time scale	300 yrs	2 ns	$t^* = 4.5 \times 10^{18}$
Cooling time	300 yrs	1 ns	$t^* = 9 \times 10^{18}$
Cooling parameter	1	2	0.5

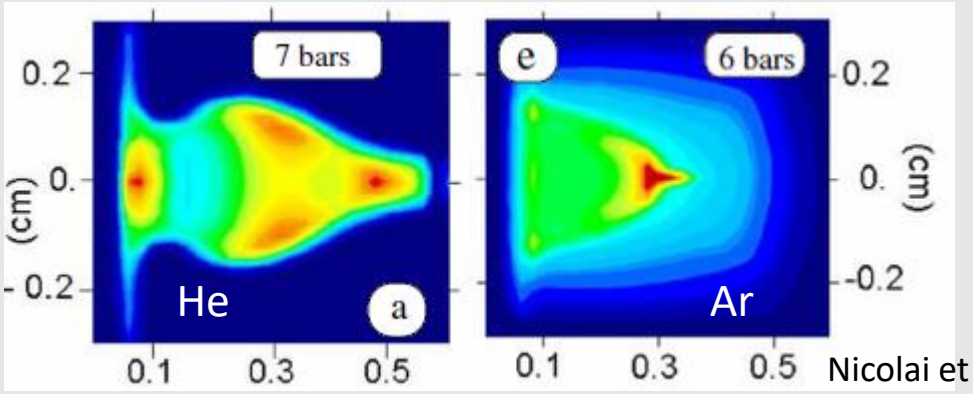

Nicolai et al PoP 2008

Simulated X-ray images are in good agreement with the experiment: evolution of the working surface, effect of the radiation losses on the jet structure

Effects of magnetic fields on jets: generation

Magnetic fields are at the origin of jet formation, control the jet propagation and stability
It is believed that jets are generated from the material in the rotating accretion discs in the polar zone confined with a toroidal magnetic field

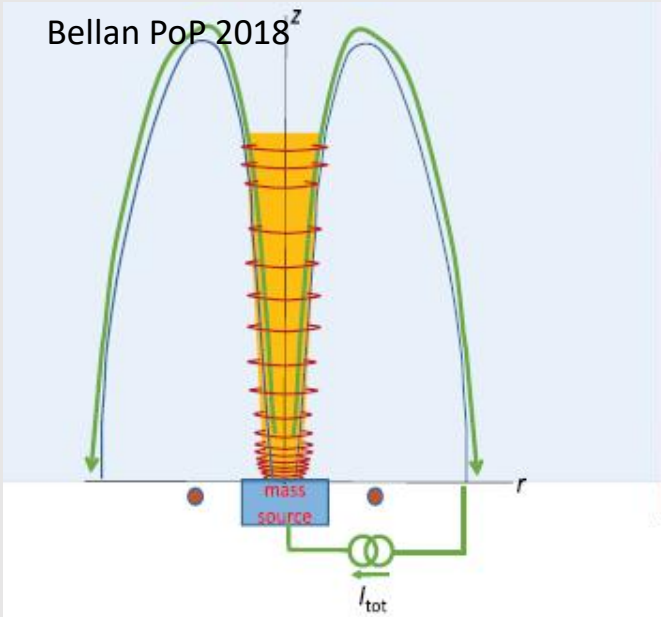

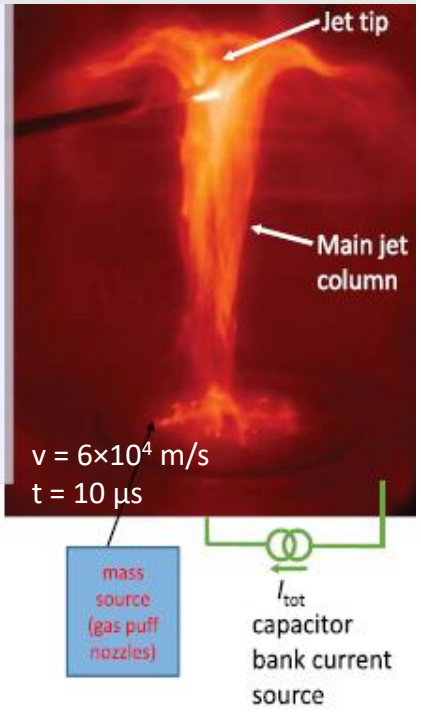

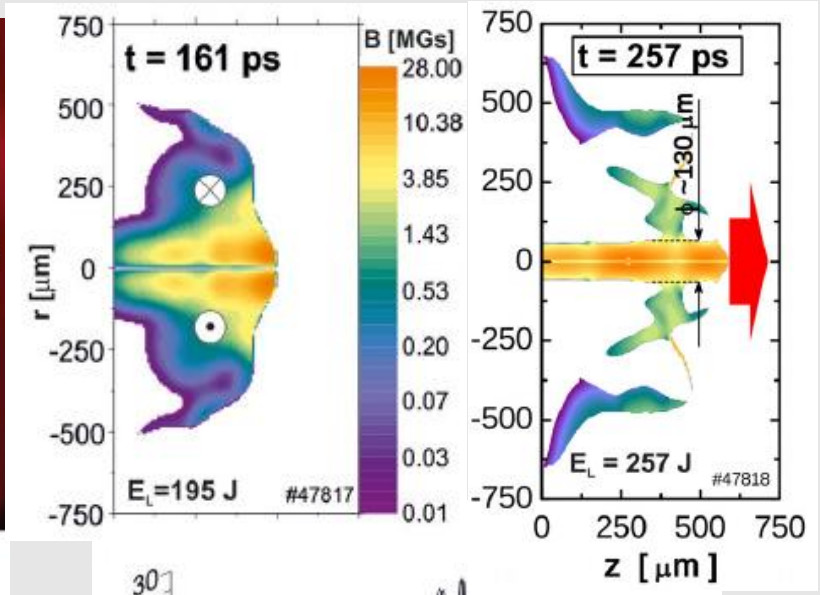

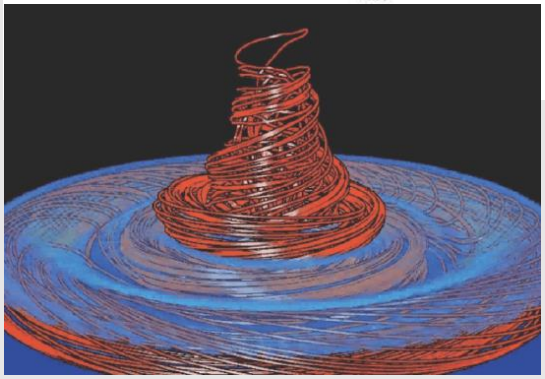

Experiments with Z pinch and laser plasmas confirm the "magnetic tower" mechanism of jet generation

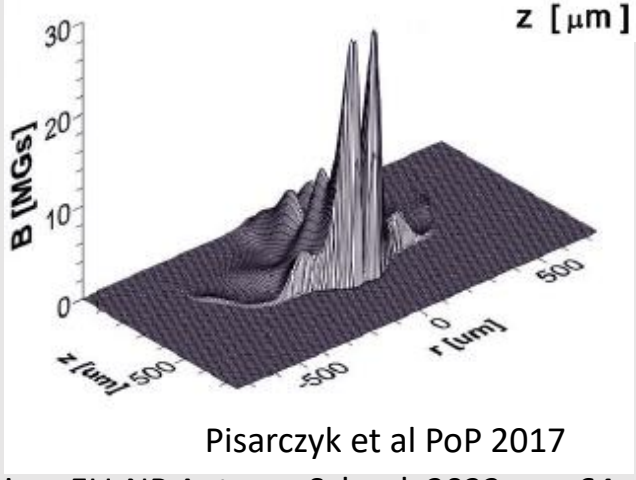

Pisarczyk et al PoP 2017

Effects of magnetic fields on jets: collimation

Magnetic fields parallel to the jet propagation collimate them

Revet et al Nat Comm 2021

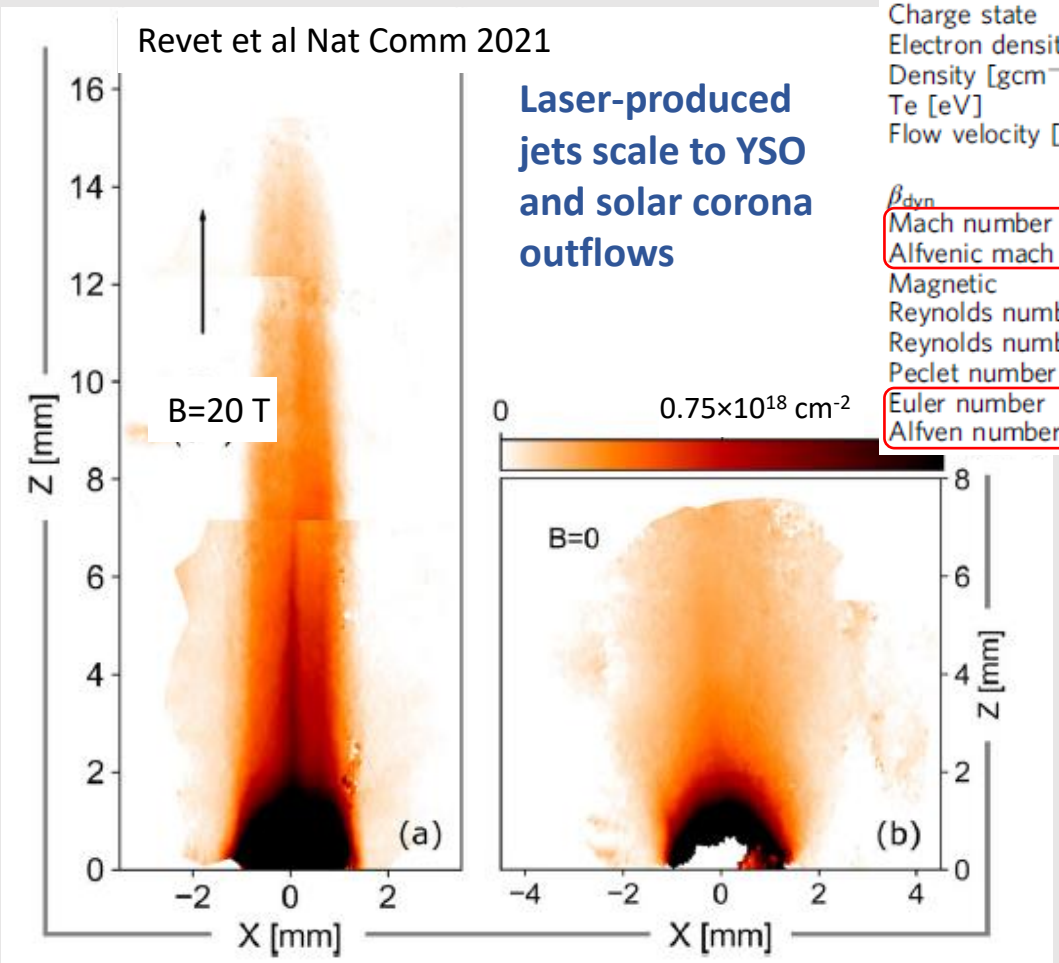

Laser-produced jets scale to YSO and solar corona outflows

	Laboratory	YSO jet	Sun's coronal outflow
B-field [G]	2×10^{5}	2.4×10^{-2}	$30-3$
Material	CF_2 (Teflon)	H	H
Atomic number	16.7	1.28	1.29
Spatial (Radial) scale [cm]	1×10^{-1}	4.5×10^{13} (3 AU)	2×10^{8}
Charge state	8	2×10^{-2}	1
Electron density [cm^{-3}]	2×10^{19}	6.5×10^{4}	3×10^{10}
Density [gcm^{-3}]	7×10^{-5}	7×10^{-18}	6.4×10^{-14}
Te [eV]	300	3	3.4
Flow velocity [kms^{-1}]	550 (100-1000)	250 (100-400)	200
β_{dyn}	133	191	$0.7-7$
Mach number	3	13	1.5
Alfvenic mach number	3	8	$0.5-1.4$
Magnetic Reynolds number	3×10^{3}	4×10^{17}	3.5×10^{12}
Reynolds number	5×10^{4}	2×10^{1}	1.7×10^{3}
Peclet number	2	2×10^{4}	31
Euler number	9	17	2
Alfven number	6×10^{-4}	20×10^{-4}	$40\times10^{-4}-4\times10^{-4}$

Jets interacting with transverse magnetic fields are unstable

Collisionless shocks and particle acceleration – *similar physics but at different conditions*

Collisionless shocks

Electrostatic collisionless shocks have been predicted in 1950s and discovered in the Earth's magnetosphere in 1962 by Mariner II mission

Entropy dissipation in the supercritical electrostatic shock is realized by the ion reflection from the electrostatic potential

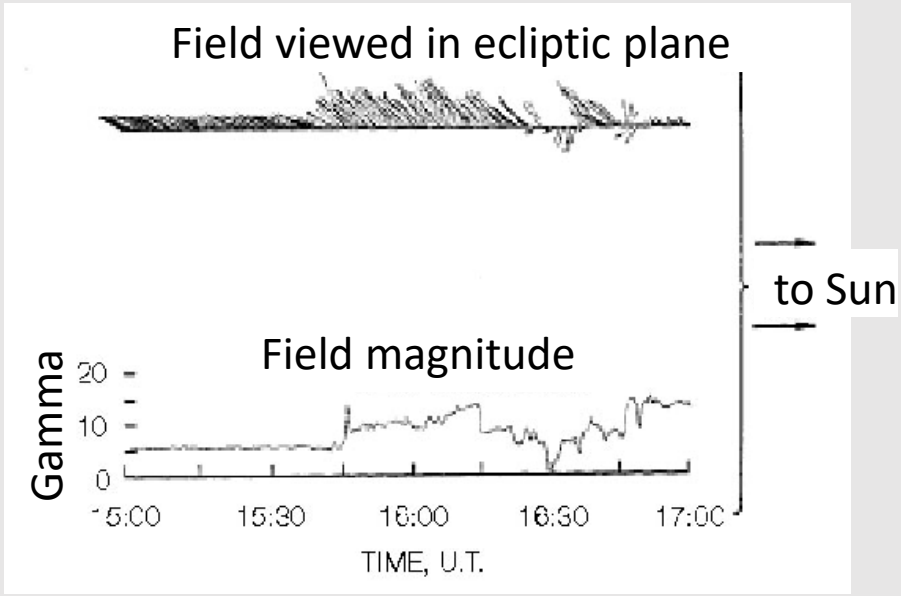

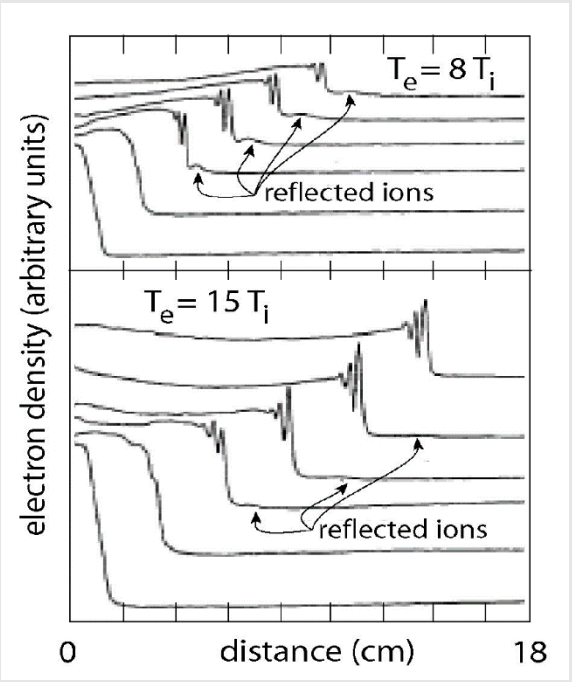

Treumann, Astron. Astrophys. Rev. 2009
Sonett et al, J. Geophys. Res. 1963
Taylor et al, Phys. Rev. Lett. 1970

Electrostatic shocks are produced by wavebreaking and two-stream instability

Collisionless shocks in laboratory

Laser driven electrostatic shocks are well documented: experiment on VULCAN – laser plasma expansion in a low density ambient gas

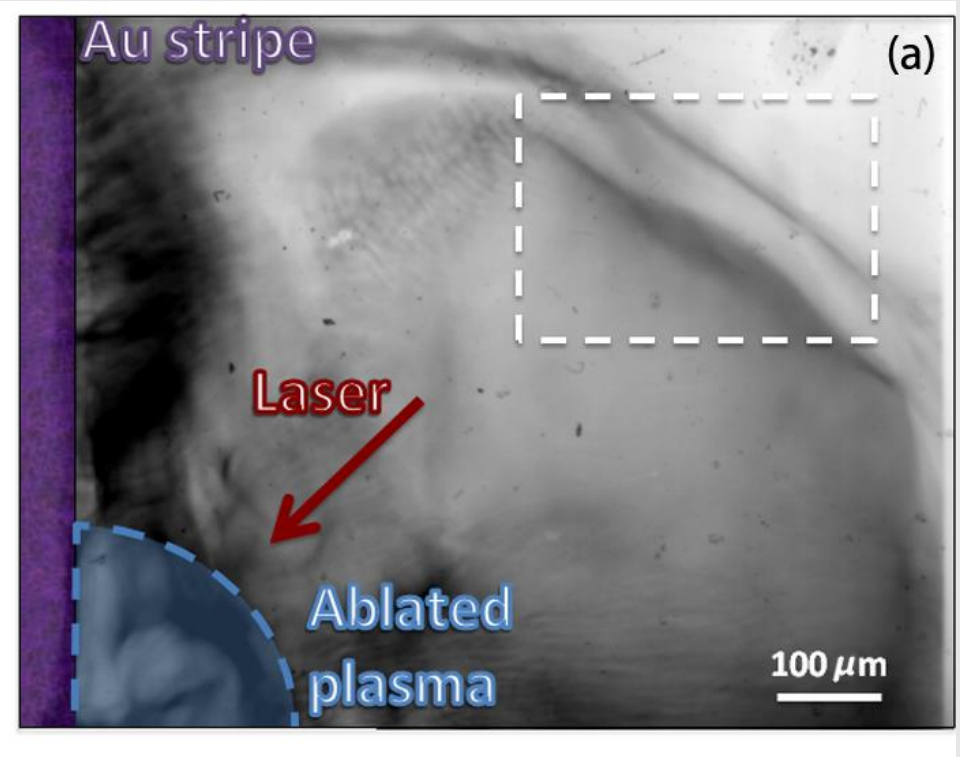

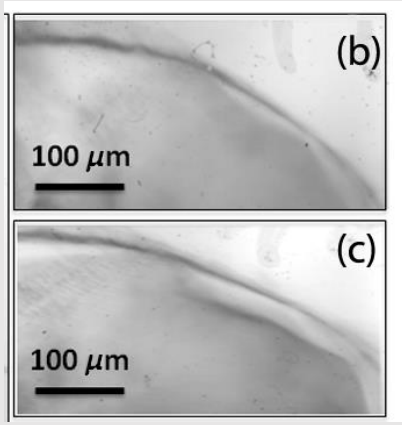

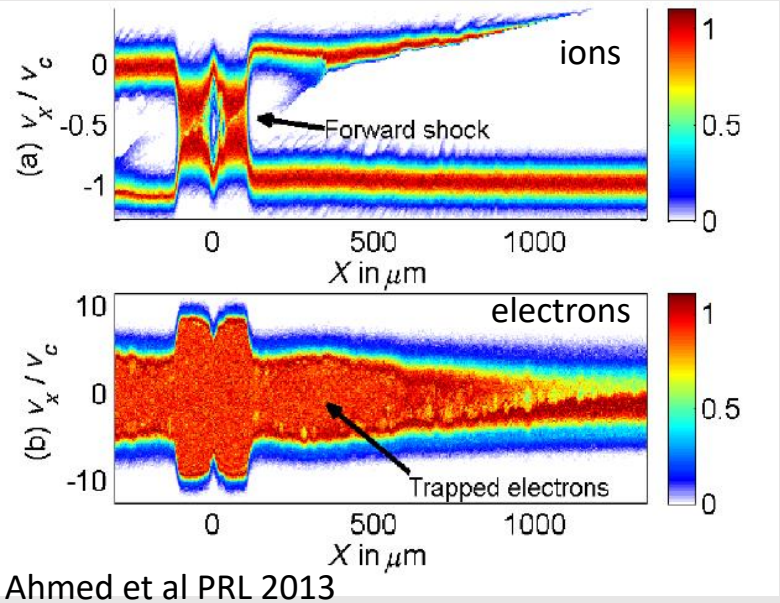

Ahmed et al PRL 2013

Signatures of the shock:

- **Downstream density > upstream density**
- **Downstream velocity> upstream velocity**
- **Downstream plasma heating**
- **Accelerated particles**

Electrostatic and electromagnetic shocks

Electromagnetic shocks provide a possibility for multi-pass particle acceleration in inductive convection electric field excited by magnetic field perpendicular to flow direction

Necessary conditions: $\lambda_{\mathrm{mfp}} \gg \ell_{\mathrm{int}} \gg \ell_{\mathrm{EM}}$

- **Excitation electromagnetic Weibel instability: high speed flows**
- **Interaction time > 30 instability growth time: large laser energy**
- **Transverse magnetic field may accelerate the shock formation by electron magnetization**

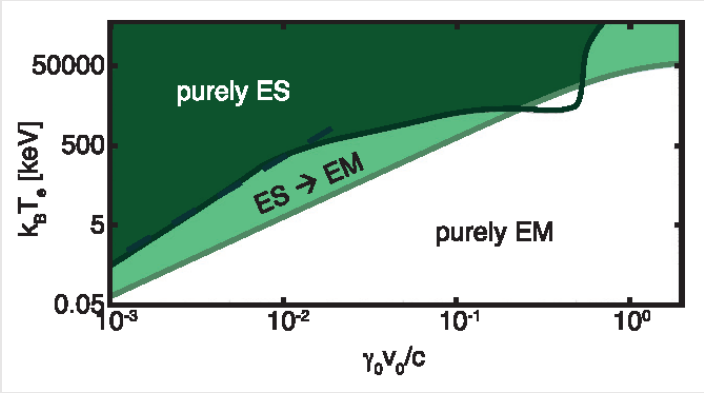

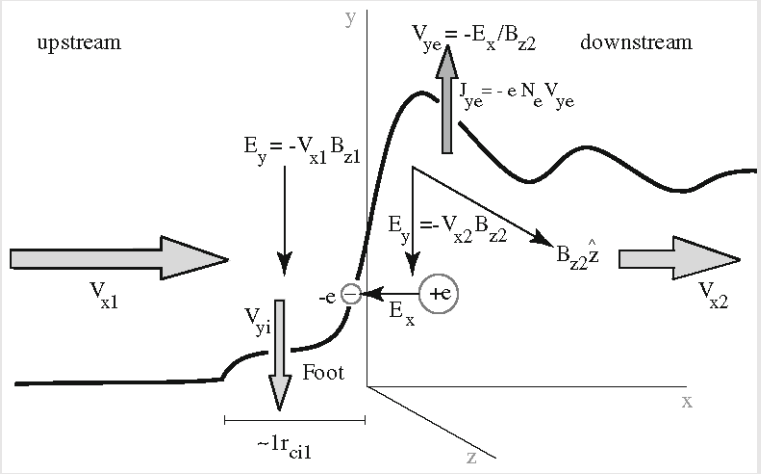

Treumann, Astron. Astrophys. Rev. 2009
Stockem Novo et al PPCF2015

Excitation of the Weibel instability on OMEGA

Weibel instability excitation have been observed in colliding plasma streams, but it did not enter in the shock formation regime

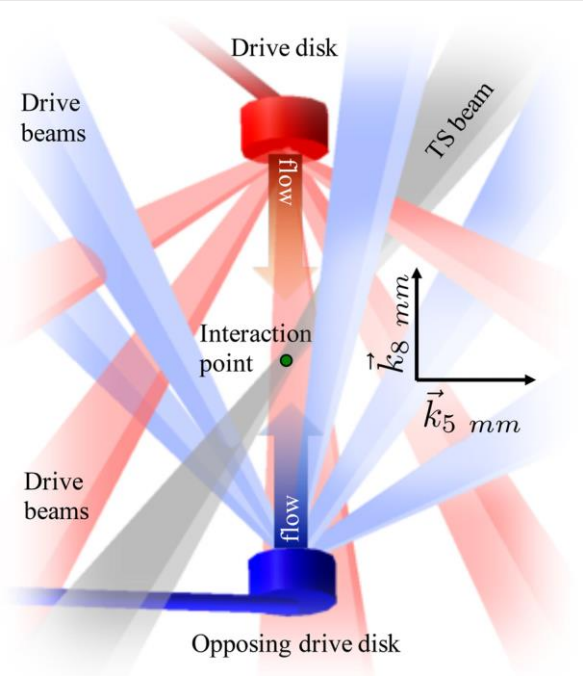

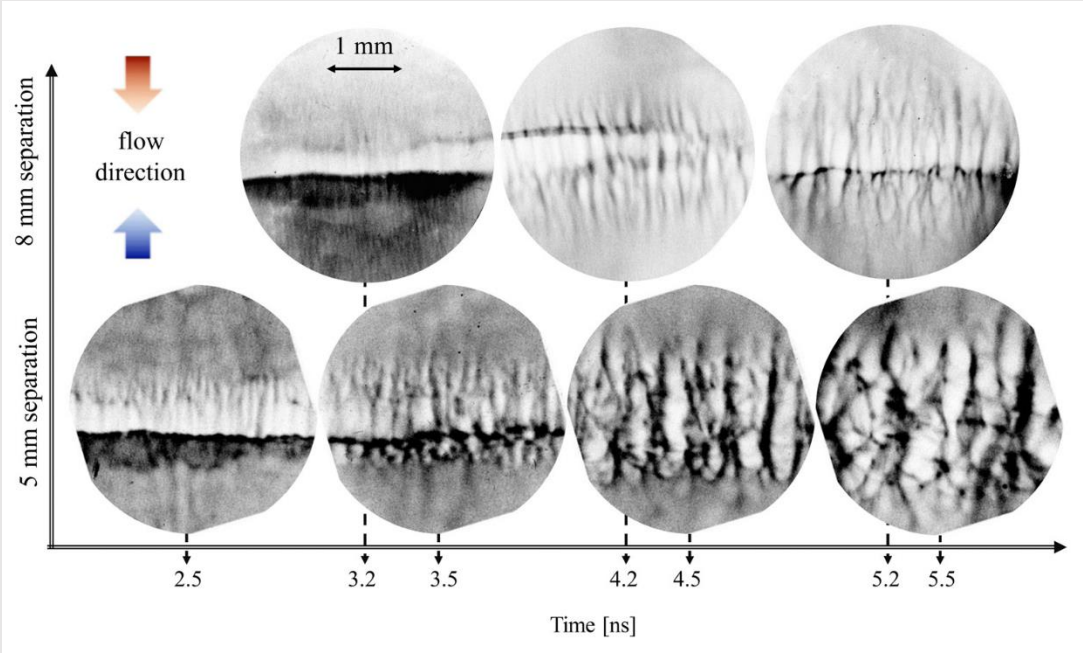

OMEGA experiment: 2 counter-streaming plasmas are driven by 4 laser beams each:

- **plasma velocity 600-800 km/s**
- **density 1-2×10^{18} cm^{-3}**

Interaction time is insufficient for sufficient dissipation of the flow energy and shock formation

Huntington et al PoP 2017

Creation of a collisionless shock on NIF

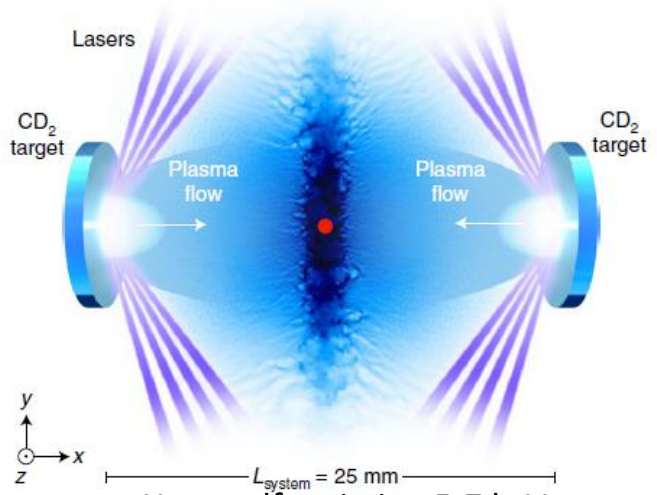

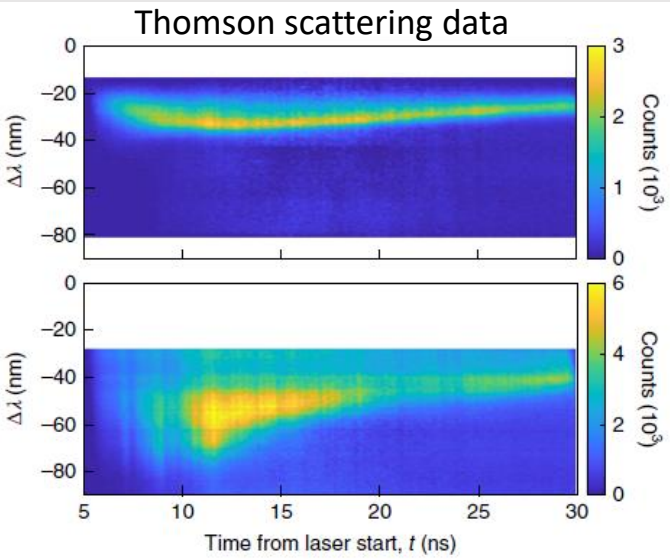

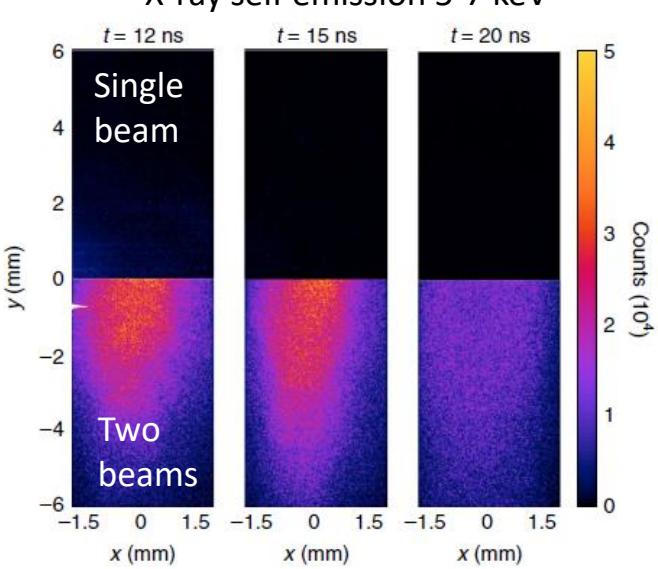

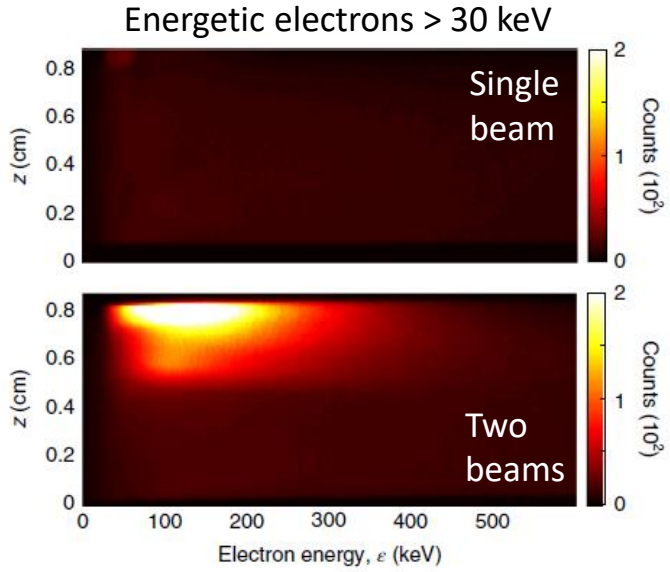

Experiment on NIF was conducted at a larger laser energy of 455 kJ and with longer pulses of 3 ns so the shock has time to develop

Plasma flow velocity 1800 km/s

Density 5×10^{19} cm^{-3}

Ion-ion mfp 80 cm

Much number 12

Shock formation time 6 ns

Fiuza et al Nat Phys 2020

Comparison with numerical simulations & SNR

This experiment can be scaled to supernova remnant shocks

Parameter	NIF experiments	Typical young SNR (for example, SN 1006)
Shock velocity (km s^{-1})	1,000–2,000	3,000–5,000
Ambient magnetic field (G)	2×10^{4}	3×10^{-6}
Ambient plasma density (cm^{-3})	5×10^{19}	0.2
Ambient plasma temperature (eV)	500	1
System size (cm)	2.5	3×10^{19}
Collisionality ($L_{system}/L_{m.f.p.}$)	0.03	0.01
Sonic Mach number (v_{sh}/c_S)	12	400
Alfvén Mach number (v_{sh}/v_A)	400	400

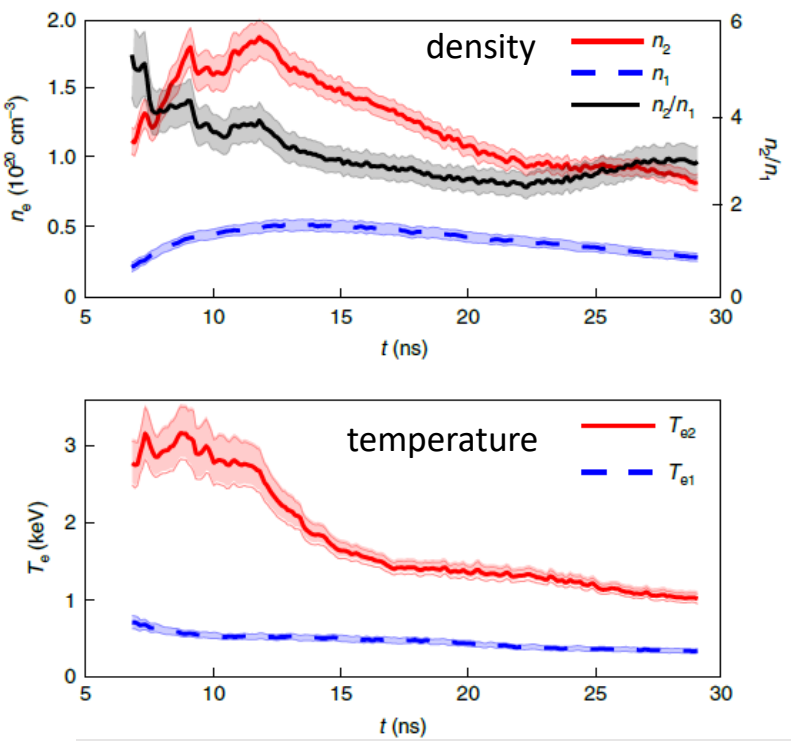

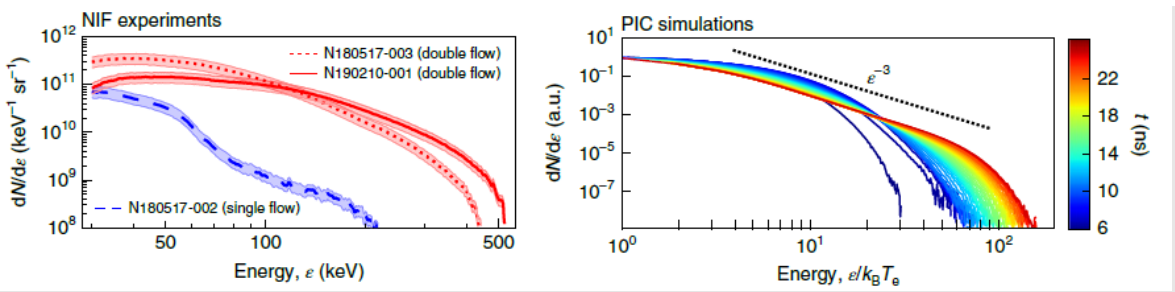

Electron acceleration to energies 500 keV agrees with simulations: acceleration in the magnetic turbulence near the shock front

Multi-pass acceleration is not yet achieved

Fiuza et al Nat Phys 2020

Relativistic laboratory astrophysics

Ultra-intense high power lasers open new chapter in the laboratory astrophysics: studies of processes related to quantum electrodynamics

- **Radiation reaction**
- **Positron production**
- **Electron-positron plasmas**
- **Gamma-gamma collisions**
- **Vacuum polarization**

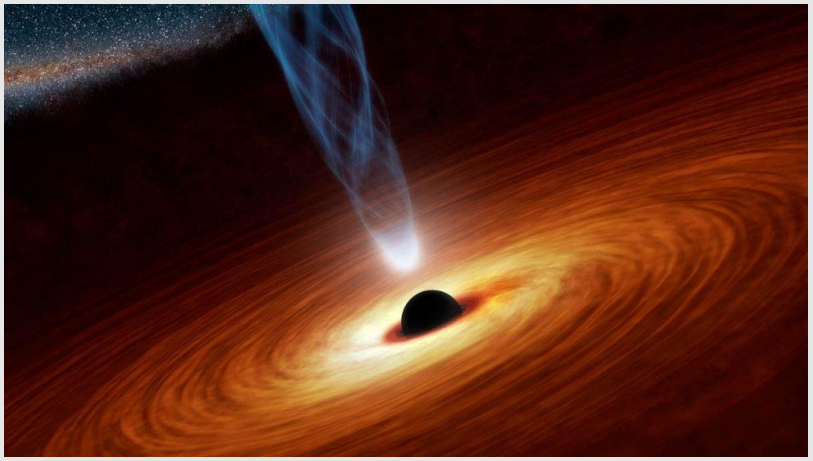

It is supposed that jets produced in AGN are made of electrons and positrons produced in gamma-gamma collisions

$$\gamma + \gamma \rightarrow e^+ + e^-$$

Breit-Wheeler process is a basic phenomenon in the Universe, not yet observed in laboratory. Limit on the maximum energy of gamma rays:

Scattering on the cosmic background radiation: max at 1 TeV, max length 213 Mpc

Nikishov JETP 1962

Reproducing BW process in laboratory

The cross section of BW process is quite large ~ 1 barn, but it is very difficult to create a sufficiently dense photon beam and target.

$$N_{ee} = N_{\gamma 1} N_{\gamma 2} \frac{\sigma_{\gamma\gamma}}{D_\gamma^2}$$

Two options are considered:

- **Dense target – hohlraum $T_{\gamma 1} \sim 300$ eV length 1 cm and density $n_{\gamma 1} \sim 10^{22}$ cm^{-3} but one would need 100 gammas with energy of 1 GeV in order to create 1 pair: a combination of high energy 10 kJ and high power 1 PW lasers**
- **Two beams of 1 MeV energy and size $D \sim 1$ mm – one needs 0.1 J energy in each beam to create 1 pair: two 1 PW short pulse lasers will be sufficient**

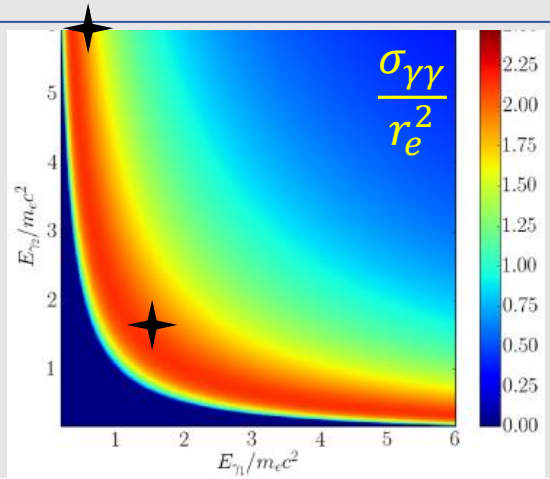

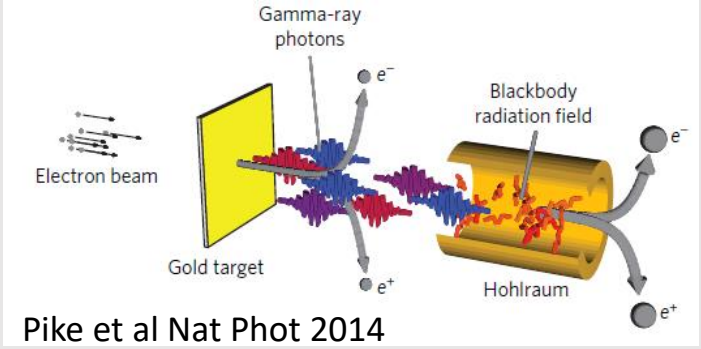

Pike et al Nat Phot 2014

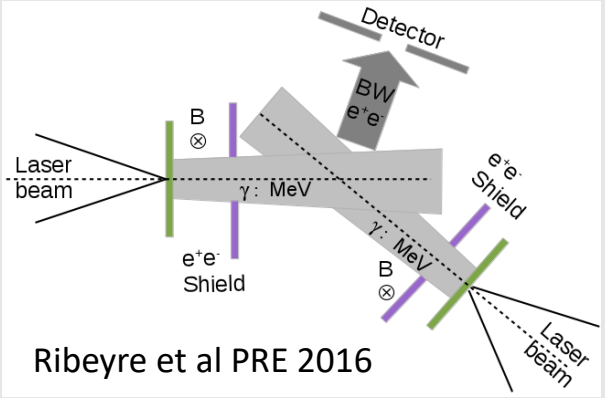

Ribeyre et al PRE 2016

Gamma-ray sources & pair distribution

Several sources of intense gammas can be considered

Pair angular distribution can be controlled

Source	Bremsstrahlung	Synchrotron	Compton	Betatron
Laser energy	100 J		10 J	
Photon energy	1 – 50 MeV		1 – 10 MeV	
Beam energy	1 – 10 J		1 – 10 µJ	
Efficiency	1 – 3 %		10^{-7} – 10^{-6}	
Divergence	10 – 30°		0.1°	
Number pairs	10^{4}		10^{-3}	

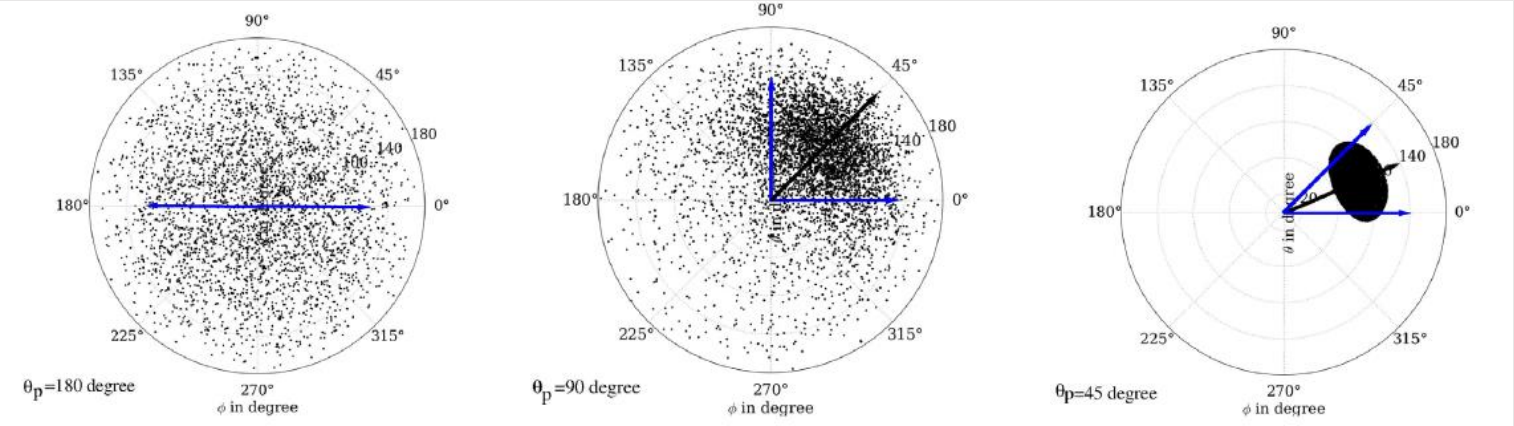

Ribeyre et al PPCF 2017

Concluding remarks

Progress in laser technology opens areas of high energy and high power laser applications in fundamental science and industry:

High energy lasers:

- **Create materials at extreme conditions**
- **Reproduce conditions and physics processes which do not exist on the Earth**
- **Provide input and validate astrophysical models and theories**

High power lasers:

- **Provide efficient and flexible diagnostic tools – X-ray radiography, proton and neutron radiography**
- **Validate QED models at extreme conditions, extension from electrons to other leptons**
- **Applications in medicine and industry**

Magnetic vs inertial: pro and contra

Standard power plant produces 1 GW electrical energy, that is about 2.5 GW fusion

Magnetic fusion is a continuous process: external energy is needed only to start the process – self-heating process

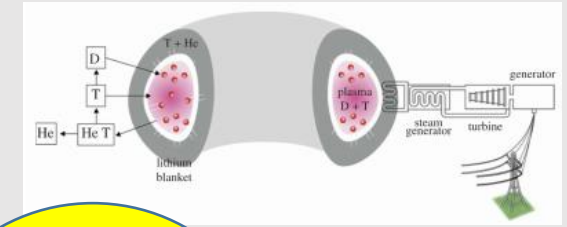

- Plasma density $n_i \leq 10^{14}$ cm^{-3} is limited by the available magnetic field strength $B \leq 10$ T
- Small reaction rate ~ 0.05 s^{-1}
- Large number of particles $\sim 4 \times 10^{22}$
- Large fuel mass ~ 0.15 g
- Large tritium inventory
- Large plasma volume ~ 400 m^3
- Large heating energy ~ 200 MJ
- Long confinement time ~ 4 s
- Small heating power ~ 40 MW
- Known (but complicated) technology
- Big capital investments
- Many installations, long experience
- International program: JET → ITER

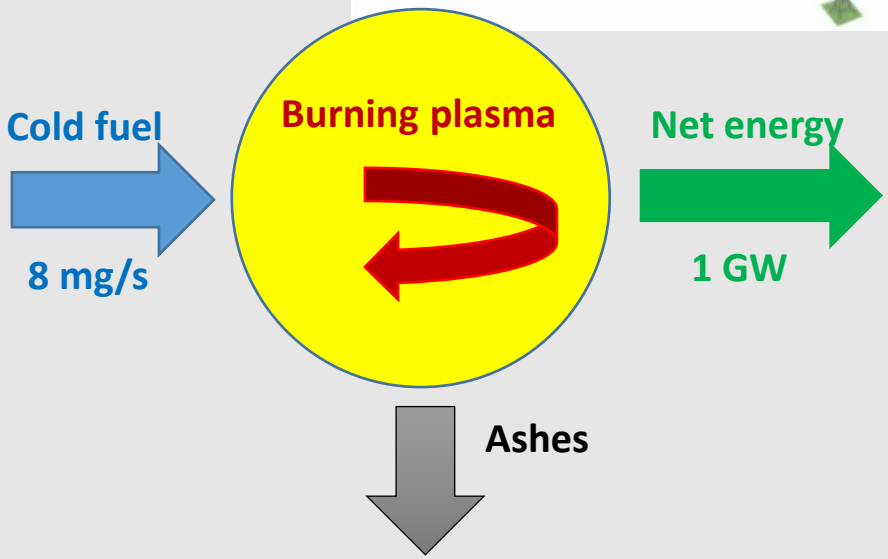

- Magnetic confinement in a toroidal geometry
- Self-heating process needs to be demonstrated
- Continuous fuel burn needs to be demonstrated

Inertial vs magnetic: pro and contra

Inertial fusion is a pulsed process: external energy is needed at the start of each cycle

- One explosion/s 2.5 GJ = 600 kg TNT/s too much, typical figure: 250 MJ/shot
- Small fuel mass ~ 2 mg
- Low tritium inventory
- Heating energy is reduced to $5-10$ kJ by heating only $\sim 1\%$ of the fuel
- Strong compression > 2000 in volume
- Short combustion time ~ 100 ps
- Low driver efficiency $\leq 10\%$
- Incomplete combustion $\leq 30\%$, debris
- Potentially compact reactor and low capital investments, max laser energy $\leq 1-3$ MJ
- Separable technology, but does not yet corresponds to the reactor requirements (energy, power, rep-rate)
- Limited number of installations: NIF and LMJ, double use

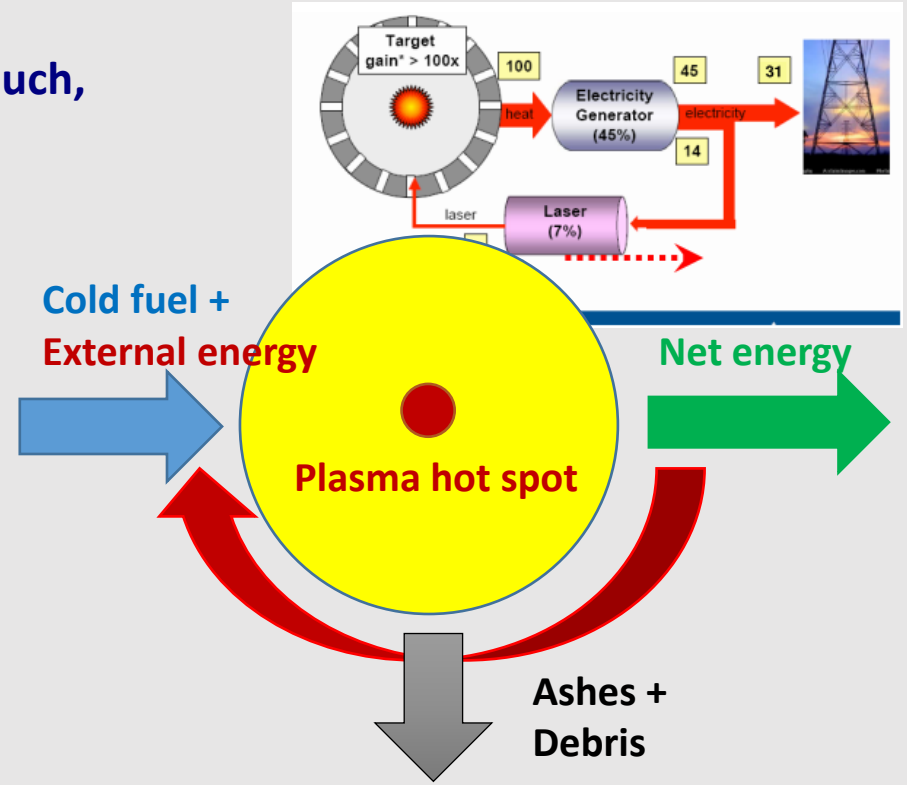

- Thin spherical shell: unstable implosion
- Ignition from the hot spot needs to be demonstrated
- Operation in the rep-rate regime needs to be demonstrated

Tikhonchuk Phil. Trans. R.Soc 2020

Direct vs indirect: pro and contra

Ignition conditions impose a relation between the hot spot areal mass and temperature

$$(\rho R)_{hs} T_i > 0.3\ \mathrm{g/cm^2} \times 5\ \mathrm{keV}$$

minimum hot spot energy $\sim 5 - 10$ kJ

In indirect drive approach target is irradiated by x-rays in a hohlraum

- More homogeneous irradiation, more stable implosion
- Nonlinear laser plasma interaction effects are suppressed, lower fuel preheat
- Good target protection from external perturbations
- Weak laser energy coupling to target
- Difficult target diagnostics
- Large amount of debris: hohlraum mass = fuel mass $\times$ 1000 or more
- Double use, defense funded installations

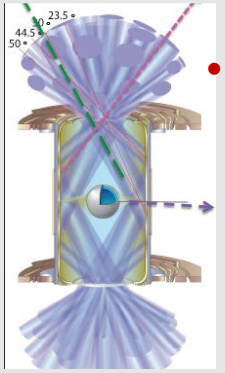

In direct drive approach target is irradiated by overlapping laser beams

- More efficient laser energy coupling to the target
- Small amount of debris
- Better diagnostic and implosion control
- High risk of nonlinear laser plasma interaction and fuel preheat
- Target protection needs to be reinforced
- Very few dedicated installations, laser beam geometry incompatible with ID